# Nanomaterials for Nanotheranostics: Tuning Their Properties According to Disease Needs

Xin Yi Wong[†,‡], Amadeo Sena-Torralba[†], Ruslan Álvarez Diduk[†], Kasturi Muthoosamy[§,*], Arben Merkoçi[†,‖,*]

[†] Nanobioelectronics & Biosensors Group, Catalan Institute of Nanoscience and Nanotechnology (ICN2), CSIC and BIST, Campus UAB, Bellaterra, 08193 Barcelona, Spain

[‡] Department of Chemical & Environmental Engineering, Faculty of Engineering, University of Nottingham Malaysia, 43500 Semenyih, Selangor, Malaysia

[§] Nanotechnology Research Group, Centre of Nanotechnology and Advanced Materials, University of Nottingham Malaysia, 43500 Semenyih, Selangor, Malaysia

[‖] ICREA, Institució Catalana de Recerca i Estudis Avançats, Pg. Lluis Companys 23, 08010 Barcelona, Spain

*Address correspondence to: kasturi.muthoosamy@nottingham.edu.my, arben.merkoci@icn2.cat

**TABLE OF CONTENTS GRAPHIC**


**ABSTRACT**

Nanotheranostics is one of the biggest scientific breakthroughs in nanomedicine. Most of the currently available diagnosis and therapies are invasive, time-consuming and associated with severe toxic side effects. Nanotheranostics, on the other hand, has the potential to bridge this gap by harnessing the capabilities of nanotechnology and nanomaterials for combined therapeutics and diagnostics with markedly enhanced efficacy. However, nanomaterial applications in nanotheranostics are still in its infancy. This is due to the fact that each disease has a particular microenvironment with well-defined characteristics, which promotes deeper selection criteria of nanomaterials to meet the disease needs. In this review, we have outlined how nanomaterials are designed and tailored for nanotheranostics of cancer, and other diseases such as neurodegenerative, autoimmune (particularly on rheumatoid arthritis) and cardiovascular diseases. The penetrability and retention of a nanomaterial in the biological system, the therapeutic strategy used and the imaging mode selected are some of the aspects discussed for each disease. The specific properties of the nanomaterials in terms of feasibility, physicochemical challenges, progress in clinical trials, its toxicity and their future application on translational medicine are addressed. Our review meticulously and

critically examines the applications of nanotheranostics with various nanomaterials, including graphene, across several diseases; offering a broader perspective of this emerging field.

**KEYWORDS**

nanotheranostics, nanomaterials, cancer, solid tumor, liquid tumor, neurodegenerative diseases, autoimmune diseases, cardiovascular diseases, clinical trials, graphene

John Funkhouser, the PharmaNetics president and CEO, was credited by scientists in year 2002 for introducing the term theranostics (a portmanteau of **Thera**peutics and Diag**nostics**), which epitomes the development of nanoparticle system for personalized medicine.[1,2] Theranostics (or theragnostics) refers to comprehensive effort that integrates diagnostic and therapy in a single system/platform.[3,4]

With the emergence of nanotechnologies and nanomaterials, the concept of nanotheranostics was then introduced (Figure 1). Nanotheranostics was able to provide non-invasive imaging, targeting and therapy at the disease sites, without affecting surrounding healthy cells.[3,5] Hence, the use of empirical treatment can be avoided (therapy given based on experience, usually without a prior definitive medical diagnosis and likely to cause infectious disease), greatly improve the prognoses and subsequently expedite clinician's therapeutic decisions. Therefore, early diagnosis will increase the patient's survival rate, and the optimized treatment will contribute to high therapeutic efficiency along with best safety profile.[3,6] Furthermore, over-dosing of drugs and cost of treatment can be effectively reduced. Nanotheranostics will also enable real-time monitoring of the drug release and its biodistribution in patients.[7]

Nanomaterials can be broadly categorized according to their composition, such as metal, carbon, inorganic and organic nanoparticles (NPs).[8,9] Generally, theranostic nanomaterials

can be made up of different chemical constructs: targeting moiety (for specific cellular binding), therapeutic agents (for drug delivery), diagnostic agents (for non-invasive imaging), and polymer coating or matrix that imparts colloidal stability and provide functional groups for bio-conjugation.[3,6] Some of the important advantages of nanomaterials are undoubtedly their small size and large functional surface area to volume ratio, in addition to interesting optical and electrical properties. These properties allow the diagnostic and therapeutic agent to be adsorbed, dissolved or covalently attached to the surface, to form nanoparticle-drug/imaging/targeting complexes.[10] The complex can subsequently signal (diagnostics) and deliver the agents to the cancer cells or other targeted sites to perform the therapy.[11,12] Ideally, after the controlled release of encapsulated drug molecules, the residual nanoparticle will be safely degraded and excreted from the body.[10]

Recently, the application of nanomaterials with multiple physical imaging modalities and therapeutic capabilities has received increasing attention. There are several excellent review papers with similar topics made, [8,13–17] however, these papers are either focused on specific disease/cancer/illness, or emphasized on the theranostic properties of a specific nanomaterial. In this review, we stratify the information on the basis of cancer- or disease-specific, enabling comprehensive comparison of the nanomaterials for theranostics of up to three different diseases. Specifically, we focus on the nanotheranostics of cancer (including solid and liquid tumor) and several diseases: neurodegenerative, autoimmune and cardiovascular diseases (see Table 1). The physiochemical properties of various nanomaterials, including graphene, a rising star in the 21$^{st}$ century, have been critically reviewed. We also discuss the physical and biological barriers that impede application of nanotheranostics *in vivo*, and provide an overview of different nanomaterials that are currently in clinical trials. A future outlook of this rapidly growing field will be given as a conclusion. By putting this information together, this review may shed light on understanding nanomaterials for nanotheranostics while we are

expecting continuous breakthrough in this field.

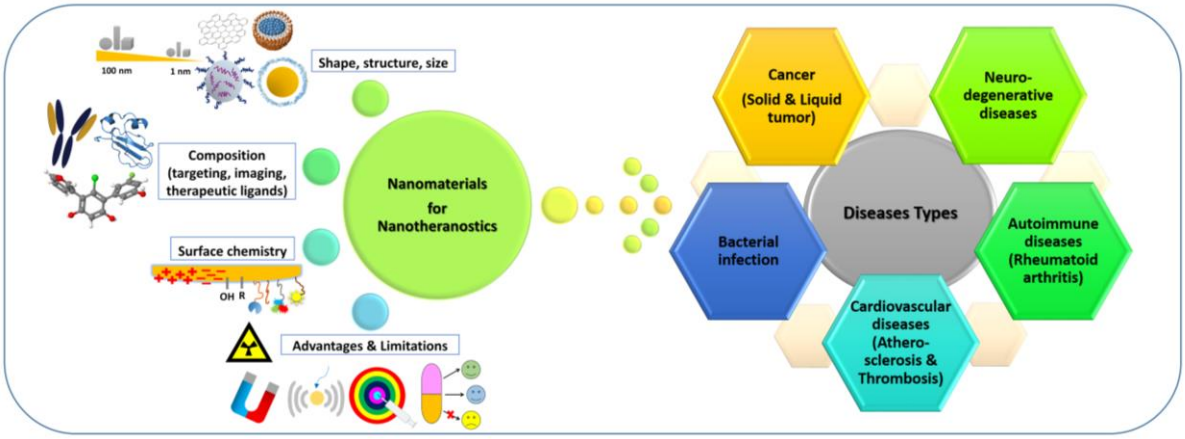


**Figure 1 Nanotheranostics: The use of nanomaterials with integrated diagnostic and therapeutic properties across several diseases.**

**Physical and biological barriers that impede the application of nanotheranostics *in vivo***

The human body has multi-tiered physical, physiological, chemical and biological barriers to protect it against foreign species/substances. Examples of the barriers that nanomaterials may encounter in biological systems are the skin, air-blood barrier in the lungs, reproductive system, circulation and blood-brain barrier.[18,19] Nanomaterials must be precisely engineered to overcome these biological barriers and perform nanotherapeutics at the disease site.[20] While it is important to find a balance between therapeutic potential and toxicity of nanomaterials, their biological effects on human body are not fully understood due to the complexity of nanomaterial/biological barrier interaction.

In this section, we will discuss the interactions of nanomaterials with serum proteins and mononuclear phagocyte system (MPS) in the tumor microenvironment, and provide an overview of the barriers to the intratumoral delivery of therapeutic nanomaterials.

**(i) Interaction of nanomaterials with serum proteins**

When nanomaterials circulate throughout the body they are exposed to a complex fluid containing blood, lymph, biomolecules, cytoplasm, *etc*.[21,22] Protein and other biomolecules

such as albumin, transferrin, gamma globulin and fibrinogen, will compete for binding on the surface of nanomaterials. This will slightly change the secondary structure of the proteins and lead to the formation of both soft and hard protein corona.[22–24] Formation of protein corona on nanomaterials will affect the surface of nanomaterials and their subsequent interaction with biological molecules (biodistribution and penetrance) and cellular compartments.[18,25] The composition, properties and formation of protein corona are influenced by physiochemical properties (size, shape, surface area, charge, chemical composition, functionalization, colloidal stability, porosity, *etc*.) of nanomaterials. Nanomaterials could exert both positive (act as carriers to immobilize enzyme, improve activity and stability of proteins) and negative impacts (induce potential toxicity to cells and organs) on proteins.[26] Supramolecularly built protein corona can also be exploited to shield nanomaterials' interaction with serum proteins and macrophages while retaining its targeting specificity *in vitro* and *in vivo*.[24]

Positively charged nanomaterials facilitate cellular uptake and improve lysosomal escape without induction of toxicity, showing more specific interaction with negatively charged biological membranes.[18] Single-layer and multi-layered graphene oxide have been proven to exhibit different behaviors in cell culture medium.[27] The various types of carbon nanomaterials (fullerene, carbon nanotubes, graphene and their derivatives) have particular effects on the structure or activity of the proteins. For instance, the graphene sheet has a stronger adsorption capacity for serum proteins than carbon nanotubes. Yet, the enzymatic degradation of graphene and fullerenes derivatives is much complicated than carbon nanotubes.[26]

The individual and in combination properties of nanomaterials play an important role in determining their path, biological effect and immunological fate in biological systems.

**(ii) Interaction of nanomaterials with MPS**

One of the factors for low drug-delivery efficacy to the tumor and low therapeutic outcomes is due to the MPS. The MPS mainly involves liver, spleen and lymph nodes. MPS serves as a delivery barrier for invading pathogens, particulates and dead or damaged host cells.[28] Among the MPS, Kupffer cells are the major phagocytic cells (*e.g.* macrophages) residing inside the liver sinusoid.[23] In principle, cationic nanomaterials have higher affinity for macrophages than neutral and anionic nanomaterials.[23] Attachment of surface protein, such as opsonins on the nanomaterials may increase the chance of nanomaterials being recognized by the scavenger receptors on the Kupffer cells. This will result in opsonisation and subsequent phagocytosis.[18,19,23] The nanomaterials will be ultimately taken up and cleared by macrophages. Generally, MPS cuts off more than 95 % of the administered nanomaterials.[23] Mammalian cells engulf intracellular contents using autophagosome, a double-membrane vesicle, fuse with lysosomes, and later degrade or recycle the autophagic contents. This process is known as autophagy.[25] Autophagy is vital in maintaining the homeostasis of cells. Dysregulation of autophagy in degrading overexpressed prions proteins may lead to neurodegenerative disorders; while active autophagy aids in chemotherapeutic treatments of cancer cells.[25] $Fe_3O_4$ NPs were found to have the ability to induce autophagy in human cervical carcinoma cells. Positive correlations between size/molecular weight of protein and adsorption of protein on a 20 nm $Fe_3O_4$ NPs were confirmed.[25] However, the higher the adsorption of protein on $Fe_3O_4$ NPs, the lower the cell uptake of NPs and consequently lower cell autophagy responses.[25]

An increase in the dosage of nanomaterials, on the other hand, raises toxicity concerns induced by the accumulation of nanomaterials in organs such as liver and spleen.[23] Solvents and chemicals involved during the synthesis of nanomaterials are one of the causes of toxicity *in vivo*.[17] Their long-term cytotoxicity and related immune response should be taken into consideration.

Four strategies (surface modification, tuning of physiochemical properties of nanomaterials, biomimetic design inspired by nature and modulation of the MPS) have been identified to oppose uptake by the MPS, lower off-target rate and enhance cancer therapeutic efficacy.[23] For instance, modifying the surface of nanomaterials with zwitterions, polyethylene glycol, carbohydrate moieties and dysopsonic proteins allow bypass of phagocyte-mediated cellular barriers, which in turn increases nanomaterials blood circulation time and theranostics efficacy.[24] Another interesting strategy to protect the nanomaterials from phagocytosis is by using the extracts of cell membranes from blood or tumor cells. The extracts can be used to coat the nanomaterials, camouflaging the nanomaterials from uptake by the MPS.

**(iii) Barriers of intratumoral delivery**

Tumor microenvironment is generally composed of tumor cells, the extracellular matrix, stromal cells, cells from the immune systems (macrophages, lymphocytes, natural killer cells), *etc.*[12,19] Macrophages act as immune cells to maintain immunohomeostasis. The failure of existing therapies is mainly attributed to the tumor microenvironment limiting drug access to the tumor cells.[12,29] This is because upon entering through the blood vessel leakage, nanomaterials would interact with the microenvironment factors.

The intratumoral microenvironment serves as a physical and biological barrier for the delivery of therapeutic nanomaterial to the solid tumor (*e.g.* pancreatic cancer).[18] In normal tissues, the extracellular matrix is loose and elastic, with sufficient oxygen supply, and the overall redox environment is homeostasis.[30] In contrast, the basement membrane in the tumor is thicker, with higher cross-linked extracellular matrix, hypoxic, acidic and has harsh redox environment.[31,32] Differentiated macrophages, named as M2-type tumor-associated macrophages, will trap and degrade the functional nanomaterials delivered into the tumor.[30] High tumor interstitial fluid pressure will also force the nanomaterials back to blood

circulation, further preventing them from reaching the tumor sites.[30] These pathophysiological properties greatly impede intratumoral delivery of nanomaterials. Dissolution (or generation of metal ions in target organs and cellular barriers), is another common phenomenon in metal and metal oxide nanomaterials in biological systems due to their high surface area and reactivity.[18] Different strategies, such as the use of stromal depletion molecules, targeting of transforming growth factor-beta (TGF-β) and interleukin-6 (IL-6) pathways, *etc*. have been studied to overcome the stromal barrier.[18,33,34] Pei *et al*. (2019)[29] also demonstrated that simultaneous targeting of both TGF-β signaling and KRAS mutation attenuates the dense stroma barrier, enhances tumor blood perfusion and improves therapeutic efficiency in pancreatic cancer.

In short, it is important to understand the interaction between nanomaterials and tumor microenvironmental factors before constructing functional nanomaterials that are expected to be able to overcome the above-mentioned challenges.

## CANCER

Cancer is a broad name given to the diseases featured with uncontrolled rapid cell division that may form growths called tumors. Nobel Laureate Otto Warburg discovered that low oxygen was a hallmark of cancer cells. Cancer cells "reprogram" themselves under stressful conditions (lack of oxygen, limited nutrient resources or energy, *etc*.), with a faster growth rate than the rate of new blood vessel formation.[35,36]

Cancer can be further classified into solid and liquid tumors, each with differences in terms of their tumor vascularity and heterogeneity, thus requiring different diagnostic and targeting strategies.[37] For centuries, surgery, chemotherapy and radiation therapy remain as the most common cancer therapies. However, these few alternatives often come with the possibility of recurrence after the treatment (since not all cancer cells can be completely removed by

surgery), severe toxic side effects (chemotherapy and radiotherapy) and limited specificities to cancer cells.[38,39] Due to their low molecular weight, conventional chemotherapeutic drugs generally have low half-lives in the blood and are rapidly distributed in healthy tissues and organs, limiting their therapeutic efficacy.[40] Furthermore, the use of centralized diagnostic platform in most of the cancer management can be complex, time-consuming and not tailored to patients and malignancies.[37]

Theranostic nanomedicine possess the ability for specific cancer biomarker detection and concurrent cancer cells ablation, in a simple and non-invasive way, making them suitable candidates for nanotheranostics.[37] For instance, the nanomedicine can be delivered and accumulated at the tumor sites to perform therapeutic action. Yet, the drug delivery is still limited in poorly vascularized regions, some cancer cells are able to continue proliferating.[10,39] In contrast, liquid tumors (such as leukemia and lymphoma) are spread throughout the bloodstream, its diagnostics and therapies are often challenged by poor selectivity, low therapeutic efficacy, multi-drug resistance and long-term side effects.[37] Tumor microenvironment varies between cancer types of different or the same anatomical region.[12] The discovery of the right diagnostics and therapeutics intervention is highly important in cancer treatments.

Continuous research efforts in nanotheranostics from drug delivery vesicles to imaging of contrast agents and targeting modalities have rapidly driven nano-oncology towards an all-in-one, localized early detection and treatment. This section will comprehensively review the recent advances regarding the development of different therapies (besides chemotherapy) and imaging modalities (such as optical, photoacoustic imaging, magnetic resonance imaging (MRI)) for solid and liquid tumors diagnosis and treatment, using functional nanomaterials.

**Solid tumor**

Solid tumor is an abnormal mass of tissues, may be benign (non-cancerous) or malignant (cancerous). Examples of solid tumors are carcinomas (tumors formed in epithelial cells) and sarcomas (tumors in blood vessels, bones, fat tissues, muscles, *etc*.).

Hypoxia, a condition in which the body tissues are deprived of oxygen, mainly due to the disorganized vasculature and poor blood circulation, is an important characteristic of solid tumors.[41,42] The hypoxia microenvironment may confer the resistance of tumors to cancer treatment,[31] especially photodynamic therapy (PDT), an externally activable and oxygen-dependent therapeutic modality.[38] PDT works by using cytotoxic oxygen species (such as singlet oxygen or reactive oxygen species (ROS)) generated from photosensitizer molecules upon light exposure, which destruct tissue structure and subsequently kill cancer cells.[41] Besides, solid tumors are 2-3 times more radio-resistant than normoxic tumors.[43] Hence, the hypoxic and radio-resistance nature of solid tumors cause the cancer treatment even more challenging.[44]

Intracellular environment of tumor cells is also rich in hydrogen ions ($H^+$) and hydrogen peroxide ($H_2O_2$) due to rapid glycolytic metabolism and superoxide dismutase over-expression.[45] This contributes to the weakly acidic extracellular pH (pH 6.0-6.8) in tumors, in contrast to weakly basic normal tissues (pH 7.2-7.4).[5,41] Hence, an ideal solid tumor theranostic nanomaterial should be sensitive enough to respond to the minute difference in extracellular pH between blood and tumors.[46] Other common cancer phenotypes are high abundance of antioxidants and elevated glutathione (GSH) level (about 4-fold higher than normal cells).[5,39,42]

In addition, the original size of the nanocarrier should be maintained below 160 nm for optimum deposition on the tumor tissues and exploit the enhanced permeability and retention (EPR) effect.[47] EPR is a phenomenon where nanomedicine leaks preferentially into tumor

tissue, through the permeable tumor vasculature. The nanomedicine will be retained in the tumor bed owing to the reduced lymphatic drainage.[36,48] EPR effect aids in the delivery (with a relatively modest effect of less than a 2-fold increase) and accumulation of nanomedicine at the solid tumors, and subsequently improves the therapeutic efficacy.[23,32,49] The potential side effects are greatly reduced, since there is very low accumulation of nanomedicine within the normal tissue.[36] The ability of the NPs to cluster into large size aggregates after successful cellular internalization could prevent the lysosomal exocytosis, which may minimize the loss of their therapeutic activity.[47] Nevertheless, the drug delivery remains limited in poorly vascularized regions of the tumors, some cancer cells are still able to survive.[10,18,32] Also, the efficiency of EPR effect is highly dependent on cancer type.[18]

Researchers have been putting efforts to design and tailor different stimuli-responsive nanomaterials to overcome multiple biological and physiological barriers in drug delivery, and simultaneously serve as a nanotheranostic platform for cancer. The following section provides comprehensive review on the nanotheranostic features of each nanomaterial, together with their advantages and limitations.

**Gold nanostructures**

Gold (Au) nanostructure is a collective term given to different shape of gold nanoparticles (AuNPs). It has received increasing attention for being able to provide a versatile and multifaceted platform for biomedical applications.[38,49–51] Apart from having excellent biocompatibility and facile surface chemical features, Au nanostructures are able to act as photothermal transducers. They are capable of absorbing visible or NIR radiation and then convert them into heat with high efficiency to destroy nearby biological structures (coined as photothermal therapy, PTT).[31,41,42,45,47] The potential side effects of using Au nanostructures for cancer treatment can be reduced to minimum by controlling the intensity of light and

amount of injected nanomaterials, making it a highly selective material in cancer treatment.[17,52–55]

Hepatocellular carcinoma (HCC), a type of solid tumor, is the most common primary liver cancer.[56] Being the third leading cause of cancer death worldwide, HCC has often been chosen as the focus of many clinical research.[57,58] HCC tumors, like other solid tumors, have scant stroma and necrosis in the central area due to poor vascularization. HCC is nodular and can either appear as a single solitary tumor with a large mass or multiple small tumors.[56] A tumor microenvironment responsive and triple-synergistic therapeutic nanoplatform based on AuNPs with Cu (II)-aptamer complexes has been developed for HCC treatment [Figure 2a (ii)].[41] Aptamer is a small and easy to synthesize secondary structure ligand made up of single DNA or RNA sequence. Aptamers confer lower immunogenicity and have high targeting affinity to cell surface receptors,[59] whereas chlorin e6 (Ce6) is a widely used photosensitiser.[38,60] Possessing high singlet oxygen generation capability, Ce6 labelled aptamer has been chosen to specifically target the HCC cells and activate PDT. The binding of Ce6 labelled aptamer onto AuNPs not only avoids rapid clearance of AuNPs from the body, but also serves as a cargo for the Cu (II) coordinated chemotherapeutic prodrug AQ4N (or banoxantrone, a hypoxia activated prodrug to enhance anti-tumor effects). The high level of intracellular GSH and acidic extracellular pH in cancerous cells induce the release of the AQ4N. The electrostatic aggregation of AuNPs induced by the free Cu (II) also switches on the PTT effects to ablate solid tumors. This system successfully permits the synergistic PDT/PTT/chemotherapy of HCC by single laser irradiation at 670 nm.[41] However, this approach has some limitations especially when selecting AQ4N as the prodrug. Since AQ4N has ultra-high aqueous solubility (260 mg/mL), large dose and multiple dosing (≥ 100 mg/kg) are required during combination therapy.[61] Although the potential side effects of AQ4N loaded nanomedicines have not been reported thus far, low AQ4N loading content and

encapsulation efficiency, non-specific release and short-term *in vivo* retention time (half-life *in vivo* ≤ 6 h) are some of the concerns.

On the other hand, it is technically difficult to keep photoirradiation localized only on cancer cells due to uncontrollable distribution of the photothermal agents in the intracellular micro-environment.[62] Alternatively, laser beam allows precise focusing to a tiny region of tumor cells. It has therefore been used as a stimulus to cross-link photothermal AuNPs covalently with the surface diazirine groups of polyethylene glycol (PEG) ligands [see Figure 2a (i)].[63] Upon 405 nm laser irradiation, diazirine groups generate a highly active carbene intermediate that can form covalent bonds with ligands within close proximity of AuNPs. The interparticle cross-linking of AuNPs has significantly improved photothermal ablation effects, with an optical-thermal conversion efficiency of about 78.8 % as compared to 21.6 % for the non-cross-linked AuNPs. This innovative approach has effectively shifted the surface plasmon resonance of 20.5 nm AuNPs to NIR region. It was also noted that the as-synthesized photocross-linked AuNPs have longer blood circulation time and shorter biological half-life than particle aggregates.[63] Nevertheless, the penetration depth of 405 nm laser remains limited. In fact, for *in vivo* imaging application, the chosen NPs need to have the ability to be imaged at greater tissue penetration depth (including thick bone penetration for imaging of brain tumors, air-filled cavities for imaging of lung tumors, *etc.*), without compromising the spatial resolution.[17,39,64] NIR shows better penetration depth in the tissue than visible light, yet, its clinical utility is still hindered due to auto-fluorescence, potential blink, scattering and photobleaching effects in various tissues.[54,59] In fact, it is difficult to compare and evaluate the efficacy of different Au nanostructures in nanotheranostics, as their behavior is highly dependent on various parameters, such as size, shape and surface functional group.[65] Au nanocages, with cubic shape, are particularly attractive as photothermal transducers for nanotherapeutics, owing to their interesting features such as flexible tuning of the localized

surface plasmon resonance (LSPR) peaks to any wavelength of interest (in the range of 600-1200 nm) and a large NIR absorption cross section (five orders of magnitude greater than the conventional organic dyes). With a compact size of about 40 nm, the hollow and porous structures of Au nanocages permit drug encapsulation with controlled release upon irradiation with NIR light.[52] In another study, it was reported that cationic NPs exhibit superior cellular internalization, but inferior systemic circulation compared to their anionic and neutral counterparts [46]. In view of this, the idea of integration of photothermal Au nanocages with zwitterionic stealth ligand has been proposed. As aforementioned, zwitterionic medication endows NPs with surface properties resistant to aggregation, binding plasma proteins and macrophage uptake, prolonging blood circulation time.[59] Zwitterionic polymers coated on Au nanocages has successfully extended the NPs' systemic circulation lifetime by 4-fold, without compromising its cellular internalization, breast tumor targeting ability and PTT efficacy. Sensitive to the changes in cell's extracellular pH, the zwitterionic ligands on Au nanocages switch from "zwitterionic" at physiological pH (7.0-7.4) to "cationic" at acidic pH (≤ 6.5). Triggering of this charge reversal makes the NPs attach to the surface of cancer cells, leading to targeted accumulation within tumors.[46]

Cervical cancer is the fourth most common cancer in women and has the fourth highest mortality rate (among cancers in women).[66] Additionally, it is a solid tumor associated with human papillomavirus infection.[66] An example of synergistic PTT and drug delivery for cervical cancer is the use of multi-layered single-walled carbon nanotubes, termed SWNT@BSA@Au-S-PEG-FA@DOX, which was prepared using a facile layer-by-layer assembly process.[67] Carbon nanotubes display hemodynamic properties as its shape greatly affects its circulation time and biodistribution. [68] For example, the needle-like morphology of nanotubes contributes to increased specific area for interaction with plasma proteins and cells; permits cell penetration *via* both endocytosis and diffusion across the plasma

membrane; and allows longer circulation time (up to 10 times longer) in blood, as compared to spherical nanomaterials.[69] Coating of bovine serum albumin (BSA) on oxidized and cut-single-walled carbon nanotubes (SWNTs) provides abundant active sites for the nucleation of Au seeds, subsequently converting Au into AuNPs by *in situ* reduction. Possessing ideal photothermal properties, the SWNT@BSA@Au was further modified with folic acid terminated-polyglycol (FA-PEG-SH), which endows the material with high water-dispersibility, biocompatibility and selectivity towards human cervical cancer cells. Doxorubicin (DOX) was subsequently loaded onto the system, with a high loading ratio of up to 590 %. The resulting complex exhibited high efficacy, especially when combined with PPT (irradiation of the tumor with a 808 nm laser, 1 W/cm$^2$ or 5 min, 24 h after systemic injection of the nanomedicine). Besides, release of DOX is induced by the pH value and temperature in the tumor microenvironment, adding selectivity to the system. The system completely eradicated tumors *in vivo* without systemic toxicity, as substantiated by several hematological and biochemical parameters and histopathological analysis.[67] However, it is of utmost importance to note that the usage of high laser irradiance (1-48 W/cm$^2$) is practically not applicable for clinical treatment of tumors, as they exceed the skin tolerance threshold values (maximum permissible exposure of skin at 808 nm is 350 mW/cm$^2$, with an exposure time of 10-1000 s).[70] Future studies can be focused on the interactions between SWNTs and actual biological environment such as blood, since the presence of protein corona in the biological fluids might affect the BSA coatings on SWNTs and subsequently modulate their biological fate.[69]

Gold nanorod (AuNR) is an excellent photothermal agent owing to their adjustable longitudinal surface plasmon resonance and high light-to-heat conversion efficiency.[71,72] These rod-shaped NPs allow prolonged blood circulation time and facilitate deeper mammary tumors penetration than nanospheres with the same diameter.[40,71] Dendrimers are inherent

polymeric scaffolds for encapsulation of small inorganic NPs (2-20 nm) used to further increase blood circulation time, solubility and dimensional stability of nanohybrids.[73] A smart nanohybrid, termed Au nanorod/dendrimer-assembly nanohybrids (AuNR@Da NHs), with size of about 130 nm, has been constructed by supramolecular encapsulation of 83.0 w/w% AuNR into dendrimer assemblies.[73] The amphiphilic dendrimer assemblies are composed of PEGylated and antitumor adriamycin (ADR)-decorated dendrons, containing tumor microenvironmental matrix metalloproteinase (MMP)-cleavable linkages, intracellular GSH-degradable disulfide bonds and pH-breakable hydrazone bonds that are highly responsive towards tumor microenvironment. Li *et al.* (2018)[73] investigated the biological adapting ability of the nanohybrids under different biomimetic stimulations. The group proved that AuNR@Da NHs could adapt sequential biological barriers through triple-responsive features: enzyme/redox/pH, to facilitate deep tissue penetration and high internalization in tumors, particularly in human ovarian tumors that are deep within the abdominal cavity and most of the time difficult to palpate.[74] The permeability of nanohybrids in ovarian tumors are further improved, credit to the efficient photothermal properties of AuNRs in AuNR@Da NHs (about 70 %, as compared to single AuNRs about 60 %). The amount of internalized AuNR and ADR mediated by nanohybrids, were about 27-fold and 6.6 times higher, respectively, than individual AuNR-treated. Furthermore, the nanohybrids were capable of generating hyperthermia (up to 67 °C), with tumor accumulation of more than 2.3 times higher. NIR-induced hyperthermia subsequently induces the rupture of the lysosome, accelerates the endosomal release of ADR/AuNRs and thus inhibits the human ovarian tumor cells *in vivo.* In brief, AuNR@DA NHs with laser irradiation offered strong curative effects, with an inhibition rate of 80.7 %, on synergistic chemo-photothermal treatment for combating multidrug resistance.[73]

Overall, targeting and therapeutic efficacy of Au nanostructures can be enhanced by tuning its physiochemical properties such as size, surface chemistry and shape. On the other hand, tumor pathological characteristics also play an important role in penetration of nanomedicines in tumor, as tumor microenvironment is highly heterogeneous between different types of tumors. Hence, characterization of both Au nanostructures and pathological properties of tumors are equally important in the design of nanomedicine with nanotheranostic properties.

**Other nanomaterials**

Inorganic nanomaterials are multifunctional NPs platform synthesized from metals, metal oxides and metal sulfides. Inorganic nanomaterials are relatively stable over large ranges of pH and temperature,[10] resistant to enzymatic or photochemical degradation,[70] thus suitable for nanotheranostics in tumor microenvironment.[70,75]

Copper sulfide (CuS) NPs are featured with several properties compared to other commonly used NPs, such as prominent absorbance, effective heat conversion, small particle size, easy modification and facile synthesis.[76] A tumor-targeting nanocomposite (CuS@BSA-MBA-cRGD) with photothermal effect for targeting of liver-intestinal metabolism pathway was synthesized recently.[77] The biocompatibility and stability of CuS NPs were improved *via* capping effect of BSA. Then, NIR fluorescence probe (MBA) and tumor-targeting ligand cyclic arginine-glycine-aspartic acid (cRGD) peptide were further conjugated on the surface of CuS@BSA. Peptides are another commonly used ligand targeting moiety, with advantages in terms of chemical stability, ease of synthesis and reduced immunogenicity.[59] cRGD can target the cell-adhesion molecule, $\alpha_v\beta_3$ integrin, that is over-expressed on tumor new-blood vessels and some tumor cells.[78] The as-synthesized CuS@BSA-MBA-cRGD served as an infrared thermal imaging contrast agent for infrared thermal imaging and as a photothermal agent for tumor ablation *via* PTT. However, the obtained nanocomposite has a mean diameter

of about 51.2 nm,[77] raising concerns regarding its uptake by reticuloendothelial system (RES) organs that may cause slower elimination from the body and potential toxicity after effective treatment.[79]

Generally, most of the nanomaterial-based PDT requires an additional photosensitizer or high-power laser sources for effective therapy. However, the high concentration of NPs and laser irradiation with long irradiation time may lead to a heat generation during NIR therapy. The rise in temperature will subsequently lead to cell death rather than ROS generation for PDT. Srivani *et al.* (2018)[70] proposed copper bismuth sulfide ($Cu_3BiS_3$) nanocrystals as an innovative human breast tumor treatment alternative, after showing the potential of $Cu_3BiS_3$ inducing PDT without any photosensitizer, at safe laser zone (808 nm, 10 mW/cm$^2$, 10 min), and in the deep tissue penetrative NIR region. Bi, with high x-ray attenuation, could serve as an efficient x-ray contrast probe; while Cu ions, with broad NIR absorption, could serve as NIR-responsive PDT and PTT agents. Upregulation of Cu ion leaching upon irradiation coupled with Bi efficiently capturing more photons is believed to contribute to the realization of $Cu_3BiS_3$ in exceptional PDT effects at low laser power.[70] Although the group has shown that the as-synthesized $Cu_3BiS_3$ nanocrystals are highly biocompatible without any genotoxic effects, yet, the uptake of this 12 nm nanocrystals by RES organs, their *in vivo* degradation behavior and clearance after PDT still require further investigation. Besides, the influence of $Cu_3BiS_3$ nanocrystals on the biogenesis and activity of cellular organelles require further understanding as organelle dysfunctions will lead to dramatic consequences on human health.

A photosensitiser-Pd@Pt nanosystem has been designed for highly efficient PDT in human breast tumors [see Figure 2b (ii)].[44] Palladium (Pd)-based nanomaterials have good catalase-like activity, which can decompose $H_2O_2$ to produce oxygen and water. This subsequently improves the hypoxic environment of solid tumor.[44] However, like other inorganic nanomaterials, Pd has chemically/biologically inert framework, which raises concerns over

the low biodegradation and biosafety issues.[10] Functional inorganic 2D biomaterials, $MnO_2$ nanosheets, have been introduced recently for improved theranostic performance [see Figure 2b (iv)].[80] Preliminary studies demonstrate its biocompatibility as Manganese (Mn) is one of the necessary trace elements in the human body. The ultra-thin $MnO_2$ nanosheets structure, with an average thickness of 2 nm, is highly sensitive towards the endogenous (acidic and reducing) tumor microenvironment.[80] It was found that the $MnO_2$ nanosheets started to disintegrate and release $Mn^{2+}$ only within 3 min in acidic (pH 5.0) and reducing ([GSH] = 5.0 mM) solutions, with longitudinal relaxitivity ($r_1$) of 5.45 $mM^{-1}s^{-1}$ and 4.81 $mM^{-1}s^{-1}$, respectively. The $r_1$ of $MnO_2$ nanosheets in neutral solution was only 0.87 $mM^{-1}s^{-1}$. High values of $r_1$ coupled with various direct photographic images demonstrated the potential of $MnO_2$ nanosheets structure as the contrast agents for MRI, since the higher accessibility of the released $Mn^{2+}$ to water molecules could enhance brightening effect of MRI signal. $MnO_2$ nanosheets also possess high intrinsic photothermal-conversion capability for PTT. Furthermore, surface modification of the $MnO_2$ nanosheets with soybean phospholipid improved the stability of the nanosheets in physiological condition.[80] Mesoporous NiO (mNiO) NPs also appear as a photothermal conversion agent for cancer PTT [see Figure 2b (iii)].[81] Artemisinin (ART) is a traditional Chinese medicine that is believed to inhibit tumor growth. Attachment of mNiO NPs and terbium complexes bestow mNiO with luminescence imaging features. The mNiO-Tb serves as a MRI contrast agent, a luminescence imaging probe and a vehicle for ART. Synergistic PTT and radical-induced therapy of cervical tumors was achieved using this ART-loaded mNiO nanoplatform.[81] Nonetheless, the selective damage mechanism of ART to cancer cells remains elusive, and the toxicity of ART derivatives to normal cells needs to be explored.

Perfluorocarbon (PFC) is a chemically inert molecule with high oxygen-carrying capacity and good biocompatibility for *in vivo* application.[47] Owing to the intrinsic hydrophobic nature

of the PFC compounds, their clinical application usually involves encapsulation by a carrier matrix. Porous hollow magnetic $Fe_3O_4$ NPs (PHMNPs) have a large central cavity for the loading of small molecules and/or the therapeutic cargo, while retaining favorable biological properties of conventional iron oxide NPs (intrinsically super-paramagnetic, as a contrast agent for MRI). In view of this, PFC and etoposide (EP) were loaded onto PHMNPs. Oxygen was released at a moderate rate from the PHMNPs over an extended period of time, effectively reducing the hypoxia-induced EP resistance of liver tumor cells and facilitating concurrent chemotherapy. Modification of the surface of PHMNPs with lactobionic acid (LA)-containing amphiphilic polymers (LA-PEG-S-S-C18PMH), through hydrophobic interaction, facilitates selective targeting of LA against the asialoglycoprotein receptor present on the plasma membrane of hepatocytes.[47] Besides, the intracellular agglomeration of the nanocarriers after GSH-triggered removal of the hydrophilic LA-PEG segment could significantly enhance intracellular accumulation and improve therapeutic efficacy.[47]

In addition, the upconversion NPs (UCNP)-based theranostic micelles have been proposed for dual-modality imaging and PDT in HCC [see Figure 2b (i)].[82] Loading of mitoxantrone (MX) and anti-epithelial cell adhesion molecule (anti-EpCAM) onto PEGylated UCNP micelles has improved the biocompatibility and synergistic antitumor efficiency of the system, without any noticeable systemic toxicity.[82] Like other commonly used UCNP-based therapeutic approach, the as-synthesized 23.4 nm UCNPs are difficult to fabricate in ultra-small (< 15 nm diameter) sizes. The quantum yield of these UCNPs was not reported. Besides, since water has an absorption peak around 980 nm, laser excitation at 980 nm will result in unnecessary tissue heating during PDT. It is of interest to develop UCNPs which can be excited by other NIR wavelengths and allow deeper tissue penetration. Lastly, overall understanding of nanotoxicology of UCNPs (NPs distribution, excretion, metabolism, pharmacokinetics *etc.*) in animal models is of utmost importance.[83]

Quantum dots (QDs) is a luminescent inorganic nanomaterial with rich surface chemistry and optical properties. The application of QDs in biomedical field has been challenged by its non-specific internalization and toxicity.[84] Shi *et al.* (2018)[84] covalently coupled folic acid (FA) and 5-fluorouracil acetic acid (FUA) on the surface of QDs, to produce a HCC targeted therapy system, named FA-QDs-FUA. FA is responsible for the specific targeting of the system to the hepatocarcinoma cells; while QDs acts as the delivery vehicles and imaging agent. FUA which interferes with nucleic acid synthesis, has been chosen as the therapeutic agent. PEG has been selected as the linker chain to facilitate attachment of FUA to the QDs' surface and dramatically suppress the non-specific interaction of QDs. The optimal proportion of FA: PEG-QDs: FUA = 10: 1: 100 was used. Noteworthy, the content of FA in the system is controlled within 10 %, since excess FA may promote undesired tumor cell growth. The system was observed to exert reduced toxic side effects and better anti-tumor efficacy.[84] Nevertheless, the particle size of FA-QDs-FUA was about 220.28 nm, which is bigger than 160 nm, raising concerns about the cellular uptake and accumulation of the FA-QDs-FUA at tumor sites. Another similar work has been reported by Ma *et al.* (2018).[85] The group coupled second near-infrared window fluorescent (NIR-II) $Ag_2Se$ QDs with gadopentetate dimeglumine injection (Gd-DTPA) for dual-modality: $T_1$-weighted MRI and fluorescence imaging. The excellent temporal resolution and high tissue penetration depth were achieved by fluorescence imaging, further supporting the potential of QDs as multifunctional contrast agents for multimodal imaging in clinical diagnosis.[85]

Magnetic metal oxide nanomaterials (MMONPs) are negative contrast agents for $T_2$-weighted MRI. In response to intratumoral oxidability and acidity, MMONPs degrade and release corresponding metal ions that can serve as highly efficient positive $T_1$-weighted contrast agent. The ratio of increase of $T_1$ signals against decrease of $T_2$ signals ($T_1$/ $T_2$) from MMONPs, is known as ratiometric MRI, which is highly selective for solid tumor imaging.[45]

Cobalt oxide nanoprism ($Co_3O_4$), a type of MMONPs, has been selected and tuned for selective ratiometric MRI tumor imaging and synergistic cancer theranostics (PTT, chemodynamic and chemotherapy). The as-prepared $Co_3O_4$ nanoprism is cuboidal, with a thickness of 3.26 nm and a length of 33.29 nm, instead of triangular structure. This could be due to the presence of high concentration of surfactant used during the synthesis which subsequently inhibited nanomaterial growth in specific spatial directions.[45] It is interesting to note that although the sharp vertices of the triangular nanoprism may lead to stronger near-field enhancements for plasmonic applications, unfortunately, its high surface energy vertices most likely will make the nanoprism highly unstable and readily degradable.[86] Nevertheless, the $Co_3O_4$ nanoprism possess significant photothermal conversion efficiency ($\eta$= 60.07 %), outstanding MRI contrast ($r_2$= 5.42 $mM^{-1}s^{-1}$) and good DOX delivery (29.36 mg/g), with a low detection limit (50 nM) and broad linear range (0-50 μM).[45] In turn, the cuboidal structure and fast degradation property of the as-prepared $Co_3O_4$ nanoprism could contribute to enhanced drug delivery and controllable drug release.

Radiotherapy is another major modality of cancer therapy. However, radio-resistance, one of the intrinsic features of solid tumors, often gives rise to unsatisfactory therapeutic outcome and subsequent tumor relapse.[13,43] Du *et al.* (2017)[87] constructed a multifunctional theranostic agent, with a mean diameter of 15 nm, integrating radiation therapy with high-depth PTT. Functionalization of amphiphilic D-α-tocopherol PEG 1000 succinate (TPGS-$Cu_3BiS_3$) with bimetallic chalcogenide nanocrystals (NCs) increased the deposition of X-ray irradiation energy within cancer cells and triggered radiation damage *in vivo.* Moreover, conversion of NIR light (1064 nm) into heat greatly improved tumor oxygenation *via* increasing the blood flow, overcoming the hypoxia-associated radio-resistance of the tumor. The presence of copper ions is capable of catalyzing the conversion of endogenic $H_2O_2$ into highly reactive hydroxyl radicals and increase the level of oxygen radicals, hence further destroy the cancer

cells. The as-synthesized NCs also have strong absorption in the second NIR window (1000-1400 nm), allowing a deeper tissue penetration ability, with low scattering and energy absorption by tissues, than in the first NIR window (650-950 nm).[87] High atomic number NPs such as platinum, gold and bismuth are high electron emitters. These elements can act as radiosensitizers and amplify the effects of radiation.[88] Bismuth heteropolytungstate ($BiP_5W_{30}$) nanoclusters have also been explored as radiosensitizers for radiotherapy enhancement.[43] Owing to the electron structure and multi-electron property, $BiP_5W_{30}$ nanoclusters deplete GSH *via* redox reaction, catalyze the decomposition of $H_2O_2$ to HO• (about 1.3-fold) to enhance ROS generation upon x-ray radiation. The coupling of $BiP_5W_{30}$ nanoclusters with reduced graphene oxide (rGO) formed a heterostructure that not only promotes electron-hole separation to improve radio-catalytic activity (about 4-fold) but also improves the oxygen level within tumors since rGO can promote mild photothermal effect.[43]

Overall, inorganic nanomaterials serve as a platform for biomedicine, yet the often-neglected characterization and fairly weak fundamental understanding of its structure-function correlations often limits its predictive capabilities in nanotheranostics.

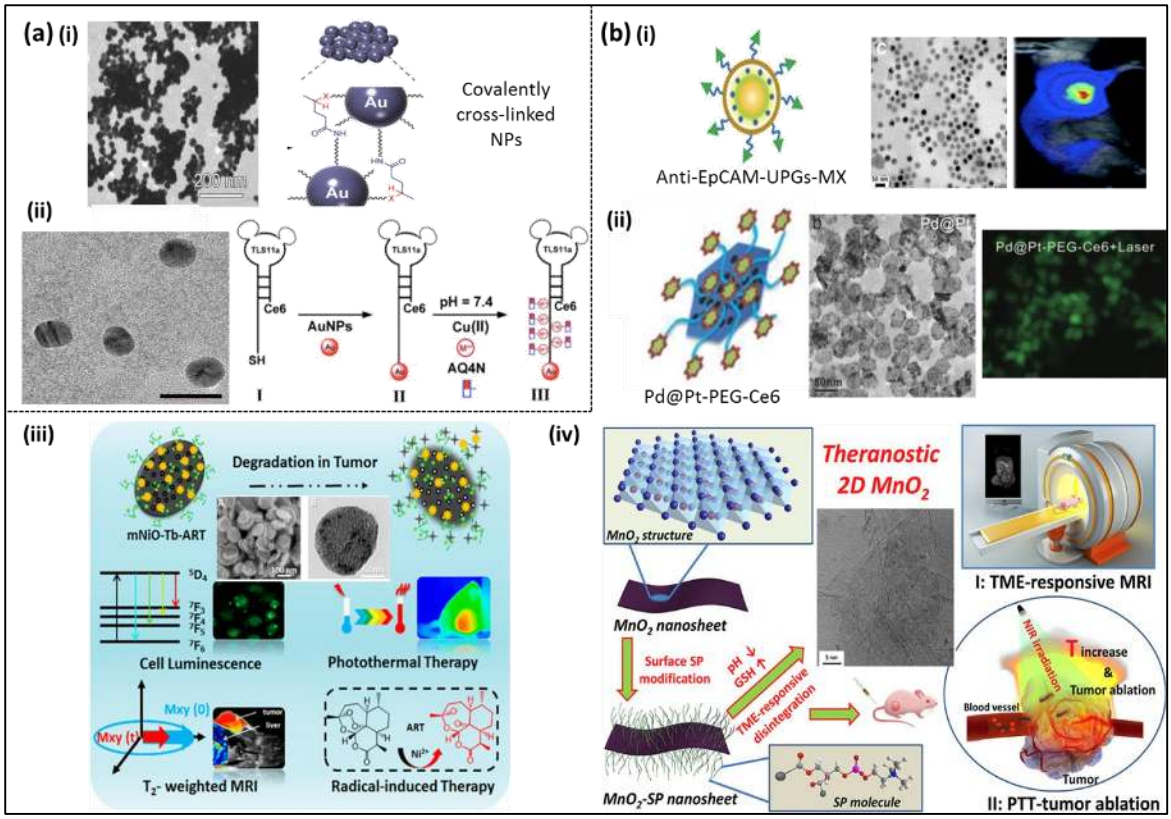


**Figure 2 Brief overview of nanomaterials used for solid tumor theranostics, with their respective TEM images. (a) Gold nanoclusters (i) The photocross-linkable Au nanoparticles for photothermal therapy and photoacoustic imaging of tumors *in vivo.* Adapted with permission from ref [42]. Copyright 2019 Ivyspring International Publisher. (ii) Preparation of the smart Cu (II)-aptamer complexes based gold nanoplatform for synergistic PDT/PTT/chemotherapy of hepatocellular carcinoma. Adapted with permission from ref [41]. Copyright 2017 Ivyspring International Publisher. (b) Inorganic nanomaterials (i) The structure of PEGylated upconversion-based micelles which permits dual-modality magnetic resonance/upconversion luminescence-guided synergistic chemotherapy and photodynamic therapy in hepatocellular carcinoma. Adapted with permission from ref [82]. Copyright 2018 Royal Society of Chemistry. (ii) A photosensitizer-Pd@Pt nanosystem (Pd@Pt-PEG-Ce6) in enhancement of tumor-specific photodynamic therapy. Adapted with permission from ref [44]. Copyright 2018 John Wiley and Sons. (iii) The artemisinin-loaded mesoporous nanoplatform for**

**synergistic photothermal and radical-induced tumor theranostics. Adapted with permission from ref [81]. Copyright 2018 American Chemical Society. (iv) Overview of 2D ultrathin $MnO_2$ nanosheets in magnetic resonance imaging and ultrasensitive stimuli-responsive photothermal therapy. Adapted with permission from ref [80]. Copyright 2018 Elsevier.**

**Polymeric nanoparticles**

Polymeric NPs is a collective term given for any type of polymer NPs, but specifically for nanospheres and nanocapsules built from synthetic polymers (*e.g*. poly(organophosphazene) (POP), poly(ethylene glycol) (PEG), *etc*.) or natural polymers (*e.g*. chitosan, gelatin, *etc*.).[10] The highly electron-delocalized structures, excellent light-harvesting and light amplifying properties, versatile surface modification, excellent photostability and biocompatibility of polymeric NPs contribute to their rapid advancements in solid tumor theranostics. Besides, with the size range between 10-1000 nm, polymeric NPs have proven to be viable carriers of therapeutic agents.

Encapsulation of methotrexate (MTX), a chemotherapeutic agent, in polymeric NPs is crucial in controlling its toxicity and side effects.[89] Two different block copolymers (poly(ethylene glycol)-*b*-poly(glutamic acid)-*b*-poly(ethylene glycol) (GEG) and poly(ethylene glycol)-*b*-poly(glutamic acid) (EG) conjugated with FA have been designed and used to encapsulate MTX. Both NPs, named M-GEG and M-EGFA NPs, are employed for passive and active targeting of cervical carcinoma, respectively [see Figure 3a (ii)].[89] FA has been used as a homing device to actively target and direct M-EGFA NPs towards the tumor, facilitating targeted drug release at the tumor site. On the other hand, M-GEG NPs passively target and accumulate at the cancer cells, by exploiting the EPR effect. Subsequently, M-GEG NPs release MTX inside the cytoplasm at a controlled rate to induce cell apoptosis. This mechanism of M-GEG NPs allowed long-term cytotoxicity action on the tumor cells while

minimizing side effect to healthy tissues.[89] The entrapment efficiency for both polymeric NPs was found to be about 93-96 %, with drug-loading content of about 38-47 %. Both polymeric NPs have improved the systemic circulation and intracellular delivery of MTX. The potential of these polymeric NPs as alternative to conventional chemotherapy for human cervical carcinoma are supported by their complete biological evaluation in terms of cytotoxicity, intracellular drug uptake and release, as well as induction of apoptosis.[89] Future research can be expected on fabrication of stimuli-responsive block copolymers, for specific targeting and precise control of the drug-release and versatility in clinical applications.

On the other hand, poly(ethylene glycol)-*b*-poly(ε-caprolactone) (PEG-PCL) is a biodegradable and biocompatible block polymer.[90] PEGylation delays renal filtration, prolongs plasma circulation and reduces non-specific uptake of nanomaterials by macrophages.[18,19,91] Encapsulation of silicon naphthalocyanine (SiNc), a photostable fluorescence molecule, within the hydrophobic core of the PEG-PCL NPs serves as a real-time activatable theranostic nanoplatform [see Figure 3a (i)].[90] The as-synthesized nanoprobe is predominantly fluorescent at tumor/cancer site (quantum yield at about 11.8 %). This is mainly because the poor water soluble SiNc (<1 ng/mL) in the PEG-PCL NPs tend to aggregate in aqueous environment and lead to fluorescence self-quenching. However, once SiNc infiltrated into the core of the solid tumor, the complex acidic intracellular environment (pH 6.5-6.8) and the interior of the endosome/lysosome (pH 4.5-6.5) will disrupt the structural integrity, trigger the leaching of SiNc from the nanoprobe, leading to NIR fluorescence recovery.[90] The nanoprobe reveals high cancer-to-normal tissue contrast ratio (about 1.6-1.9-fold) specifically at the tumor sites, and with none or minimal fluorescence signal in healthy organs.[90] This highly sensitive fluorescence switching nanoplatform successfully broaden the imaging and treatment window, making it highly promising for further clinical studies. The group also validated that heat can be efficiently generated by the

nanoprobe up to 12 mm deep within tumors from the point of NIR light (1.3 W/cm$^2$) for PTT, which is beneficial for nanotheranostics of ovarian cancer which usually started in one or both ovaries or fallopian tubes located in the female pelvis. Moreover, the chemistry involved in the SiNc-mediated combinatorial phototherapy can be easily tailored *via* photo irradiation dosage.[90] On the other hand, self-assembly of PEG-PCL with folate-PEG-cholesterol micelles forms a spherical and self-luminescing nanosystem (called POCL nanoreactor) with a diameter of about 50 nm.[92] POCL encapsulates bis[3,4,6-trichloro-2-(pentyloxycarbonyl) phenyl]oxalate (CPPO, a chemical power source with high reactivity to $H_2O_2$), poly[(9,9'-dioctyl-2,7-divinylene-fluorenylene)-alt-2-methoxy-5-(2-ethyl-hexyloxy)-1,4-phenylene] (PFPV, a chemiluminescence converter), and tetraphenylporphyrin (TPP, a photosensitizer with NIR emission and singlet oxygen. The folate ligand on the POCL surface allows specific targeting at the tumor site. Upon trigger by the high level of $H_2O_2$ at the tumor site ($10^{-6}$ M, normal condition = $10^{-7}$ M), POCL can be used for chemiluminescence imaging and PDT *via* a series of intraparticle relayed resonance energy transfer. The tumor cells are converted to a "light on" state and subsequently destroyed by the generated singlet oxygen. With such an excellent NIR light emission and singlet oxygen generation abilities, POCL showed a high image contrast in fluorescence imaging with a high antitumor effect and low systemic toxicity.[92]

Ursolic acid (UA), a pentacyclic triterpenoid extracted from *Hedyotis diffusa* Willd, has shown great potential in cancer therapy but their efficacy is extremely hindered by limited water solubility and poor pharmacokinetics *in vivo*. Yan *et al.* (2018)[93] has employed cationic nanomicelles derived from pluronic F127 as a delivery vehicle of UA for colorectal cancer treatment. Pluronic F127 is a widely-used biocompatible polymeric drug delivery vehicle, comprising of polyethylene oxide–poly-propylene oxide–polyethylene oxide (PEO–PPO–PEO) chains. The PPO segment of pluronic F127 allows incorporation of lipophilic drugs

while hydrophilic segment of F127 prevents adsorption and aggregation with other bio-macromolecules. Since the positively charged NPs have stronger affinity with negatively charged cell membranes, therefore, cationic polymer of stearoyl chloride grafted polyethylenimine copolymer ($C_{18}$-PEI) was functionalized to increase UA uptake by colorectal cancer cells.[93] This UA loaded cationic nanomicelles, termed as FUP, was fabricated through simple self-assembly of UA, F127 and $C_{18}$-PEI in ethyl alcohol. FUP can effectively block colorectal cancer cell proliferation by interfering cell cycle arrest at the G1 checkpoint and induce cell apoptosis mechanism.[93] Nonetheless, further studies on the degradation behavior and clearance of NPs after performing therapy are necessary. Photoacoustic imaging (PAI) is a biomedical imaging modality combining the high contrast of optical imaging with the high spatial resolution of ultrasound imaging.[5,42,45,72] PAI can also be defined as the non-radiative conversion of light energy into sound energy.[17] Based on the use of non-ionizing laser pulses, PAI non-invasively visualizes anatomical structures with greater penetration depth (several cms) and specificity than conventional optical imaging, suitable for imaging superficial tumors at breast and skin.[94] On the other hand, high intensity focused ultrasound (HIFU) is a minimally invasive therapeutic modality. HIFU concentrates multiple intersecting beams of ultrasound into the targeted tumor region. Subsequently, it generates hyperthermia and mechanical effects to destroy the affected areas.[95] A multifunctional poly(lactic-*co*-glycolic acid) (PLGA) nanocapsule, termed $Cu_{2-x}S$/PFBO@PLGA or in short CPPNs, encapsulating PAI contrast copper sulfide nanodots ($Cu_{2-x}S$ NDs) and a typical HIFU synergistic liquid, perfluorooctyl bromide (PFOB) has been constructed using emulsion solvent evaporation strategy.[95] The high performance of $Cu_{2-x}S$ NDs in the absorption and conversion of NIR confers high PAI contrast capability to the CPPNs, by which the location of the CPPNs within a tumor can be monitored successfully under PAI. Shifting absorption from the first to the second NIR-window could enhance PAI

contrast in imaging of deep lying living structures *in vivo*.[17] Due to the encapsulated PFOB, the cavitation effect in CPPNs is improved, thus enhances the ablation efficacy under HIFU exposure. With a particle size of 123.7 nm, CPPNs show its potential as a theranostic agent for future photoacoustic image-guided HIFU synergistic therapy of breast cancer.[95] However, high level of ultrasound energy (usually more than 100 W/cm$^2$) may cause damages to healthy tissues, especially along the path of ultrasound propagation, hence leading to severe side effects.[96]

Aggregation-induced emission (AIE) is a concept originated from the phenomena that a class of fluorogens are non-emissive as free molecules but luminescent as aggregates.[57,97] AIE-based bioprobes are suitable to use in real-time imaging probes, credit to their low background, high sensitivity and resistance to photobleaching. A smart nano delivery system, named STD nano-micelle (STD-NM), with ST and TD peptide functionalization and AIE "switch on" characteristics has been presented for precise theranostics and apoptosis monitoring of colon cancer.[97] Comprising of pH-triggered targeting peptide STP (sequence: SKDEEWHKNNFPLSPG), a caspase-3 responsive peptide linker (sequence: DEVD) and an AIE molecule tetraphenylethylene (TPE), ST could recover the fluorescence of the nanocarrier during apoptosis. Meanwhile, TD, a tumor acidity-activated peptide made up of the cell-penetrating peptides TAT and 2,3-dimethylmaleic anhydride, maintained the "stealth" stability of the nanocarrier in the physiological environment.[97] Upon exposure to tumor microenvironment, STP and TAT were switchably stimulated and activate the peptides to penetrate through the colon cancer cells and subsequently release the anticancer drugs (*cis*-platinum and DOX) into the tumors. The AIE signal will then be "switched on". Gene analysis by RNA-seq has also been performed, supporting the superior therapeutic effect of anticancer drugs-loaded STD-NM treatment. [97]

Generally, poor spatial resolution, shallow tissue penetration and relatively low quantum yield of NIR-emissive polymeric NPs than other common fluorescent imaging probes are some of the concerns for polymeric NPs in theranostics. The interaction between light-induced charge transfer of polymeric NPs with other biological activities requires further detailed study.

**Lipid nanoparticles**

Solid lipid NPs are made up of rigid core of hydrophobic lipids surrounded by a monolayer of phospholipids. This structure improves their biocompatibility and stability in biological environment, making them suitable as a carrier system.[98]

A multifunctional hypoxia-responsive theranostic liposome co-encapsulating a photosensitizer Ce6, hypoxia-activated prodrug tirapazamine (TPZ) and gene probe miRNA-155 was designed for synergistic PDT-chemotherapy of breast cancer.[99] The liposome was fabricated using an innovative hypoxia-responsive 2-nitroimidazole derivative conjugated PEG amphoteric polymer. The gene probe is a molecular beacon probe with the loop sequence complementary to the target miRNA-155. In absence of target, the fluorescence of the gene probe is switched off; upon hybridization with the target, the fluorescence is switched on, and effectively used for detection and diagnosis of intracellular oncogenic miRNA biomarker in breast cancer.[99] Subsequent laser irradiation (670 nm, 0.48 W/cm$^2$, 10 min) induced Ce6-mediated PDT by consuming oxygen to generate intracellular ROS, such as singlet oxygen, which causes severe hypoxia. The PDT-induced hypoxia led to the disassembly of the liposome, intracellular TPZ leakage to cell nucleus and induce DNA damage and cell apoptosis.[99] A detailed nanotoxicology study of the as-produced liposome system is imperative for possible clinical application as TPZ is currently under Phase III clinical trial.

An ultrasound molecular probe based on lipid NPs has been introduced for precision theranostics at an early stage of HCC [see Figure 3b (i)].[100] As common lipid NPs lack of specific targeting ability, hyaluronic acid (HA) has been chosen as a ligand to actively target the overexpressed CD44 cell adhesion factor on HCC. Cysteine-flanked cell-penetrating peptide (CPP), CG-TAT-GC, has been selected to improve the delivery of macromolecular substances into the nucleus without causing cytotoxicity.[100] The as-synthesized lipid NPs is known as HA-mediated cell penetrating peptide-modified with 10-hydroxycamptothecin-loaded on a phase-transformation lipid NPs (HA/CPPs-10-HCPT-NPs). Upon trigger by low-intensity focused ultrasound (LIFU) sonication, the NPs in tumor tissue and cells undergo acoustic droplet vaporization (ADV) and are transformed into microbubbles.[100] The resultant microbubbles not only able to provide significant contrast enhancement in tumor-site imaging, but also increase permeability of NPs into tumor blood vessels and cell membrane.[96] Since the acoustic intensity of LIFU sonication is usually low, no more than 3.2 W/cm$^2$, it is less likely to cause tissue necrosis as compared to HIFU.[96] This fascinating mechanism successfully induces local release of antitumor drug in the cytoplasm and nucleus.[100] However, there are some concerns with this approach. Although the ligand-mediated active targeting has been used to improve the targeting efficiency, it is important to fully understand and avoid the adverse side-effects due to off-target distribution of the CPP and its cargo which might induce mutations, cytotoxicity or initiate immune responses in the host. Secondly, the pharmacokinetics, stability and circulation time of the system in bloodstream should also be further investigated. In addition, since the effect of ultrasound is highly localized, their applicability in tumor metastasis is highly compromised.

On the other hand, abnormal levels of $H_2O_2$ (about 50-100 μM) often correlate with physiological and pathological conditions like inflammation and cancers. Generally, the concentration of $H_2O_2$ in physiological environments should be below 50 μM.[101] Liposomal

nanoprobe loaded with horseradish peroxidase (HRP) and its substrate, 2,2-azino-bis(3-ethylbenzothiazoline-6-sulfonic acid) (ABTS), has been presented for *in vivo* detection of inflammation, photoacoustic detection and imaging of $H_2O_2$ (down to sub/micro molar concentrations) [see Figure 3b (ii)].[101] In the presence of endogenous $H_2O_2$, HRP loaded in liposomes would catalyze ABTS (colorless) into its oxidized form (greenish) and show strong NIR absorbance (700-900 nm), allowing sensitive PAI of early stage tumors (as small as 2 mm in size). Meanwhile, based on the difference in $H_2O_2$ contents, the nanoprobe also allows diagnosis and imaging of LPS- (a lipoglycan that triggers inflammation) and bacteria-induced inflammation, orthotopic brain tumors, breast tumors and metastatic tumors. Besides, this spherical shape liposomal NPs with an average diameter of about 100 nm concurrently achieve selective PTT of tumors with high efficacy and minimal non-specific heating damage to surrounding normal tissues.[101] However, the loading capacity of ABTS and HRP were found to be limited at about 23.17 and 5 %, respectively. This could be due to premature release of the drug from the lipid matrix as changes in temperature during administration may cause polymorphic transitions of the lipid matrix.[10] The depth-dependent light attenuation and interference of unwanted background signals remain challenges for the clinical application of PAI.

Superparamagnetic iron oxide nanoparticles-loaded solid lipid (SPIONs) is made from iron, one of the most abundant metals present in metabolism. SPIONs have big potential as theranostic agent as they display interesting cellular and *in vivo* interactions with no dramatic toxicity.[69,102,103] A smart nanovehicle with DOX and SPIONs delivery system, in short DOX/SPIONs-loaded DFSLNs, has been constructed for oral chemo/magnetothermal combination therapy of colon cancer.[98] Despite the system combined both DOX chemotherapy and hyperthermia therapy (generated from SPIONs) with high frequency magnetic field (HFMF), its therapeutic efficacy is still limited by the systemic drug

absorption into blood circulation. Thereby, the group innovatively coated folate (FA) and dextran on the surface of the NPs in a sequential layer-by-layer manner.[98] Although the fabrication of SPIONs can be relatively easy and reproducible, biocompatible polymer layer, such as PEG and polyvinyl alcohol (PVA), is normally coated on the SPIONs surface to improve their biocompatibility and stealthiness for specific targeting. This is because naked SPIONs tend to sediment and aggregate at physiological conditions, resulting in an increased risk of toxicity.[69] Coating of the polysaccharide dextran shell layer on the NPs surface not only evaded the cellular transport and systemic absorption by at least 2 folds, but also enhanced the particle accumulation at the tumor sites by specific association with dextranase present only in colon. The subsequent enzymatic degradation and removal of dextran coating led to the exposure of the FA residues that further facilitate cellular level targeting and uptake of the system by receptor-mediated endocytosis. The preliminary results demonstrated prominent therapeutic efficacy (a 15-fold decrease in tumor mass of mice than the PBS control) of DOX/SPIONs-loaded DFSLNs for the oral administration, with no apparent systemic side effects or toxicity.[98] The particle size of DOX/SPIONs-loaded DFSLNs is approximately 132 nm. In fact, the optimal size of the nanomaterials designed for colorectal cancer should be between 10-100 nm in order to avoid triggering of immune response and clearance by glomerular filtration in the kidneys.[104] The spherical shape of the nanomaterials would encourage longer circulation time in blood and faster uptake by colorectal cancer cells.[105]

In short, the potential side effects arising from the off-target distribution of the molecular or drug-loaded lipid NPs require more studies for validation on the effectiveness of the delivery system. The pharmacokinetics, stability and circulation time of the nanomedicine in the bloodstream should also be further investigated.

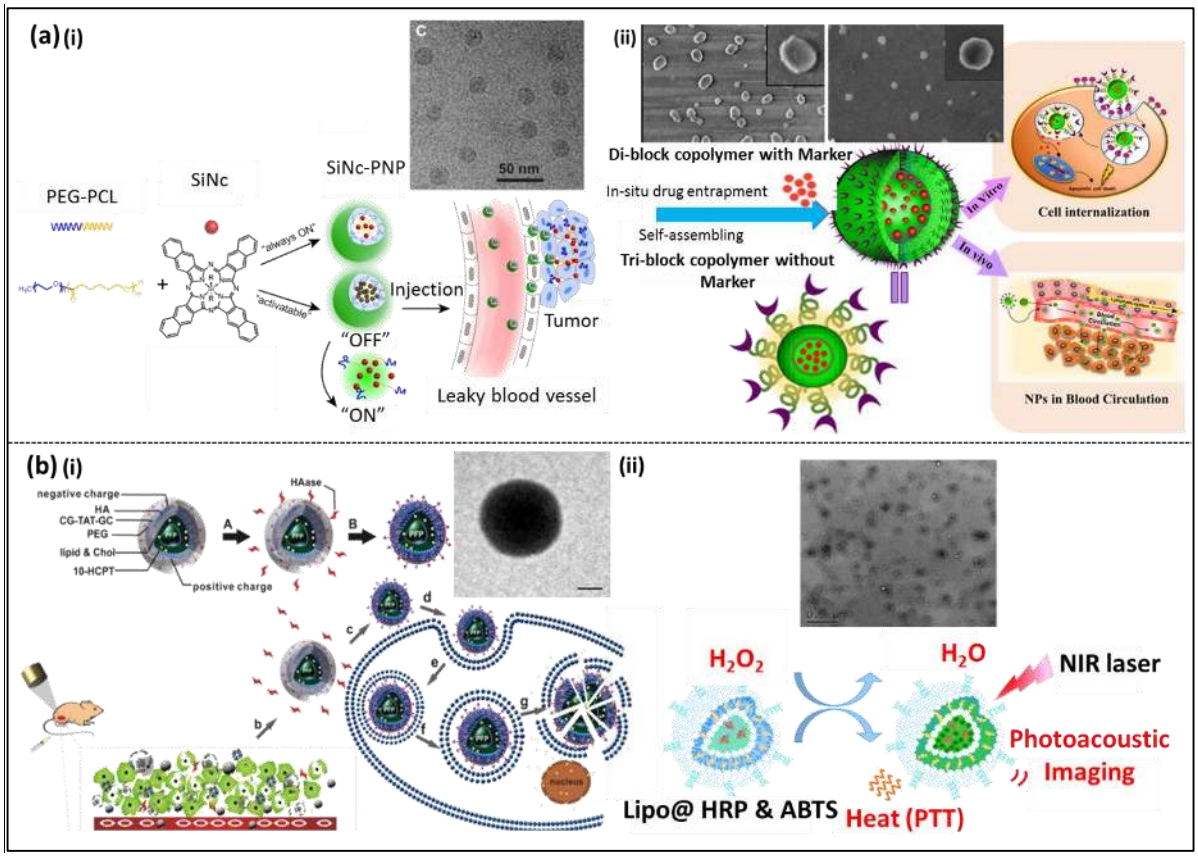


**Figure 3 Brief overview of nanomaterials used for solid tumor theranostics, with their respective TEM images. (a) Polymeric nanoparticles (i) Illustration of a tumor-activatable silicon naphthalocyanine (SiNc) encapsulated in a copolymer, PEG-PCL nanoparticles, that permits NIR fluorescence-guided surgery and combinatorial phototherapy of ovarian cancer tumors. Adapted with permission from ref [90]. Copyright 2018 Ivyspring International Publisher. (ii) Overview of block copolymer (PEG and PGA) based nanoparticles in passive and active theranostic intervention of cervical cancer. Adapted with permission from ref [89]. Copyright 2017 American Chemical Society. (b) Lipid nanoparticles (i) A multifunctional ultrasound molecular probe (cell-penetrating peptide-modified targeted drug-loaded phase-transformation lipid nanoparticles) with low-intensity focused ultrasound in hepatocellular carcinoma. Adapted with permission from ref [100]. Copyright 2018 Ivyspring International Publisher. (ii) A $H_2O_2$-responsive liposomal nanoprobe capable for photoacoustic**

**inflammation imaging and photothermal therapy of early-stage of small tumors and metastatic lymph nodes. Adapted with permission from ref [101]. Copyright 2017 PNAS.**

## Graphene

Graphene and its derivatives have become the spotlight of nanotheranostics since the last decade, owing to their electrically tunable surface chemistry and mechanical robustness.[102,106–108] The $sp^2$-hybridised carbon atoms in a honeycomb network provide graphene with a large surface area, enabling the compounds to adsorb/functionalize on both sides of its planar surface. Moreover, the large molecular weight of graphene oxide (GO) enhances the imaging contrast,[109] while its electrical properties allow long-range fluorescence resonance energy transfer (FRET).[110] GO presented low uptake in the RES and long blood circulation time at 1 mg/kg body weight within days.[111]

Melanoma is a form of skin cancer caused by excessive exposure to the sun's ultraviolet radiation.[112,113] A work using only GO (without the co-presence of any photosensitizers) to sensitize the formation of singlet oxygen for dual nanomaterial-mediated PDT and PTT of solid melanoma tumors was reported in 2016.[114] The group proved that the nano-sized graphene is suitable for *in vivo* fluorescence imaging operated using inexpensive laser setups. GO is able to absorb NIR light that subsequently induces the generation of singlet oxygen and offers deeper tissue penetration depths.[114]

However, the relatively hydrophobic nature of graphene makes it difficult to be taken up by cells, which in turn minimize their therapeutic efficacy. Hwang *et al*. (2016)[110] has therefore suggested to graft a biopolymer of HA and a CD44 receptor-specific polysaccharide, onto the GO surface (see Figure 4a).[110] The as-synthesized 170 nm HA-GO conjugate improved stability and solubility of GO in ionic solutions, without any aggregation. With such an idea, the group has also successfully developed an interesting fluorescence-switchable theranostic platform that is able to sense oncogenic miR-21 using anti-sense miR-21 peptide nucleic acid

probes and show therapeutic effect on breast cancer simultaneously.[110] On the other hand, GO/gold nanorods (GO/GNR) theranostic nanohybrids have been synthesized *in situ* at room temperature for precise tumor computed tomography (CT) imaging and PTT of pancreatic cancer.[115] GO is chosen as the template for the synthesis of GNR due to the presence of many oxygen-containing functional groups which can improve solubility and biocompatibility of the system.[115] Meanwhile, the synthesis method is straightforward, environmental-friendly, highly adaptable for different types of synthesis of GO/NPs and most importantly does not form any aggregates. The GO/GNRs showed photothermal effect *in vitro*, with good optical morphological stability up to six cycles of 808 nm laser irradiation.[115]

Graphene quantum dot (GQD) is a zero-dimensional carbon material with excellent chemical stability, optical and electronic properties, biocompatible and allow easy surface modifications.[116,117] Besides, GQD can produce ROS with significantly high quantum yield (greater than 1.0) for PDT, due to their excellent electron donating and accepting capability.[118] GQD has the property of extremely high intrinsic mobility of charge carriers.[119] The work of loading IR780 iodide (IR780) onto FA-functionalized GQD *via* π-π stacking interactions has been reported recently.[119] The GQDs-FA contains a large and intact $sp^2$ domain with carboxyl groups around the edge which exhibits excellent water solubility and suitable for further conjugation (see Figure 4b).[119] IR780 is an effective theranostic agent for simultaneous NIR fluorescence imaging and PTT. Yet, its application is often hampered by its insolubility in different solvents due to the presence of the rigid chlorocyclohexenyl ring in the structure. Interestingly, the water solubility of IR780 (33.19 %) is increased by over 2400-fold when loaded onto the GQDs-FA system, with a high photothermal conversion efficiency (87.9 %). The photostability and tumor-targeting ability were greatly improved too. Most importantly, IR780/GQDs-FA, with a particle size of about 9 nm, is capable of producing sufficient hyperthermia to effectively kill cervical cancer cells and completely

eradicate tumors upon 808 nm laser irradiation.[119] For future studies, it would be advantageous if pH-responsive features could be incorporated into this system, so that the therapeutic mechanism will be initiated once exposed to acidic tumor microenvironment. Generally, the clinical translation of PDT is often challenged due to the low yield of ROS, poor tissue penetration depth of the photosensitizer and short lifetime of ROS.[57,120] A mitochondrial specific PDT, named UCNP-GQD/TRITC, has been presented with the use of rare-earth doped UCNPs mediated NIR-GQD.[120] UCNPs are a kind of inorganic nanomaterials capable of emitting efficient and sharp visible or UV light when excited at NIR. These features of UCNPs permit high penetration depth in biological tissues with high detection sensitivity.[121] Generation of singlet oxygen by the GQD becomes more prominent after UV light emission from UCNPs (see Figure 4c).[120] The high concentration of singlet oxygen observed in mitochondria is due to intrinsic advantages of GQD as well as the highly efficient energy transfer from UCNPs to GQD. Furthermore, surface modification of UCNP-GQD with mitochondrial-targeting fluorescent probe, tetramethylrhodamine-5-isothiocyanate (TRITC), allows the system to target mitochondria precisely and triggers breast cancer cells apoptosis irreversibly (with an inhibition ratio of more than 75 %).[120] However, toxicity from long-term exposure and high quantum yield of singlet oxygen, surface-dependent therapeutic responses, and biological corrosion resistance (a phenomenon in which metallic ions and particles are released in a complex aqueous environment through electrochemical processes)[122] of the GQD are some of the concerns raised regarding this strategy. Also, since GQD (with a 6 nm diameter) is attached on the surface of UCNPs *via* amide linkages, it is possible that the resultant UCNP-GQD/TRITC composites would cleave off easily when the system is dispersed in a solvent. Glycyrrhetinic acid (GA), a natural product from *Glycyrrhiza glabra*, is another mitochondrion targeting ligand.[123] A biocompatible GA-functionalized GO has been fabricated and used as a carrier for targeted delivery of DOX into

mitochondria. Both *in vitro* and *in vivo* studies revealed the activation of the mitochondria-mediated apoptosis pathway, suggesting GA-GO@DOX's potential for liver cancer treatment.[123]

Zhao *et al.* (2018)[111] has presented a chitosan/dimethymaleic-modified chitosan (CS/CS-DMMA)-functionalized GO NPs, also known as GON/CS/CS-DMMA. Chitosan (CS), a natural polysaccharide that commonly exists in the hard shells of marine crustaceans, has been actively explored to construct various CS-based nanomaterials because of its biocompatibility, biodegradability and structural variability.[124] This hybrid nanocarrier is pH-sensitive and has surface charge-reversible ability, which is due to self-assembly of deprotonated carboxyl of GO NPs and the protonated amine of CS *via* electrostatic interactions. A chemotherapeutic drug, DOX, was adsorbed onto the GO *via* π-π stacking interaction between the large π conjugated structures of GO and the aromatic structure of DOX. The outer CS-DMMA polyelectrolyte shell of the nanocarrier is negatively charged which prevented premature release of the co-loaded DOX, when circulating in the blood system. Upon reaching the slightly acidic microenvironment (pH 6.5) of liver cancer, the nanocarrier switches to positive charge, due to detachment of chitosan coating, which re-expose the amino groups of the positively charged CS. Consequently, GON/CS/CS-DMMA was capable of delivering DOX effectively at a controlled release rate.[111] In another study, reduction and functionalization of GO using dopamine formed reduced graphene oxide/polydopamine (RGO-PDA).[109] The formed PDA stabilizes the RGO against agglomeration and fouling effects. It also attenuates the *in vivo* toxicity of RGO and allows covalent surface modification with desired molecules. Conjugation of BSA (as a drug carrier, capturing agent for 4T1 breast cancer cells) onto the RGO-PDA system further permits a higher loading of MRI contrast agent diethylenetriaminepentaacetic acid (DTPA)-Mn(II) complex and anticancer drug (MTX). This multifunctional and biocompatible theranostic

hybrid system is electrochemically proved to allow higher sensitivity (by a factor of four) towards breast tumor.[109]

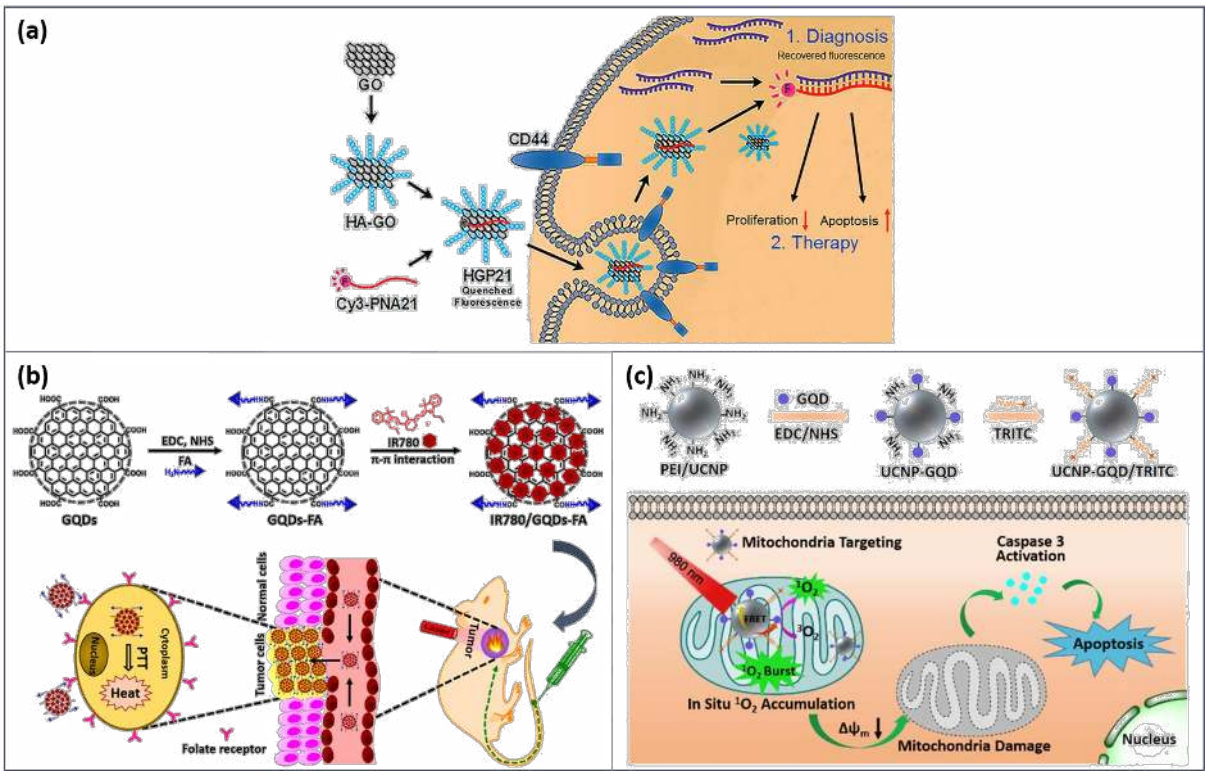


**Figure 4 Brief overview of graphene for nanotheranostics. (a) Illustration of hyaluronic acid-coated graphene oxide synthesis and its theranostic effect by targeting oncogenic miR-21. Reprinted with permission from ref [110]. Copyright 2017 Elsevier. (b) Schematic illustration of the IR780 iodide on folic acid-functionalized graphene quantum dots for targeted PTT. Reprinted with permission from ref [119]. Copyright 2017 American Chemical Society. (c) Overview of mitochondrial specific PTT by rare-earth nanoparticles mediated near-infrared graphene quantum dots. Reprinted with permission from ref [120]. Copyright 2018 Elsevier.**

### Liquid tumor

Although the nanotheranostic strategies are focused more on the diagnosis and therapy of solid tumors, a considerable increase in their application to liquid tumors has been noted in recent years. However, while it is true that liquid tumors are classified as leukemia,

lymphoma and myeloma, only the former two have generated interest in the scientific community.[37] The strategy to carry out nanotheranostics in tumors are selected according to several variables, the most important being the disposition and accessibility of the tumor by the nanomaterials. Liquid tumors are more accessible than solid tumors, since they are present throughout the bloodstream, whereas in solid tumors, the nanostructures must cross tissue barriers to detect and treat.[125] In this section, we will evaluate how and why the specific nanomaterials are selected to carry out nanotheranostic strategies in liquid tumors.

**Metal nanoparticles**

Metal NPs are presented as an interesting strategy for the detection and therapy of lymphoma and leukemia. Their ability to generate heat from the optical energy allows them to be nanoagents for PTT. However, its application for liquid tumor theranostics have not been fully studied and this is due to the fact that these types of circulating tumors are not located at a certain point and therefore may cause ablation of adjacent tissue.[126] In this context, 100 nm-sized iron oxide NPs (IONPs) functionalized with FA have been evaluated as promising platform for imaging followed by therapy of tumors related to the lymphatic system. Coating with FA does not require the use of linkers and therefore prevents the NPs from being oversized and enhances its accessibility to the lymph vessels. Moreover, FA provides stability to the NPs as it provides a negative surface charge, and this increases its retention in vessels. Finally, FA on the IONPs could specifically recognize the folate receptor that is overexpressed on the surface of cancer cells.[127] However, IONPs tend to aggregate when placed in biological suspensions and therefore its heating ability is reduced. In order to exceed this limitation, IONPs have been functionalized with a protective mesoporous silica shell, which gives high heating and relaxivity properties when applied *in vivo,* while keeping its size below 100 nm.[128] Moreover, it should be noted that unlike other metal NPs, these modified IONPs allow positive MRI contrast by displaying bright region and therefore allows

effective visualization of the tumor. However, although this nanoparticle has interesting properties, its effectiveness for magnetic hyperthermia therapy of circulating cancer has yet to be demonstrated. The nanomaterial that has proved to be an excellent nanotheranostic agent for *in vivo* leukemia treatment is Cu-Au alloy nanostructures, where the higher thermal conductivity of the copper allows excellent heating under laser irradiation once the tumor is visualized by NIR imaging. This nanoplatform was proven to target and destroy cancer cells in mice within five minutes (see Figure 5a).[129] Despite this, issues concerning renal clearance and lymphatic fenestration are hindering the current nanotheranostic strategies for liquid tumor treatment. In this context, it is essential to select nanomaterials with a size range from 20-50 nm, as they have proven to enhance *in vivo* tumor penetration and inhibition.[130]

**Lanthanide-doped nanoparticles**

The lanthanide oxyfluoride NPs appear as an alternative to lipid and polymeric based delivery systems, which have low retention and non-specific cellular uptake, respectively.[131] The excellent photoluminescence property of the lanthanide and the conjugation of the nanoparticle with anti CD33 antibody enable it to be an interesting nanotheranostic agent for myeloid leukemia. These NPs are conjugated with anti CD33 that allows retention and internalization in $CD33^+$ AML cells, which otherwise could not accumulate in the blood vessels and therefore making it effective for diagnosis and therapy. (see Figure 5b).[131] They have shown to be successful antitumor agents both *in vivo* and *ex vivo* by acting as a specific delivery vehicle of PMI peptide, which antagonizes the inhibitors of the tumor suppressor protein p53.

**Polymeric nanoparticles**

Polymeric NPs have been applied mostly for image-guided anticancer drug delivery. In this context, several types of polymeric NPs have been used depending on the diagnostic strategy to be followed. For the treatment of non-Hodgkin lymphoma, amphiphilic polymers

composed of hydrophobic fluorescent curcumin and hydrophilic PEG were designed as self-assembled anti-cancer drug nanovesicles [see Figure 5c (i)].[132] Limitations associated with the drug, such as low solubility and low bioavailability, was curtailed with PEG. The most attractive aspect of this nanomaterial is the ability of curcumin to act as both a strong fluorescent probe and an anti-cancer drug, avoiding the need of a fluorophore.[133] Furthermore, a multifunctional imaging theranostic approach based on core-shell chitosan-HA NPs has been applied in murine model of B-cell lymphoma.[134] Since they are initially conjugated with fluorophores and then loaded with paramagnetic tracers, the most suitable imaging agent can be chosen depending on the tumor type; fluorescent reflectance imaging for scanning of superficial structures such as sentinel lymph node and MRI for deep tissue visualization. Another advantage is that the HA has numerous active groups that are useful for specific targeting. In this context, these polymeric NPs were decorated with a specific mimotope (pA20-36) that exclusively recognize A20 lymphoma cells and induce cell apoptosis. Moreover, amphiphilic perylene diimide (PDI) derivatives were developed and further self-assembled into a series of PDI NPs with different sizes of 30, 60, 100, and 200 nm. They have been proven to perform activable PAI and effective PTT [see Figure 5c (ii)].[135]

**Lipid nanoparticles**

Lipid NPs have also been applied as carriers for lymphoma theranostics, but as an alternative to improve cell internalization and simultaneous drug delivery. Liposomes that contain SPIONs and functionalized with rituximab antibody has been developed as theranostic agent for central nervous system lymphoma (see Figure 5d).[136] Blood-brain barrier regulates the movement of molecules, ions and cells between the continuous non-fenestrated microvasculature and the central nervous system.[137] The restrictive nature of the blood-brain barrier pose challenges for targeted drug delivery to the central nervous system, and it is

usually associated with neurological diseases including neurodegenerative diseases.[138] In this case, free rituximab is not able to cross the blood-brain barrier, hence it requires a drug delivery system to perform effective therapy. The liposome is used as a rituximab vehicle, with sizes of less than 200 nm. Surface modification of liposome with a non-ionic surfactant allows penetration into the blood-brain barrier and therefore can develop its antitumor function. The liposome which also contains SPIONs allows *in vivo* MRI with both $T_1$ and $T_2$ modes. Nevertheless, the anti-lymphoma activities of the liposome have only been tested *in vitro* and therefore this strategy only remains as a promising tool for clinical translation.[136]

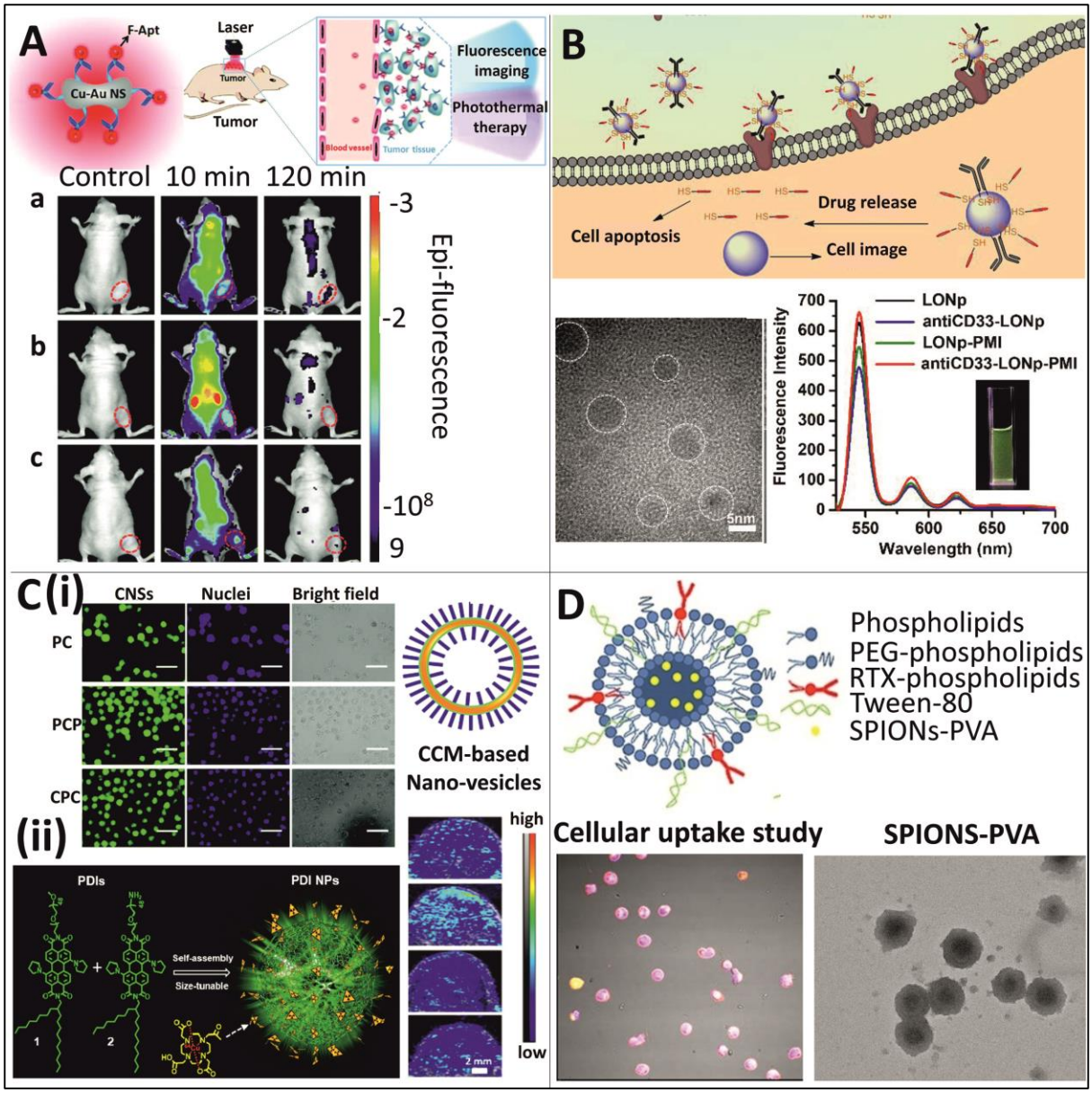


**Figure 5 Nanomaterials applied as theranostic agents for liquid tumor. (a) Metal nanoparticles. Cu–Au alloy nanostructures coated with aptamers for NIR imaging and photothermal therapy in *in vivo* leukemia cancer theranostics. Adapted with permission from ref [129]. Copyright 2016 Royal Society of Chemistry. (b) Lanthanide-doped nanoparticles. Lanthanide-doped nanoparticles conjugated with an anti-CD33 antibody and a p53-activating peptide for acute myeloid leukemia therapy. Adapted with permission from ref [131]. Copyright 2018 Elsevier. (c) Polymeric nanoparticles. (i) Curcumisome loading on nanovesicles for fluorescence imaging and drug delivery**

**strategy in leukemia theranostics. Adapted with permission from ref [132]. Copyright 2015 Royal Society of Chemistry. (ii) Application of perylene diimide nanoparticle on lymph node mapping and cancer photoacoustic imaging and photothermal therapy. Adapted with permission from ref [135]. Copyright 2017 American Chemical Society. (d) Lipid nanoparticles. Application of liposome-containing SPIONs conjugated with anti-CD20 antibody as a theranostic agent for central nervous system lymphoma. Adapted with permission from ref [136]. Copyright 2018 Elsevier.**

## NEURODEGENERATIVE DISEASES

Neurodegenerative diseases are a set of heterogeneous disorders that result in a progressive loss of certain neuronal systems and finally loss of cognitive abilities. Alzheimer's disease (AD), Parkinson's disease, amyotrophic lateral sclerosis and Huntington's disease are the prototypes of degenerative diseases.[139] Among them, AD is the most common neurodegenerative disorder, and this is the reason that most of the nanotheranostic strategies applied on brain diseases are focused on this specific disorder. While it is true that the causative mechanism of the disease is unknown, there are several hypotheses that consider the deregulation of metal levels in the brain is associated with multiple pathological factors of the disease, such as amyloid aggregation and oxidative stress. In this context, the nanotheranostic platforms are classified according to the therapeutic strategy to be performed, which is usually the amyloid-β aggregation inhibition and metal chelation.[140]

### Nanomaterials for amyloid-β aggregation inhibition

The application of nanotheranostics to AD is a clear example of how nanoplatform is designed according to the type of therapy to be performed. Unlike nanotheranostics for cancer disease, in which the therapy is usually tumor thermal ablation or specific drug delivery, for AD the therapy is usually based on the inhibition of the Aβ aggregation, since

these have a direct relationship with the disease's poor prognosis. In this context, three NIR dyes (DMA-SLOH, DBA-SLOH, and DPA-SLM) for *in vivo* imaging of Aβ species and inhibition of Aβ aggregation have been developed (see Figure 6a).[141] The advantage of using fluorescence imaging is that the use of high cost and low sensitivity MRI and positron emission tomography (PET) imaging (in which radioactive compounds and use of sophisticated instruments) are completely avoided. Moreover, the use of NIR fluorescence reduces the interference caused by native fluorescence biological compounds, which have wavelength emission peak below 550 nm. Furthermore, the NIR dyes are proven to have excellent blood-brain barrier permeability, good biostability and renal clearance ability.[141] However, since the strategies of nanotheranostics reported for inhibiting the aggregation of β-amyloids have shown to fail in clinical trials, a multifunctional nanocomposite has been developed for the specific targeting of Tau and its aggregation inhibition. Tau aggregation is an independent amyloid-β AD pathology that leads to mitochondrial dysfunction and consequently oxidative stress generation and cognitive deficit. The nanocomposite consists of a mesoporous silica nanoparticle that acts as a carrier of ceria and iron oxide nanocrystals, for antioxidant function and MRI probe, respectively (see Figure 6b).[142] The Tau aggregation inhibition is due to the loading of the carrier with methylene blue. This nanomaterial proved to be an effective *in vivo* theranostic agent due to its retention capability in the axon and its synergic therapeutic effect on AD. Despite this, in order to promote clinical translation of this nanoplatform, the nanocomposite must fulfill the Lipinski's rules, which determine its capability to cross the blood-brain barrier.[143]

**Nanomaterials for $Cu^{2+}$ chelation**

The process of Aβ aggregation is promoted by the increase in the concentration of trace metal ions, such as $Cu^{2+}$; therefore, determining its concentration in the brain is an essential tool for diagnosis of AD. In this context, fluorescence chelators, BTTA composed of a cyclen group

and a benzothiazole aniline group (BTA) has been developed, in which BTA allows specific fluorescence imaging of Aβ species and the cyclen group acts as an attenuator of the metal induced Aβ aggregation (see Figure 6c).[144] This nanotheranostic agent satisfies the restrictive terms of Lipinski's rules and has demonstrated its functionality *in vitro* and its ability to penetrate the blood-brain barrier *in vivo*. However, it should be noted that it requires structural modifications for longer fluorescence emissions or even NIR emission with acceptable penetration depth.[144] For this reason, UCNPs modified with complex 8-hydroxyquinoline-2-carboxylic acid (HQC) have been developed. The fluorescence emission of the UCNPs is quenched when $Cu^{2+}$ is detected, due to luminescence resonance energy transfer. As the $Cu^{2+}$ is captured by HQC, it inhibits the aggregation of Aβ and subsequently eliminates the toxic Aβ intermediates (see Figure 6d).[145] Although this nanomaterial was reported as a promising nanotheranostic agent in human brain, it is noteworthy that the *in vivo* experiment was performed on zebrafish, which has a transparent brain compared to a complex human brain. In order to determine the efficacy of this nanotheranostic agent for AD patients, further *in vivo* assays should be conducted.

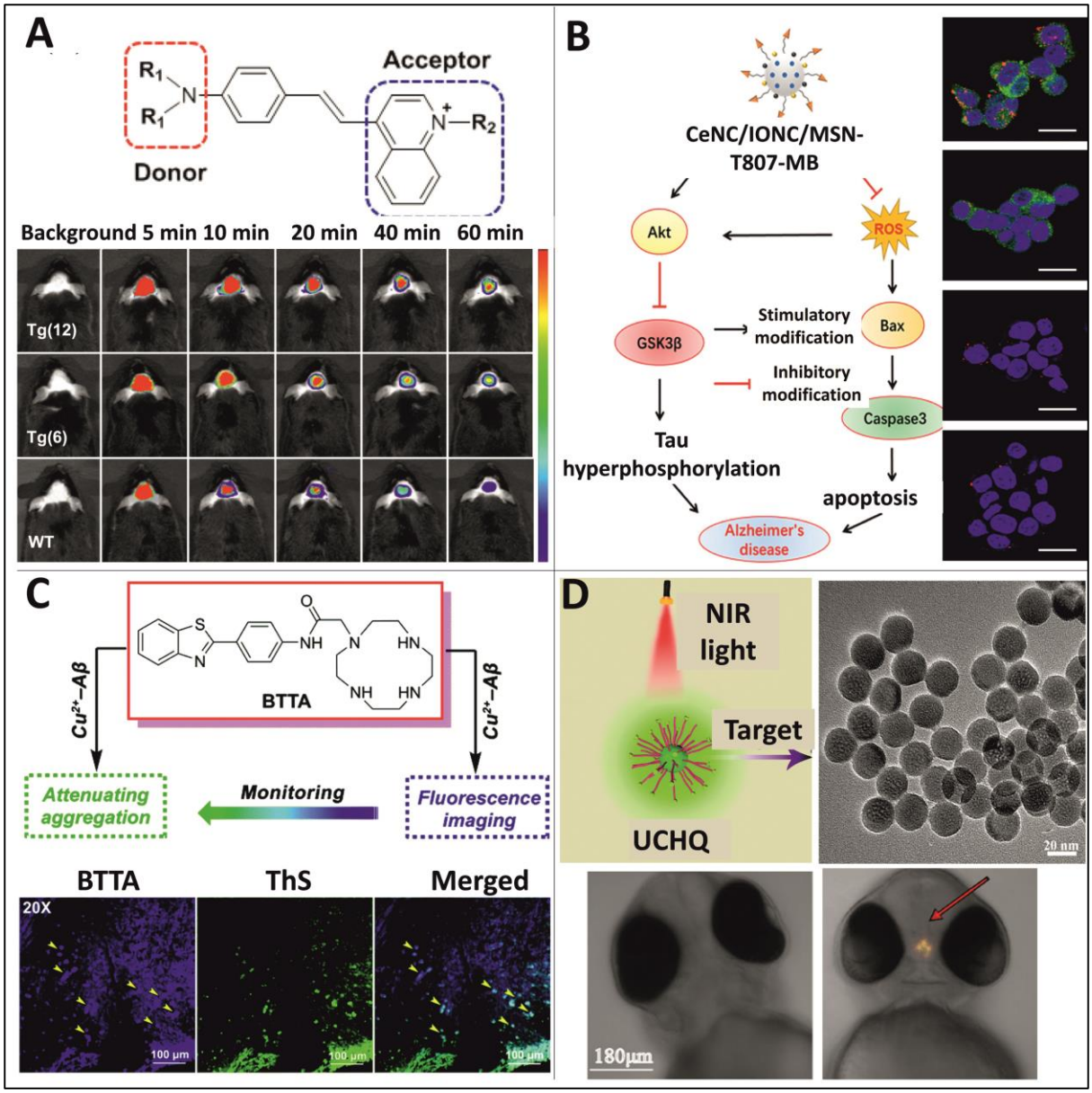


**Figure 6 Nanomaterials applied as theranostic agents for neurodegenerative diseases. (a) NIR dyes for *in vivo* imaging of Aβ species and Aβ aggregation inhibition. Adapted with permission from ref [141]. Copyright 2016 Elsevier. (b) ceria and iron oxide nanocrystals functionalized nanocomposite as a nanotheranostic agent for MRI and Tau aggregation inhibitor. Adapted with permission from ref [142]. Copyright 2018 American Chemical Society. (c) BTTA for fluorescence imaging and $Cu^{2+}$ chelators applied in Alzheimer's disease. Adapted with permission from ref [144]. Copyright 2016 Royal Society of Chemistry. (d) Upconversion nanoparticles for NIR Alzheimer's**

**disease detection and therapy based on $Cu^{2+}$ chelation. Adapted with permission from ref [145]. Copyright 2016 Elsevier.**

## AUTOIMMUNE DISEASES

The immune system in our body protects us from disease and infection. However, if a person has an autoimmune disease, the body's defense mechanism will launch an attack against specific cells, body tissues and organs of the host. Autoimmune diseases can affect many parts of the body and significantly affect the patient's well-being. Environmental, infectious and genetic factors are some possible factors initiating or exacerbating autoimmune diseases. There are more than 80 types of autoimmune diseases; with the classic symptom of inflammation. Current clinical treatment modalities are generally non-specific and focus on reduction of inflammation. Moreover, the use of anti-inflammatory drugs lack of desired specificity, has severe toxic effects and limited therapeutic benefits.[146]

NPs can be used as a drug delivery system to specifically target cells and tissues. Co-delivery of targeting and therapeutic agents using NPs can greatly improve pharmacokinetics and enhance bioavailability of therapeutics. NPs used for the treatment of autoimmune diseases can be classified as colloidal NPs (consist of a metal core stabilized by an organic/polymeric coating) and organic-based NPs (either polymeric or lipid-based).[147] The biodegradability, biocompatibility, biodistribution and clearance of NPs are very important issues to take into consideration when constructing an efficient NPs-based nanomedicine for autoimmune disease theranostics.

### Rheumatoid arthritis

Rheumatoid arthritis (RA) is a chronic systemic inflammatory disease, characterized by severe cartilage, bone destruction and massive synovial joint inflammation. Currently, there is no cure for RA.[148] The integration of targeting and therapeutic agents in RA into a single

nanomaterial-based theranostic platform is increasingly advancing in rheumatology. This section will present few nanomaterials that have been discovered lately, with the potential for synergistic RA theranostics.

Activated macrophages are the main "culprit" of inflammation in RA. The macrophages actively release cytokines which trigger onset and persistence of RA. Dextran sulfate (DS) is a hydrophilic polysaccharide that can specifically target the scavenger receptor (SR, one of the receptors overexpressed on the macrophages). MTX is achemotherapy drug that is commonly used for the treatment of RA. However, the utility of MTX is limited by its severe drug resistance, random distribution in the body which may cause serious side effects. Combining both the benefits of nanoscale prodrugs and modified conjugates, a biocompatible polymer-drug conjugate, namely dextran sulfate-graft-methotrexate conjugate (DS-*g*-MTX), has been designed for treatment of RA (see Figure 7a).[149] The conjugate (about 100 nm in diameter) exhibited excellent SR targeting properties, with improved anti-inflammatory efficiency in the affected joints of collagen-induced arthritis (CIA) mice.[149] Similar work has also been presented by Heo *et al*. (2017)[150] using MTX-loaded DS NPs (220 nm in diameter), with the loading efficiency of 73 % (see Figure 7b).[150] NPs permit prolonged circulation in the bloodstream, passive accumulation of drugs into inflamed synovial tissues (12-fold higher than control), with controlled drug release at desired action sites. The results further confirmed that polymeric NPs are potentially useful theranostic nanomedicine for RA.[150]

Solid lipid NPs (SLNs) are formed by a mixture of solid lipids dispersed in inner cores. SLNs are widely used as matrix for drug encapsulation, mainly because SLNs possess attractive features such as good physical stability, enhanced biocompatibility and biodegradability, protection against labile drug degeneration, controlled release and facile synthesis.[98,151] HA is another commonly used drug carriers and targeting ligands in RA treatment.[148] HA targets the over-expressed hyaluronic receptor CD44 on the surface of activated macrophages.

Encapsulation of glucocorticoid prednisolone (PD) can be carried out within the SLNs conjugated with HA and the resultant product is known as HA-SLNs/PD, with approximately 147.8 nm in diameter. Encapsulation of PD in HA-SLNs improved colloidal stability, slowed down PD release (37.6 % compared to 56.22% from free drug solution during the first 30 hours), enhanced biodistribution and therapeutic efficacy in CIA model (with a histopathology score of 2.0).[152]

Metallic NPs have been successfully translated to RA treatment due to their size and magnetic properties which can serve as a multifunctional drug delivery and theranostic platform.[148] In a study, researchers designed drug-loaded gold/iron/gold plasmonic NPs for simultaneous magnetic targeted chemo-photothermal treatment and dual (NIR absorbance and magnetic resonance) imaging of RA.[153] The NPs combine the properties of both iron (magnetic) and gold (surface plasmon resonance), and the gold exterior shell provides an anchorage site for further functionalization. Arginine-glycine-aspartic acid (RGD) peptide was conjugated onto the Au surface to target $\alpha_v\beta_3$ integrins expressed at the inflammation sites. Meanwhile, MTX was loaded inside the poly(lactic-*co*-glycolic acid, PLGA) NPs. PLGA is selected due to its excellent biodegradability, biocompatibility and stability.[154] This RGD-conjugated MTX-loaded PLGA Au/Fe/Au half-shell NPs has an average diameter of 135 nm. Upon NIR irradiation, NIR resonance of the Au half-shells generates heat at the inflammation sites to accelerate the release of MTX from PLGA NPs. Besides, the Fe half-shell layer embedded between the Au half-shell layers allows *in vivo* $T_2$- MRI and NIR absorbance imaging [(see Figure 7d).[153] The externally generated magnetic field not only speeds up the delivery of the NPs to the inflammation sites, but also enhances the retention of the NPs. The combination of NIR absorbance imaging and MRI allow higher spatial resolution of inflammation regions with outstanding contrast features, higher sensitivity and specificity. Interestingly, the MTX dosages required in this case is only 0.05% as compared

to free MTX therapy for the treatment of RA.[153] The *in vivo* behavior (such as biodistribution and vascular penetration) of the as-synthesized NPs requires in-depth studies before wide clinical application.

A combined strategy PSDT (PDT followed by sonodynamic therapy), using PLGA phase-transition NPs co-loaded with oxygen and indocyanine green (ICG), termed OI-NPs, has been proposed for theranostic of RA by Tang *et al.* (2017).[154] PSDT may reduce the sensitizer dosage and ultrasound/light energy that can alleviate side effects, while improving the curative effect dramatically. ICG can strongly absorb NIR once activated by light and ultrasound, suitable for therapy or imaging. The stability of the ICG is improved when co-loaded with oxygen onto PLGA phase-transition NPs. The synergistic oxygen and ICG are found to act as a sensitizer and oxygen carrier for PSDT. The prepared NPs have advantages in terms of biosafety and stability, at the same time showing cytotoxic effects on synoviocytes (a specialized cell type located inside the joints, responsible in producing cytokines and proteases, which cause cartilage destruction).[154] Nonetheless, the authors did not report on the performance of the as-synthesized NPs in *in vivo* model and its therapeutic effect in hypoxic environment.

Titanium dioxide ($TiO_2$) has shown potential in PDT for some diseases, mainly because of its excellent biocompatibility, easy availability and ROS generation properties upon excitation. Tetra sulfonatophenyl porphyrin (TSPP) is a porphyrin derivative that can generate ROS for PDT, but its application is often hampered by neurotoxicity, phototoxicity and non-specific accumulation in body tissues. Interestingly, the photo-activated TSPP-$TiO_2$ nanocomposites were found to be able to ameliorate RA by PDT in CIA models, when coupled with allogenic bone marrow stem cells (BMSC).[155] Meanwhile, Cu is an essential element in the human body, useful in promoting osteogenesis and chondrogenesis. Cu-based nanomaterials were reported as excellent PTT agents and photosensitizers for PDT. An approach using Cu-based

nanomaterials in RA treatment has been proposed with good biocompatibility and facile synthesis (see Figure 7c).[156] Upon NIR irradiation at 808 nm, the as-synthesized L-cysteine (Cys) assisted CuS NPs (named $Cu_{7.2}S_4$ NPs) not only showed better bone preservation, but also displayed outstanding antibacterial ability during intra-articular injection. Hence, the $Cu_{7.2}S_4$ NPs could serve as a synergistic PDT and PTT modality for RA.[156]

Drug delivery systems can be manipulated in a way that the nanomaterials only release the drug from the conjugate in response to certain conditions. This is important in avoiding systemic distribution of drugs in the body that necessitates the use of sustained high-dose therapy and may give rise to adverse effects. As such, Li *et al.* (2017) presented pH-sensitive polymeric micelles for targeted drug delivery to inflamed joints.[157] The polymeric micelles (with particle size of 45.76 nm) are stable in the bloodstream, until it reaches the inflammation sites. An imbalance between increased metabolism and insufficient oxygen supply contributes to low pH in the inflamed synovial fluid (as low as pH 6.0, in some cases even lower than 5.0).[158] Recognition of acidosis of synovial fluid triggers hydrolysis of hydrazone bonds, subsequently releasing the drug, PD in affected joint areas. Same process has also been reported for targeted drug delivery to the acidic microenvironment of solid tumors. The results demonstrated improved therapeutics efficacy, with the therapeutic benefits from each injection lasting for 48-72 hours in preclinical models,[159] fulfilling the needs of sustained prodrug activation kinetics for RA treatment. The as-prepared polymeric micelles inevitably display minimal toxicity, which could be due to micelle uptake by phagocytic cells in liver and spleen that initiates inflammatory responses.[157] Key mechanistic details that induce potential toxicity and inflammatory effects, long-term nanomaterial fates in clearance organs as well as macrophage-nanomaterial interactions are generally unexplored.[160] Future research can be anticipated on fabrication of micelles with bone regeneration capabilities in eroded joints.

Generally, the RA severity often fluctuates over time. Usually, the treatment offered, doses of drug applied and its release rates are irrespective of disease stage, resulting in non-optimal therapeutic efficacy with potential side effects. Herein, a drug-loaded hydrogel that responds to RA flare-ups in real time has been innovatively introduced.[159] A hydrogel is a three-dimensional polymer network of hydrophilic monomers that can absorb and retain a large amount of water, without affecting its shape. Since it can mimic a native tissue's architecture and functions, hydrogel often has been used as drug-delivery carriers.[161] In this case, a hydrogel is formed from the self-assembly of triglycerol monostearate (TG-18), encapsulated with drug triamcinolone acetonide (TA).[159] Synovial fluid from RA joints has higher expression of matrix metalloproteinases (MMPs) and other tissue-degrading enzymes than synovial fluid from healthy joints.[159] Therefore, upon exposure to synovial fluids from patients with RA, MMPs cleave the ester bond in TG-18, disassemble the hydrogel and release the encapsulated TA on-demand, which exclusively corresponds to the concentration of MMPs expressed in the synovial fluids. The severity of the RA is reflected by the co-loaded fluorescent dye 1,1-dioctadecyl-3,3,3,3-tetramethylindotricarbocyanine iodide (DiR).[159] Metalloproteinases-3 (MMPs-3) gene is one of the biomarkers of RA and often correlated with systemic inflammation. Although the precise role of MMPs-3 in RA progression requires further elucidation, TA is believed to be able to alter genes expression of MMPs-3.[162] However, the system still requires extensive *in vivo* biocompatibility evaluation, sustained TA drug release and encapsulation studies especially in large animal models. It is challenging to maintain a consistent release profile in the setting of constant physiochemical changes.

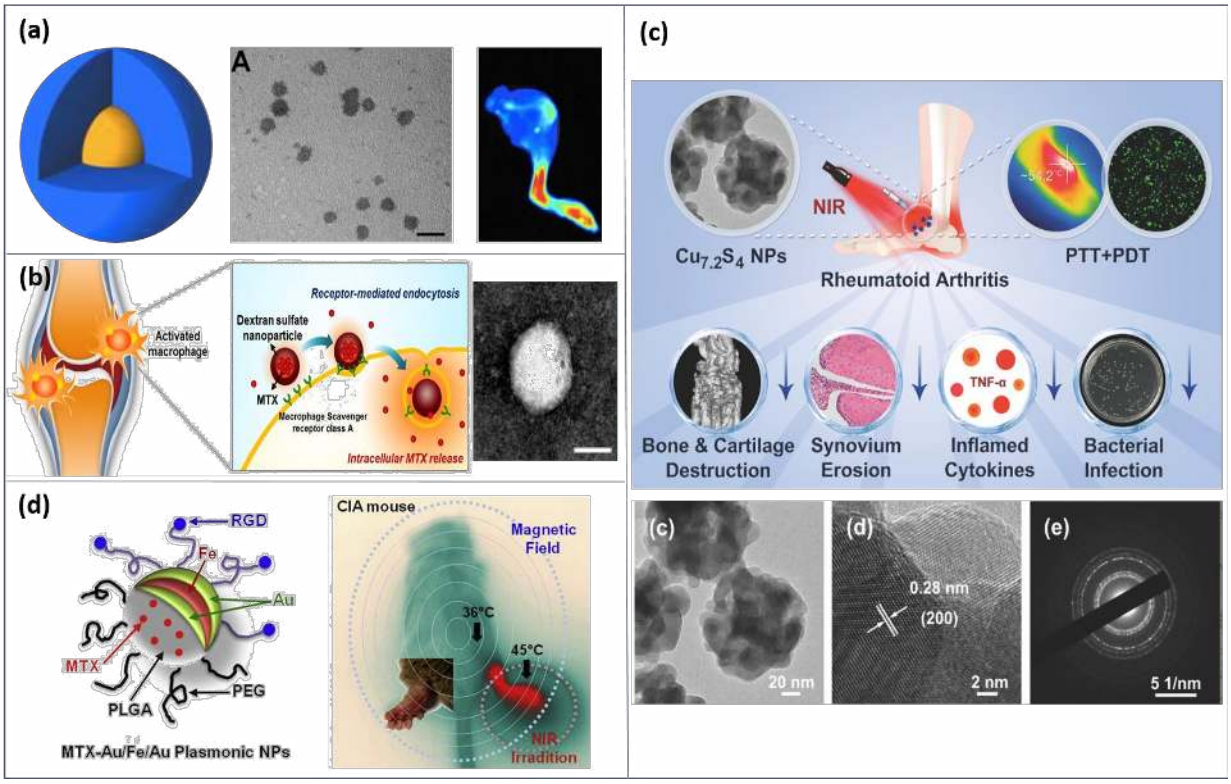


**Figure 7 Brief overview of the structure of the nanomaterials used for rheumatoid arthritis theranostics. (a) MTX prodrug, TEM microimages of DS-g-MTX and its *ex vivo* FITC image of affected joints. Adapted with permission from ref [149]. Copyright 2017 Ivyspring International Publisher. (b) DS-NPs as a nanocarrier for targeted RA theranostic. Adapted with permission from ref [150]. Copyright 2017 Elsevier. (c) Application of $Cu_{7.2}S_4$ NPs in RA theranostic when combined with PTT and PDT. The respective TEM image, SAED and interplanar crystal spacing of $Cu_{7.2}S_4$ NPs. Adapted with permission from ref [156]. Copyright 2018 John Wiley and Sons. (d) MTX-Au/Fe/Au plasmonic NPs for magnetic targeted chemo-photothermal treatment of RA. Adapted with permission from ref [153]. Copyright 2015 Elsevier.**

## CARDIOVASCULAR DISEASES

Cardiovascular diseases (CVDs) are the leading cause of non-communicable illness worldwide. Current surgical intervention and therapy for CVDs are not completely effective

and face many medical challenges. For instance, current recommended therapeutic regimes barely lead to full recovery and often involve poor efficacy, drug instability and resistance, as well as adverse effects and high costs.[163] Advances in nanomedicine offers theranostic approaches for CVDs.[161] It is observed that most of the scientific researches are focused on the study of non-invasive biological imaging applications (particularly MRI and near-infrared fluorescence (NIRF)) for early detection of atherosclerotic plaque. Additional therapeutic strategies for CVDs are highly imperative in actualizing CVDs theranostic applications.

**Atherosclerosis**

Atherosclerosis, a systemic disease affecting arteries, is the major pathological cause of CVDs. Atherosclerosis is characterized by the formation of atherosclerotic plaques, which are developed through the accumulation of cholesterol and formation of foam cells in the arterial wall.[164] Atherosclerotic plaques tend to induce hardening of the artery and thus obstruct blood circulation.[165]

Report for non-invasive fluorescence imaging of atherosclerosis in live atherosclerotic mice has been published in 2016, with the use of Simian virus 40 virus-like particles (SV40 VLPs) as a platform to load imaging probes, targeting elements and therapeutic compounds (see Figure 8a).[166] Controllable *in vitro* self-assembly and the capacity as the cargo for foreign peptides or proteins, makes SV40 VLPs stand out as a nanomaterial in various nanotheranostic applications.[167] Encapsulation of NIR QDs (QD 800) inside SV40 VLPs improved QDs photostability, brightness and detection sensitivity during fluorescence imaging of atherosclerotic plaques in mice.[166] In fact, different atherosclerosis biomarkers or targeting peptides are present at various developmental stages of atherosclerosis.[168] Vascular cell adhesion molecule-1 (VCAM-1), macrophages and fibrin have been identified and used to target atherosclerosis at early, development and late stage, respectively. The multifunctional QDs, with a diameter of 26 nm, permits its accumulation inside the

atherosclerotic plaque tissues mediated by EPR effect, in response to the inflammatory process in the vascular. Enhanced targeted delivery of anticoagulant drug Hirulog (about 6.5-fold increase) and higher anti-thrombin activity (1.8 μg/mg of tissue) at atherosclerotic plaques has been reported when QDs are functionalized with VCAM-1 targeting peptide.[166] However, the group did not provide strong justification on the atherosclerosis efficacy of these NPs, such as reduced areas of plaques, counts of infiltrated immune cells or the expression of inflammatory markers.[169] Future studies should be focused on more detailed biocompatibility evaluation of the SV40 VLPs, including blood-half life, immunogenicity and comparisons with other protein cages to justify its potential as theranostic tools for atherosclerosis.

$H_2O_2$ is a highly promising theranostic biomarker in various pathological disorders, however, its fluorescence imaging modalities are hindered by its short tissue penetration depth. ICG is a widely used photoacoustic contrast agent with a high signal to noise ratio and maximum emission at around 800 nm. Yet, its application is often challenged by instability, rapid blood clearance and non-targeting ability.[170] Jung *et al.* (2018) loaded ICG onto boronated maltodextrin (BM) NPs to form spherical ICG-BM NPs with a diameter of 500 nm.[170] Maltodextrin, one of the polysaccharides obtained from partial hydrolysis of starch, is water soluble, biocompatible, biodegradable, versatile and easy to modify. Hence, maltodextrin is suitable to be used as a diluent, coating material and carrier of diagnostic or therapeutic agents in drug delivery system. Substitution of hydroxyl groups of maltodextrin with boronic ester forms BM, rendering maltodextrin with $H_2O_2$-responsive properties. ICG-BM NPs react with $H_2O_2$ to generate echogenic carbon dioxide ($CO_2$) bubbles which significantly enhanced fluorescence (almost 2-fold higher); ultrasound (signal detectable even with low-frequency ultrasound transducer); and photoacoustic signals in $H_2O_2$-triggered manner. Moreover, ICG-BM NPs could exert therapeutic effects by scavenging the overexpressed $H_2O_2$ and

simultaneously release therapeutic 4-hydroxybenzyl alcohol (HBA). HBA displays anti-inflammatory, antioxidant and antiplatelet functions by suppressing the expression of pro-inflammatory tumor necrosis factor-alpha (TNF-α) and soluble CD 40 ligand in activated platelets,[171] thus relieving inflammation and accelerating angiogenesis.[170] Future work can be anticipated on reducing the size of ICG-BM, since NPs with sizes over 100 nm are easily recognized by macrophages and accumulate in lymph nodes, liver, spleen as well as lungs.[59] High density lipoproteins (HDL) are responsible for reverse cholesterol transport (RCT), a process to efflux excess cholesterol in the periphery back to the liver. RCT is important in protecting against CVDs. A magnetic nanostructure (MNs) functionalized with phospholipids and apolipoprotein A1 (apoA1), named HDL-MNs, has been developed to mimic the natural HDL particles present in the body (see Figure 8b).[172] The MNs are biocompatible and composed of $Fe_3O_4$ NPs, suitable to be used as contrast agents for MRI. The use of HDL-MNs for CVDs is a non-invasive imaging and therapeutic approach. Apart from being capable of precise targeting of macrophages, HDL-MNs are able to perform RCT by inducing cholesterol efflux (about 4.8 %, in natural HDL is about 4.7 %) from cholesterol-rich macrophages. The HDL-MNs have also shown 5 times higher MR contrast enhancement than commercial FDA approved $T_2$ MRI contrast agent (Ferumoxytol). The HDL-MNs are found not inducing cytotoxicity in *in vitro* setting, in macrophages of up to 350 μM HDL-MNs.[172] The hydrodynamic diameter of the nanostructure, however, is approximately 80-100 nm, which is too big for EPR-based extravasation and may impact its circulation time in blood and accumulation at atherosclerotic plaques. It is of interest to further investigate the targeting ability of this nanostructure in *in vivo* setting. In addition, the use of iron-based NPs could potentially generate harmful radicals (Fenton reaction). This may limit their use in humans for diagnosis and treatment, especially under oxidative stress-related conditions.

Recently, researchers have turned their attention to activation of transient receptor potential vanilloid subfamily 1 (TRPV1) signaling pathway as one of the alternatives for attenuating atherosclerosis (see Figure 8c).[164] Activation of TRPV1 cation channels may reduce lipid storage and formation of atherosclerotic lesions. Yet, clinical use for the normally used TRPV1 cation channels activator, capsaicin, is limited by its chronic toxicity and infusibility. Unlike the optical absorption in gold nanostructures, which is due to the surface plasmon resonance, NIR absorption of CuS NPs derives from the d-d transition of $Cu^{2+}$ ions. In other words, CuS NPs absorption would less likely be influenced by the solvent or the surrounding factors, which is perfect for *in vivo* setting. CuS NPs also possess almost analogous high heat conversion efficiencies (as high as 80 %) compared to gold nanostructures, making them remain stable under prolonged optical excitation.[173] Coupling of CuS NPs to antibodies targeting TRPV1 acts as a photothermal switch for TRPV1 signaling in vascular smooth muscles. Upon irradiation of CuS NPs by continuous wave laser at 980 nm, 5 $W/cm^2$ for 350 s, the NPs (with particle size of 13 nm) generate local heat and strong photoacoustic signal which subsequently opens TRPV1 channels and causes calcium ions ($Ca^{2+}$) influx. The increase in intracellular $Ca^{2+}$ induces autophagy, reduces lipid accumulation and foam cell formation. The cholesterol efflux was enhanced with no obvious long-term toxicity *in vivo*. With photoacoustic imaging, high resolution visualization with high temporal and spatial precision of blood vessels in the deeper cardiac regions (such as aortic arch, carotid artery and femoral artery) were achieved.[164]

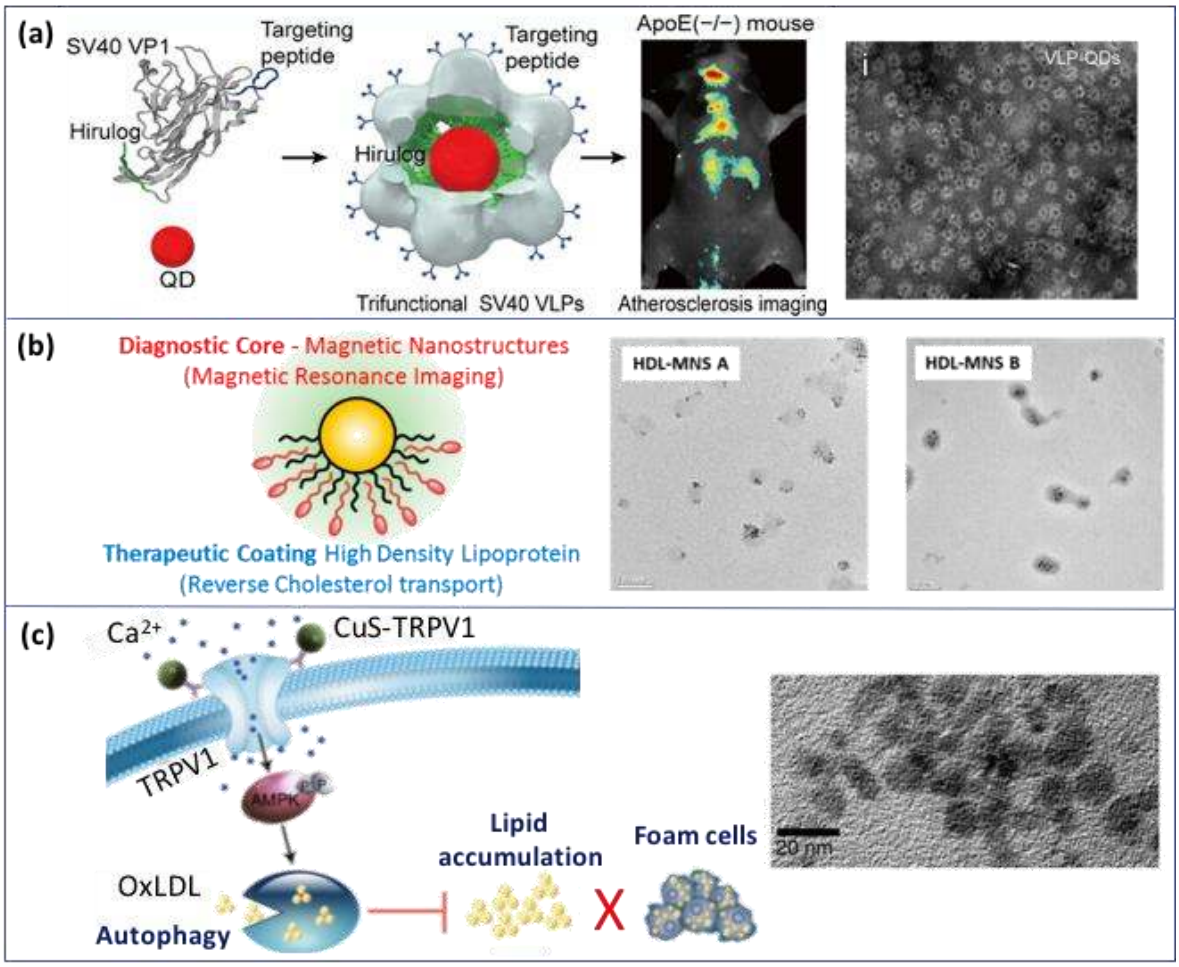


**Figure 8 Brief overview of the structure of the nanomaterials used for atherosclerosis theranostics. (a) Multifunctional virus-like particles of Simian Virus 40 NPs (SV40 VLPs) with the TEM image. Adapted with permission from ref [166]. Copyright 2016 American Chemical Society. (b) High-density lipoprotein-like magnetic nanostructures (HDL-MNs) with their TEM images when synthesized using different approaches. Adapted with permission from ref [172]. Copyright 2017 American Chemical Society. (c) Copper sulfide (CuS) NPs as a photothermal switch for TRPV1 signaling to attenuate atherosclerosis, with the TEM image. Adapted with permission from ref [164]. Copyright 2018 Springer Nature.**

**Thrombosis**

The vulnerable plaques located in the arterial wall are prone to rupture due to soft and weak fibrous cap. The rupture exposes collagen and various components to the blood, leading to the formation of blood clots (thrombi (plural); thrombus (singular)) in the lumen. This condition is known as arterial thrombosis.[164] Thrombosis rarely show any symptoms until late stage and sudden death.[174] Generally, a thrombus is made up of blood factors, mainly activated platelets and water-insoluble fibrin. P-selectin is an adhesion molecule mainly involved in the pathophysiology of thrombosis and other CVDs.[174] Li *et al.* (2018) innovatively functionalized fucoidan, a marine polysaccharide that specifically targets P-selectin in thrombus, on polysaccharide-coated microbubbles (MBs).[174] Ultrasound imaging is one of the commonly used medical diagnostic imaging modalities owing to their portability, non-invasiveness with excellent safety profile, high spatial resolution, lack of ionizing radiation, reasonable cost and real-time imaging properties.[59] The as-synthesized fucoidan functionalized microbubbles (fucoidan-MBs) exhibit high echogenicity and stability in suspension at 4°C (up to 2 months),[174] hence suitable to be used as a sensitive molecular ultrasound contrast agent by creating strong acoustic reflections that may identify thrombus. However, possible treatments for thrombosis after imaging are not discussed by the authors of this study. Future studies could, therefore, focus on theranostic capabilities, safety and efficacy of fucoidan-MBs, as well as the possibility of incorporation of antithrombotic drugs into the system.

A thrombus is also usually associated with an elevated level of $H_2O_2$. $H_2O_2$ is an important signaling messenger regulating the activity of signaling proteins, enzymes and ion channels. Upregulation of $H_2O_2$ may bring harmful oxidative damage, leading to apoptosis and tissue damage.[161] Inspired by these phenomena, fibrin-targeted imaging and anti-thrombotic nanomedicine (FTIAN) has been constructed for thrombosis theranostic (see Figure 9a).[165]

With a diameter of 160 nm, FTIAN has been prepared from self-assembly of IR820 NIR fluorescent dye-conjugated boronate antioxidant polymers (fBAP) and lipopeptides (lipid-PEG-CREKA) composed of 1,2-distearoyl-*sn*-glycero-3-phosphoethanolamine (DSPE), PEG, and a pentapeptide, CREKA (Cys-Arg-Glu-Lys-Ala). High level of $H_2O_2$ in thrombus oxidizes boronate in FTIAN and stimulates subsequent release of HBA from fBAP,[165] initiating antioxidant and anti-inflammation activities.[171] On the other hand, high affinity of CREKA in the lipopeptide towards fibrin facilitates the specific targeting of fibrin on the obstructive thrombus using FTIAN. With the use of IR820 as an NIR fluorophore and photoabsorber, the fluorescence/photoacoustic imaging of thrombi has also significantly enhanced by 5-fold. Most importantly, the intrinsic anti-thrombotic activity of FTIAN has suppressed thrombus formation (required a dose of 24 μg/kg of tirofiban only as compared to a clinically used dose of 80 μg/kg).[165]

Another thrombus-specific theranostic (T-FBM) NPs have been developed with a mean diameter of 260 nm (see Figure 9b).[171] T-FBM NPs is composed of lipopeptide, GPRPPC−PEG−DSPE (distearoylphosphatidylethanolamine). The pentapeptide, GPRPPC, is used to target the thrombus since it has high affinity to fibrin as well. PEG (3.4 k) serves as a surface corona which may prevent non-specific interaction of T-FBM NPs with plasma proteins. The ultrasound/photoacoustic contrast of T-FBM NPs has been significantly enhanced (by 5-fold) when triggered with $H_2O_2$. This is because $H_2O_2$ generate $CO_2$ bubbles to amplify the photoacoustic signal. These NPs are also suitable to be used as an anti-thrombotic nanomedicine, since the NPs can release anti-oxidant and anti-inflammatory HBA under oxidative stress-related conditions. Based on the findings, there is an obvious suppression of the thrombus formation in the studied mouse models. However, for most of the works described in this section, the researchers did not report the dose, pharmacokinetics, side effects and toxicology of the NPs used. In fact, the biocompatibility and biodegradability

of the NPs are equally important in future clinical applications. Also, unlike non-motile solid tumor, thrombi ultrasound imaging analysis is often challenged by poor contrast resulting from the interference of motion artifact caused by respiratory and cardiac activities.[174]

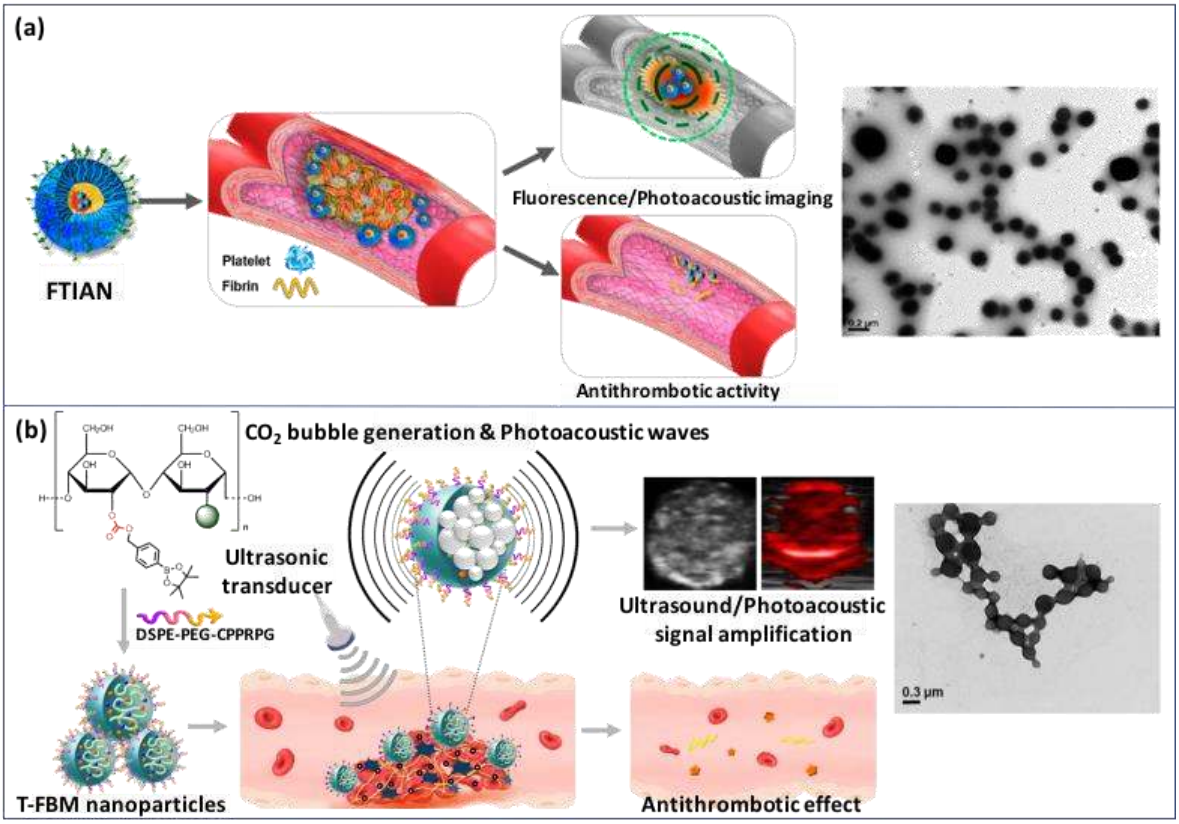


**Figure 9 Brief overview of the nanomaterials used for thrombosis theranostics, with their TEM images. (a) Fibrin-targeted and $H_2O_2$-responsive NPs as a theranostics for thrombosed vessels. Adapted with permission from ref [165]. Copyright 2017 American Chemical Society. (b) T-FBM NPs as a $H_2O_2$-activatable photoacoustic signal amplifier and a thrombus-specific nanotheranostic agent. Adapted with permission from ref [171]. Copyright 2018 American Chemical Society.**

## BACTERIAL INFECTION

Bacterial infection is one of the world's leading causes of premature deaths and mortalities. Current methodologies for diagnosis and therapy of bacterial infection are often hindered by a difficult bacteria isolation and early detection, low numbers of bacteria in the clinical

specimen, false negatives and contamination of the specimen.[1] Poor sensitivity and late diagnosis often delay the therapy and thus increase the cost and discomfort to the patients. The development of drug resistance in the bacterial pathogen and the overuse of antibiotic are also concerns in bacterial infection management. This section will discuss different nanomaterials with their potential in bacteria nanotheranostics and provides a critical review on their advantages and limitations.

The work on both *in vitro* and *in vivo* multi-modal mapping and targeted PTT against bacterial infection of gastrointestinal tract was introduced in 2015, with the use of tungsten-based theranostic agents.[175] Since then, different nanoprobes capable of selectively imaging bacteria with high anti-microbial properties have been proposed. Selenium (Se) is a semi-metallic element with low electronegativity and large atomic radius compared with sulfur, endowing Se-containing compounds with high reactivity and sensitivity.[176] Moreover, the stimulus-responsive property of Se gives the materials a big potential in construction of smart and sensitive theranostic systems responding to biomolecules.[176] Ruthenium (Ru) is a rare metal in the earth's crust with diverse biomedical and antimicrobial applications, especially in its complex form.[177] For instance, Ru complexes have been found to display synergistic antimicrobial activity with antibacterial peptide UBI29-41 (PEP)-modified Se particles (see Figure 10d).[178] This multifunctional theranostic nanoplatform, or known as Se@PEP-Ru NPs, displayed good biocompatibility, excellent selectivity and potent antimicrobial activity. The NPs strongly interact with both gram-positive and gram-negative bacteria cell membranes, followed by severely damaging the structures of the bacterial cell and cytoplasmic membranes. The wound sizes of the mice treated with Se@PEP-Ru NPs were found to decrease by about 40% at the fourth day after surgery, showing a significant therapeutic effect. Besides, since Se@PEP-Ru NPs are sensitive to sites of bacterial infection, it was found to be able to identify and distinguish bacterial infection from inflammation and

tumor-induced tissue infection with high specificity.[178] Evident fluorescence can be observed (after 4-48 hours of injection) at the site of the bacterial infection but the fluorescence was almost negligible (2-3 times weaker) at the site of inflammation. Future studies can be focused on engineering the as-synthesized Se@PEP-Ru NPs (with a size of about 78 nm) into a smaller size as the size and surface area of NPs could affect the antibacterial activity.[179] Smaller NPs (less than 10 nm) are generally more effective since it allows favorable surface area of NPs for interaction with the bacterial cell membrane and disruption of bacterial permeability and respiration.[180]

Metabolic biomolecular labelling is an emerging technology to modify the surface of cells and pathogen with chemical functional groups, which in turn allows conjugation of fluorescent dyes (for imaging purpose) or drugs (for therapeutic effect) onto cell membrane.[181] Metal-organic frameworks (MOFs) can be engineered as drug nanocarriers, thanks to their versatile chemical properties, good biocompatibility, sensitive to low pH tumor environment and fast body clearance after drug delivery. A bacteria theranostic strategy through coupling of MOFs with metabolic labelling technique has been reported recently (see Figure 10a).[181] Mao *et al.* (2018)[181] innovatively used MIL-100 (Fe) nanoparticles (with an average diameter of 120 nm) as the nanocarriers for metabolic labelling molecule and 3-azido-D-alanine (D-AzAla), to target bacterial cells. The NPs are stabilized by polymer pluronic F-127. The high $H_2O_2$ inflammatory environment stimulates degradation and rapid release of D-AzAla from MIL-100 (Fe) at the inflammation sites. Upon internalization of D-AzAla by the bacteria, unnatural azide groups will be expressed on the bacterial cell walls. Ultrasmall photosensitizer NPs with around 10 nm, named dibenzocyclooctyne (DBCO)-modified 2-(1-(5-(4-(1,2,2-tris(4-methoxyphenyl)vinyl)phenyl)thiophen-2-yl)ethylidene)malononitrile NPs (US-TPETM NPs), with aggregation-induced emission characteristics are subsequently administered. DBCO

groups on the surface of NPs will bind and react with the bacteria through *in vivo* click chemistry. The bacterial cell walls will be lightened up to produce fluorescence signals for imaging, facilitating subsequent image-guided antibacterial therapy and PDT.[181] This breakthrough in *in vivo* incorporation of unnatural functional group into bacteria for metabolic labelling and antibacterial therapy could soon enable the discovery of more effective bacterial theranostic approaches.

Luminescent porous silicon (LuPSi) has tunable porosity and surface chemistry, good biocompatibility and degradability, making them suitable as optical biosensors for bioimaging and drug delivery. LuPSi can be loaded with antibiotics ciprofloxacin (CIP) to form CIP-LuPSi for theranostic application.[182] For wound care application, a smart bandage composed of polyurethane (PU) membrane and chitosan film, has been presented by Chen *et al.* (2017) for monitoring and inhibition of wound infection.[182] High level of ROS and elevated pH (above 7.4, normal skin pH= 5.5- 6) are two main biomarkers in chronic or infected wounds.[182] The luminescent property of LuPSi is correlated with its surface chemistry. The blue luminescence of CIP was quenched by red LuPSi due to the fluorescence resonance energy transfer (FRET) effect. When the smart bandage is applied onto the infected wound that usually associated with an elevated level of ROS and alkaline ions (such as $PO_4^{3-}$ or $OH^-$), the surface of LuPSi was oxidized into an insulating oxide layer that blocked the energy transfer between LuPSi and CIP. As a result, the fluorescence of CIP recovered (from red to blue) and can be observed by naked eyes and a cell phone camera. Therefore, by detecting the ratiometric fluorescence intensity, the kinetic process of surface oxidation of CIP-LuPSi can be precisely measured. The oxidation of LuPSi also simultaneously trigger the release of CIP to inhibit bacterial activity. In the same year, Zhao *et al.* (2017) developed silica NPs coated with vancomycin-modified polyelectrolyte-cypate complexes ($SiO_2$-Cy-Van), with a size of about 72.7 nm, as a bacteria-activable theranostic

nanoprobe (see Figure 10c).[183] The polyelectrolyte acts as an adsorbate or dissociation energy barrier on silica NPs, conferring the NPs with bacteria-responsive feature, as well as enhanced biocompatibility and relatively prolonged blood circulation. The cell wall of methicillin-resistant *Staphylococcus aureus* (MRSA) bacteria is capable of forming hydrogen bonding with vancomycin (Van) on the nanoprobes. The interaction between Van and MRSA detaches the layer-by-layer assembled polyelectrolytes from silica NPs, changing the state of cypate (Cy), a dye with NIR fluorescence emission at around 825 nm, from OFF (aggregation) to ON (disaggregation). This leads to rapid MRSA-activated NIR imaging (4 hours post-injection, high sensitivity up to $10^5$ colony-forming units) and effective PTT upon 808 nm laser irradiation.[183] However, the possibility of autofluorescence and influences of bacterial environment on the sensitivity and selectivity of the nanoprobes are not clearly demonstrated. On the other hand, the idea of bacteria-responsive intelligent wound dressing proposed by Zhou *et al.* (2018)[184] has also offered a different perspective in the fabrication of nanomaterials to combat bacterial infection. The group constructed a biocompatible UV-photocrosslinkable methacrylated gelatin (GelMA) encapsulating both antimicrobials and self-quenching dye carboxyfluorescein vesicles. The working principle is that upon bacterial infection, toxins or enzymatic factors secreted from bacteria could break down the lipid vesicles and release the payloads. This eventually leads to bacterial inhibition in addition to a visual color change (due to the fluorescence recovery of carboxyfluorescein). Supported by both *in vitro* and *in vivo* studies, the release of antimicrobials occurs only when pathogenic bacteria (specifically MRSA and *Pseudomonas aeruginosa*) exist.[184]

Gold nanomaterials are antibiotic agents owing to their tunable size, facile functionalization and minimal toxicity. It is interesting that recently, gold nanoclusters (AuNCs) have been demonstrated to exhibit anti-bacterial activity,[185] especially by manipulating their surface ligand chemistry.[186] Quaternary ammonium (QA) capped AuNCs (QA-AuNCs), with the size

about 2 nm, can selectively target MRSA and Van-resistant *Enterococci* (VRE), *in vivo*.[185] Since QA-AuNCs can disrupt the bacterial cell membrane (in terms of integrity, permeability and inner potential), catalyze the generation of ROS and disturb the intracellular metabolic pathway of the bacteria, QA-AuNCs displayed excellent therapeutic effects. The intensely fluorescent QA-AuNCs interact with live/dead bacteria differently, suggesting their potential for image-guided bacteria discrimination and counting. Besides, QA-AuNCs are stable for long-term storage, even at room temperature.[185] On the other hand, it should be noted that it is difficult to compare the anti-bacterial performances of different nanomaterials, since the composite design and concentration of each multifunctional nanomaterial used can be very different, unless more comparable studies are conducted under standard experiment conditions.

Gold nanorods (AuNRs) are an excellent contrast agent for PA imaging and have characteristic strong NIR absorption. Kim *et al.* (2018) have developed a gold/silver hybrid NPs, named as Au/AgNRs, as theranostic antibacterial/photoacoustic agent (see Figure 10b).[187] Au/AgNRs (with a diameter of 104.9 nm) are formed by coating AuNRs with silver (Ag) to decrease the photoacoustic signal.[187] Oxidative etching of the Ag shell induced by the addition of ferricyanide solution (1 mM) could recover the photoacoustic contrast as the Ag is released. The release of Ag also effectively triggers and monitors the release of $Ag^+$ ions (a well-known antibacterial agent) from its reservoir AgNPs. $Ag^+$ ions exhibit strong bactericidal efficacy towards both MRSA (32 μM $Ag^+$) and *Escherichia coli* (8 μM $Ag^+$). The photoacoustic signal increased by 730 % pre- and post-etching, and the bacterial counts in infected tissues were reduced by 1000-fold (log CFU/g= 4.15 *vs* 7.75) in the treated group.[187] This is the only report that quantitates Ag release *in vivo* and correlates the released dose to antibacterial outcomes.

Hydrogels are the three-dimensional water-swollen polymer networks composed of hydrophilic polymers. It can be used as a scaffold for local bacterial drug delivery since it can achieve long retention at the focal area with low unwanted diffusion.[188] A NIR light-triggerable and thermo-sensitive hydrogel that can combat bacterial infection and promote wound healing have been introduced recently.[188] This injectable hydrogel is composed of ciprofloxacin (Cip)-loaded polydopamine NPs (PDA NPs) and glycol chitosan (GC). The aromatic rings on the surface of PDA NPs enable the adsorption of drugs *via* π-π stacking and hydrogen bonding; while the quinone groups on the surface of PDA NPs allow facile conjugation with the chemicals containing thiol or amine groups. GC is rich in amine, therefore, has been used to crosslink with PDA NPs. With a uniform size of about 30 nm, PDA NPs also possess excellent photothermal effect (the ability to convert NIR light into heat), biocompatible and biodegradable. The positive charge of GC and the adsorbability of PDA NPs are able to trap bacteria on the surface of the hydrogel with minimal leakage under physiological conditions. Once irradiated with NIR light, Cip antibiotic will be released. Meanwhile, PDA NPs in the hydrogel will be activated and subsequently generate local heat to kill the bacteria, with a bactericidal efficacy up to 98.9 %.[188]

Despite its efficacy, inorganic NPs as antibacterial agents are constrained by their non-specific biological toxicity or potential long-term *in vivo* retention. Applications of metal-free antibacterial agents such as polymers are still facing limitations, including poor biocompatibility, complicated synthetic steps, limited structural tunability and/or the need for suitable carriers to ensure the spatial stabilization at the injection site. Generally, it is difficult to compare different nanomaterials from the aspects of their photothermal conversion efficiency or bactericidal performances.

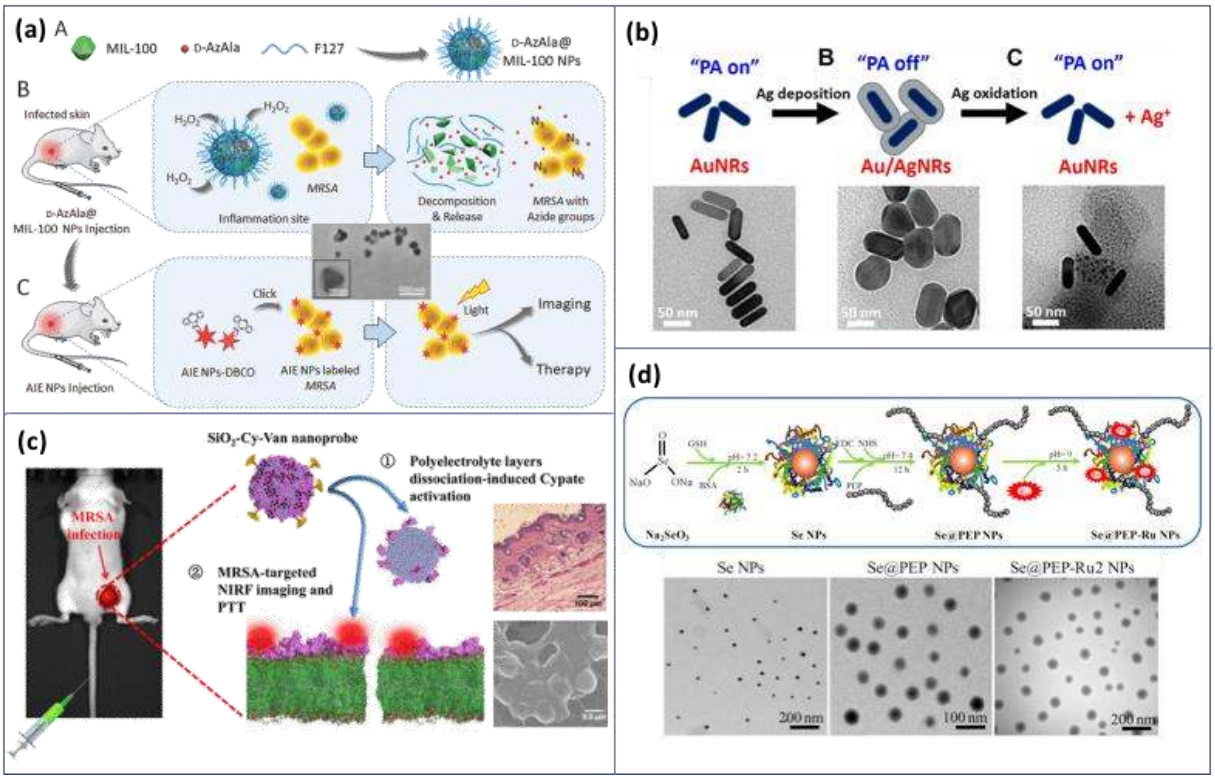


**Figure 10 Brief overview of the nanomaterials used for bacterial infections theranostics, with their TEM images. (a) $H_2O_2$-responsive MOFs assisted *in vivo* metabolic labelling of bacteria and precise antibacterial therapy. Adapted with permission from ref [181]. Copyright 2018 John Wiley and Sons. (b) Formation of Au/AgNRs hybrid NPs by Ag coating on AuNRs. The addition of ferricyanide solution results in oxidative etching of the Ag shell. Adapted with permission from ref [187]. Copyright 2018 American Chemical Society. (c) $SiO_2$-Cy-Van as a theranostic nanoprobe against MRSA infections. Adapted with permission from ref [183]. Copyright 2017 American Chemical Society. (d) Fabrication of Se@PEP-Ru NPs for identification of bacterial infection with simultaneous targeted antibacterial activity. Adapted with permission from ref [178]. Copyright 2017 Elsevier.**

**TABLE OF SUMMARY**

**Table 1 A Summary of Functional Nanomaterials Developed for Different Cancer/Diseases/Illness**

| **Cancer/Disease /Illness** | **Type of nanomaterial** | **Formulation** | **Mean size (nm)** | **Therapeutics modality** | **Imaging modality** | **Animal model** | **Brief description/ Remarks** | **Ref.** |
|---|---|---|---|---|---|---|---|---|
| Cancer (Solid tumor) | Gold nanostructures | Diazirine-decorated Au@PEG-$NH_2$ | 20.5 ± 1.9 | PTT | PAI | Female BALB/c mice | Light-addressable cross-linking at 405 nm laser irradiation | [63] |
| | | AQ4N-Cu(II)-$Apt_{Ce6}$-GNPs | 137.07 ± 4.26 | PDT, PTT, chemotherapy | Optical | Male BALB/c-nude mice | Tumor microenvironment -triggered, programmed synergistic therapy at 670 nm laser irradiation | [41] |

| | | | | | | | | |
|---|---|---|---|---|---|---|---|---|
| | | SWNT@BSA@Au-S-PEG-FA@DOX | 20–30 (estimated thickness) | PTT, chemotherapy | Optical | Female nude mice | High drug loading ratio (150–590 %); 808 nm laser irradiation | [67] |
| | | Stealth-AuNC NPs | 80-100 | PTT | Optical | BALB/c mice | 850 nm laser irradiation; longer circulation half-life (> 4-fold) | [46] |
| | | AuNR@Da NHs | 130 | PTT, chemotherapy | Fluorescence, PAI | Nude mice | Photothermal conversion (80 %); 27-fold higher internalized AuNR mediated by NHs; 6.6 times higher internalized ADR; 2.3 times | [73] |

| | | | | | | | | |
|---|---|---|---|---|---|---|---|---|
| | | | | | | | higher tumor accumulation due to NIR-induced hyperthermia | |
| | Other inorganic nanomaterials | $MnO_2$-SPs nanosheets | 295 (average thickness = 2.0 nm) | PTT | MRI | BALB/c-nude mice | Ultra-sensitivity to endogenous tumor microenvironment and exogenous NIR irradiation; 808 nm laser irradiation; high photothermal-conversion efficiency (21.4 %) | [80] |

| | | | | | | | | |
|---|---|---|---|---|---|---|---|---|
| | | Anti-EpCAM-UPGs-MX | 93.5 | Chemotherapy, PDT | MRI, upconversion luminescence | Female BALB/c mice | MX loading level (12.5 wt %); 980 nm laser irradiation | [82] |
| | | mNiO-TB-ART | 310 | PTT, radical-induced therapy | Optical luminescence, $T_2$-weight MRI | HeLa tumor mice models | $T_2$-weighted MRI, $r_2$ = 6.30 (mg $mL^{-1})^{-1}$ $s^{-1}$; NIR laser irradiation at 785 nm | [81] |
| | | Pd@Pt-PEG-Ce6 | 80 | PDT, PTT | Optical | 4T1 subcutaneous tumor mice model | Laser irradiation at 660 and 808 nm; hypoxia modulation | [44] |

| | | | | | | | | |
|---|---|---|---|---|---|---|---|---|
| | | | | | | | function with mild PTT effect | |
| | | $BiP_5W_{30}$ NCs | 1.5 (thickness of rGO) | Radiotherapy, PTT | Optical | HeLa tumor-bearing mice | Laser irradiation at 808 nm; increased radiation dose deposition within tumors; tumor microenvironment -manipulated | [43] |
| | | CuS@BSA-MBA-cRGD | 51.2 ± 2.46 | PTT | Optical (infrared thermal) | EAC tumor-bearing mice | Laser irradiation at 808 nm; synergistic tumor-targeting delivery and PTT effects | [77] |

| | | | | | | | | |
|---|---|---|---|---|---|---|---|---|
| | | TPGS-$Cu_3BiS_3$ NCs | 15 | Radiotherapy, PTT | Optical | Female BALB/c nude mice | Photothermal conversion efficiency at 1064 nm = ~67.29 %; 808 nm = ~18.27 %; 980 nm = ~61.06 % | [87] |
| | | FA-QDs-FUA | 220.28 | Chemotherapy | Optical | Balb/c Nod/Scid mice | Zeta potential= -13.3 mV; drug-loading content = 36.85 % ± 1.61 % (n= 3) | [84] |
| | | Gd-DTPA-coupled $Ag_2Se$ quantum dots | 4.08 ± 0.58 | - | Optical, MRI | Female Balb/c mice | Contrast agents in *in vivo* dual-modality $T_1$-weighted MR | [85] |

| | | | | | | | | |
|---|---|---|---|---|---|---|---|---|
| | | | | | | | imaging; NIR-IIb fluorescence imaging with high spatial resolution | |
| | | PHMNPs-S-S-PEG-LA@PFC($O_2$)/EP | 16.07 | Chemotherapy | Optical, MRI | Nude mice | High etoposide/oxygen loading capacity, tumor-targeting capability and programmable intracellular agglomeration behavior | [47] |
| | | $Cu_3BiS_3$ nanocrystals | 12 ± 4 | PTT, PDT | Optical, x-ray contrast | BALB/c nu/nu mice | Ultra-low NIR laser irradiation | [70] |

| | | | | | | | | |
|---|---|---|---|---|---|---|---|---|
| | | $Co_3O_4$ nanoprism | 3.26 x 33.29 (thickness x length) | PTT, chemodynamic, chemotherapy | MRI, optical | Nude mice | Photothermal conversion efficiency, $\eta$= 60.07 %; MRI contrast, $r_2$= 5.42 $mM^{-1}s^{-1}$; significant hydroxyl radical generation; low toxicity; DOX delivery = 29.36 mg/g; low detection limit (50 nM), broad linear range (0-50 μM); high sensitivity | [45] |

| | | | | | | | | |
|---|---|---|---|---|---|---|---|---|
| | | | | | | | and selectivity for $H_2O_2$ | |
| | Polymeric nanoparticles | SiNc-PNP, encapsulated in PEG-PCL | 40 | PTT, NPs-mediated image-guided surgery | Optical | Female athymic nude mice | Real-time intraoperative image-guided surgery; 785 nm laser irradiation; process can be tailored *via* photo irradiation dosage | [90] |
| | | M-GEG NPs, M-EGFA NPs | 105 (GEG NPs), 90 (EGFA NPs) | Chemotherapy | Optical | New Zealand albino rabbits, athymic | Sustained and targeted drug release at the tumor site | [89] |

| | | | | | | | | |
|---|---|---|---|---|---|---|---|---|
| | | | | | | mice models | | |
| | | POCL nanoreactor | 50 | PDT | Chemiluminescence | BALB/c nude mice | Self-luminescing; tumor microenvironment activated; non-invasive | [92] |
| | | FUP cationic nanomicelles | 30-150 | Chemotherapy | Optical | - | Surface charge of zeta potential +20.1 mV; antitumor apoptosis mechanism might be related to the regulation of Fas/FasL and | [93] |

| | | | | | | | | |
|---|---|---|---|---|---|---|---|---|
| | | | | | | | activation of caspase-8 and caspase- 3 | |
| | | $Cu_{2-x}S$/PFBO@PLGA | 123.7 | HIFU | PAI | Balb/c nude mice | Core/satellite/shell sandwich structure; favorable biosafety; high PAI contrast capability with enhanced ablation efficacy under HIFU | [95] |
| | | STD-$NM_{drug}$ | 25 | Chemotherapy | Optical, AIE-based | BALB/c nude mice | Therapeutic effect monitoring by AIE signal ‘switch on’; | [97] |

| | | | | | | | | |
|---|---|---|---|---|---|---|---|---|
| | | | | | two-photon | | therapeutic property supported by gene analysis (RNA-seq) | |
| | Lipid nanoparticles | HA/CPPs-10-HCPT-NPs | 284.2 ± 13.3 | Chemotherapy | Optical, ultrasound | BALB/c nude mice | Can undergo ADV and ultrasound-targeted microbubble destruction; triggered by LIFU; allow penetration into extracellular matrix, cellular membrane and nucleus | [100] |

| | | | | | | | | |
|---|---|---|---|---|---|---|---|---|
| | | Lipo@HRP&ABTS | 100 | PTT | PAI | Female BALB/c mice | Under 808 nm NIR laser irradiation; *in vivo* $H_2O_2$-responsive chromogenic assay; detection of inflammation; enable differentiation of metastatic lymph nodes | [101] |
| | | DOX/SPIONs-loaded DFSLNs | 132.1 ± 8.7 | Chemo/magnetothermal combination therapy | Optical | BALB/c mice | Hierarchical and dual targeting for the oral delivery of dual-modality local therapy | [98] |

| | | | | | | | | |
|---|---|---|---|---|---|---|---|---|
| | | Lip/Ce6/TPZ NPs | 162 ± 4 | PDT, chemotherapy | Optical | MCF-7-beared mice | Light- triggered and hypoxia-responsive; good biocompatibility with little toxicity toward normal cells without irradiation | [99] |
| Cancer (Liquid tumor) | Metal nanoparticles | FA-IONPs | 100 | PTT | MRI | LnCaP cells | Specific targeting due to FA functionalization | [127] |
| | | EMG-308 IONP | 60 | PTT | MRI | LnCaP cells | IONP aggregation prevention | [128] |
| | | Cu-Au@F-Apt NSs | 30 | PTT | Optical | Male athymic | Cu high thermal conductivity | [129] |

| | | | | | | | | |
|---|---|---|---|---|---|---|---|---|
| | | | | | | BALB/c mice | | |
| | Lanthanide-doped nanoparticles | antiCD33-LONp-PMI | 5.6 | Chemotherapy | Optical | Primary cells from patients with AML | Real time visualization of AML cells apoptotic events | [131] |
| | Polymeric nanoparticles | CCM-PEG | 228 | Chemotherapy | Optical | HL-60, HepG2, HEK293 T, HDF cells | Natural biocompatible material with anticancer activity | [132] |
| | | pA20-36 Chitosan-HA-NPs | 70 | Chemotherapy | Optical | Balb/C nude mice | Multimodal imaging depending on the site of tumor | [134] |

| | | | | | | | | |
|---|---|---|---|---|---|---|---|---|
| | | PDI NP | 60 | PTT | PA and PET | U87MG tumor-bearing nude mice | Size dependent tumor accumulation effect | [135] |
| | Lipid nanoparticles | Lip/PEG/Tween 80/SPIONs-PVA/RTX | 7-10 | Chemotherapy | MRI | Athymic nude mice | Blood-brain barrier internalization | [189] |
| Neurodegenerative diseases | Dyes | DBA-SLOH | - | Chemotherapy | Optical | APP/PS1 transgenic (Tg) mice | NIR dye | [141] |
| | Multifunctional nanocomposite | CeNC/IONC/MSN-T807-MB | 131 | Chemotherapy | MRI | Male Sprague−Dawley rats | Synergistic therapeutic effect of CeNC and MB | [142] |

| | | | | | | | | |
|---|---|---|---|---|---|---|---|---|
| | BTTA chelator | BTTA | - | Chemotherapy | Optical | C57BL/6J male mice | Fluorescent chelator | [144] |
| | Multifunctional upconversion nanoparticle | UCHQs | 114 | Chemotherapy | Optical | C57BL6 female mice | Tissue autoluminiscence circumvented by NIR excitation | [145] |
| Autoimmune diseases (Rheumatoid arthritis) | Polymer conjugate micelles | DS-*g*-MTX | 104.4 ± 14.4 | Chemotherapy | Optical | CIA mice | Targeting on SR-expressed activated macrophages | [149] |
| | Polymeric NPs (amphiphilic) | MTX-DSNPs | 220 | Chemotherapy | Optical | CIA mice | MTX loading efficiency (73.0 %); targeting on macrophages | [150] |

| | | | | | | | | |
|---|---|---|---|---|---|---|---|---|
| | | | | | | | scavenger receptor class A | |
| | Phase-transition NPs | OI-NPs | 277.80 ± 22.49 | PSDT | Optical | - | Exposed to LIFU, caused a sonodynamic reaction; laser irradiation at 808 nm | [154] |
| | Plasmonic NPs | MTX-Au/Fe/Au plasmonic NPs | 135 | PTT, chemotherapy | MRI, optical | CIA mice | NIR light irradiation at 808 nm; $T_2$ weighted MRI; magnetic targeted chemo-photothermal treatment; higher | [153] |

| | | | | | | | | |
|---|---|---|---|---|---|---|---|---|
| | | | | | | | therapeutic efficacy with smaller MTX dosage (0.05 %) | |
| | Inorganic NPs | $Cu_{7.2}S_4$NPs | 120 | PTT, PDT | Optical | CIA mice | NIR irradiation at 808 m, can prevent bacterial infection using intra-articular injection | [156] |
| Cardiovascular diseases (Atherosclerosis) | Inorganic NPs | CuS-TRPV1 | 13 ± 1.2 | PTT | PAI, optical | ApoE −/− mice | Targeting on TRPV1 signaling; NIR laser irradiation at 980 nm; showed no | [164] |

| | | | | | | | | |
|---|---|---|---|---|---|---|---|---|
| | | | | | | | obvious *in vivo* toxicity | |
| | QDs | SV40 VNPs | 26 ± 1.2 | Chemotherapy | Optical | ApoE −/− mice | Encapsulating NIR QDs, bearing atherosclerotic targeting peptides and anti-coagulant drug Hirulog; targeting on VACM-1, macrophages and fibrin | [166] |
| | Magnetic NPs | HDL-MNS | 80-100 | Reverse cholesterol transport | MRI | - | Serve as cholesterol efflux agents (4.8 %); | [172] |

| | | | | | | | | |
|---|---|---|---|---|---|---|---|---|
| | | | | | | | show a 5 times higher contrast ($r_2$ relaxivity up to 383 $mM^{-1}s^{-1}$) | |
| | Polymeric NPs | ICG-BM NPs | 500 | Antioxidant, anti-inflammatory | Fluorescence, ultrasound, photoacoustic | Balb/c male mice | Photoacoustic signal is detectable with low frequency ultrasound transducers; excellent antioxidant, anti-inflammatory, proangiogenic activities; pathological | [171] |

| | | | | | | | | |
|---|---|---|---|---|---|---|---|---|
| | | | | | | | stimulus-activatable multiple contrast amplification | |
| Cardiovascular diseases (Thrombosis) | Polymeric NPs | FTIAN | 160 | Chemotherapy | PAI, optical | $FeCl_3$-induced carotid arterial thrombosis mice model | Targeting on fibrin and elevated level of $H_2O_2$; intrinsic anti-oxidant, anti-inflammatory and anti-platelet activity; anti-thrombotic when loaded with antiplatelet drug tirofiban; irradiation of | [165] |

| | | | | | | | | |
|---|---|---|---|---|---|---|---|---|
| | | | | | | | pulsed laser at 808 nm | |
| | Inorganic NPs | T-FBM NPs | 320 | Chemotherapy | PAI, optical | $FeCl_3$-induced carotid arterial thrombosis mice model | $CO_2$ bubble generation and photoacoustic waves formation when exposed to ultrasonic transducer; $H_2O_2$-activatable ultrasound/photoacoustic signal amplification; antithrombotic effect | [171] |

| | | | | | | | | |
|---|---|---|---|---|---|---|---|---|
| | Polymer nanobubbles | Fucoidan-MBs | 2–6 μm | - | Ultrasound | Wistar male rats | Stable in suspension at 4 °C up to 2 months; exhibit high echogenicity; could completely burst under high destructive pulse | [174] |
| Bacterial infections | Composite materials | MIL-100 (Fe) NPs | 120 | PDT | Optical | MRSA-bearing mice | $H_2O_2$-responsive MOFs assisted bacteria metabolic labelling strategy; incorporation of unnatural functional group | [181] |

| | | | | | | | | |
|---|---|---|---|---|---|---|---|---|
| | | | | | | | into bacteria *in vivo* | |
| | | Se@PEP-RuNPs | 78 ± 13 | Antibacterial | Optical | BALB/cA-nude mice | High stability, excellent light stability; no obvious cytotoxicity, negligible hemolytic effect; could promote wound healing | [178] |
| | | Au/AgNRs | 104.9 | Antibacterial | PAI | Wild-type male C57BL/6 mice | Strong bactericidal efficacy towards both MRSA (32 μM $Ag^{+}$) & | [187] |

| | | | | | | | | |
|---|---|---|---|---|---|---|---|---|
| | | | | | | | *Escherichia coli* (8 μM $Ag^{+}$); PA signal increased by 730% pre- and post-etching; bacterial counts reduced by 1000-fold (log CFU/g= 4.15 *vs* 7.75) after treatment | |
| | Inorganic NPs | CIP-LuPSi | 17.3 | Bacterial inhibition *via* drug release | Optical | SD male rats | High biocompatibility & drug-loading ability; silicon-based smart bandage in wound | [182] |

| | | | | | | | | |
|---|---|---|---|---|---|---|---|---|
| | | | | | | | care and bioimaging | |
| | | $SiO_2$-Cy-Van | 72.7 ± 3.2 | Antimicrobial, PTT | Optical | MRSA-bearing mice | Activated by bacteria-responsive dissociation of the polyelectrolyte from silica NPs; rapid MRSA-activated NIRF imaging (4 hours post-injection, high sensitivity up to $10^5$ colony-forming units); effective PTT | [183] |

| | | | | | | | | |
|---|---|---|---|---|---|---|---|---|
| | | | | | | | upon 808 nm laser irradiation | |
| | | QA-AuNCs | 2 | Antibacterial | Optical | MRSA T144 mouse | Imaging-guided bacteria counting; discrimination of live/dead bacteria; non-toxic to mice at doses of up to 100 mg/kg | [185] |
| | | PDA NP-Cip/GC hydrogel | 30 | PTT, antibacterial | Optical | BALB/c female mice | NIR laser irradiation at 808 nm; bacterial killing activity with wound healing ability | [188] |

| | | | | | | | | |
|---|---|---|---|---|---|---|---|---|
| | Organic NPs | PEG-$W_{18}O_{49}$ | 18 x 5 x 1 (height x width x thickness) | PTT | X-rays, CT, MRI, ultrasound | Kunming mice | NIR laser irradiation at 808 nm; excellent colloidal stability, low cytotoxicity & neglectable hemolysis | [175] |

## CLINICAL TRANSLATION OF THERANOSTIC NANOMATERIALS

While we focus here on nanotheranostics of different diseases (see Table 2), theranostic nanomaterials in human clinical trials are still in its infancy when compared to its NPs predecessor, which focuses only on either imaging, diagnostics or therapy. There are numerous review articles on NPs for single function that are in clinical trials.[190–194] An all-in treatment (comprising of imaging, diagnosis and therapy) is lucrative, however, years of clinical trials are required in order to gain patients' confidence.

Based on our extensive search, only one nanoparticle qualifies as a theranostic agent: gadolinium nanoparticles (GdNPs), under the name of (AGuIX) where imaging, targeting and therapy were incorporated into a single system.[88] GdNPs in the AGuIX function as a radiosensitizer. GdNPs improve tumor-targeting and diagnosis of HCC using external beam radiotherapy.[195] Conjugation of cisplatin and polysiloxane on the GdNPs allows therapy and passive tumor-targeting, respectively. Besides, functionalization of AGuIX NPs with a chelator of radiometal ($^{64}$Cu or $^{68}$Ga), NIR heptamethine cyanine dye and a bioconjugatable handle form a trifunctional (PET, MRI and optical) imaging probe with fast tumor accumulation and renal clearance.[196] AGuIX demonstrated an enhanced MRI contrast than other FDA-approved Gd chelates, and is currently under Phase Ib clinical trials and estimated to be completed in April 2021.[197]

Another close relative is the NBTXR3, a hafnium oxide radio-enhancer, which have been used in various types of cancer patients and is currently in Phase II-III clinical trials. Besides these, there are various NPs in clinical trials that have successfully incorporated dual-functions: either as imaging and targeting or imaging and therapeutic agent. Magnetic NPs have been used for anemic patients as therapy and recently developed as an MRI-contrast agent. Some commercially known brands (such as Ferumoxtran and Ferumoxytol) are ultra-

small SPIONs NPs coated with either dextran or synthetic carbohydrate shell. SPIONs NPs were initially tested clinically on various types of cancer (such as head, neck, prostate and cervical cancer) by differentiating cancerous and non-cancerous lymph nodes with the aid of an MRI. [104,198] Recently, SPIONs NPs have been used in diagnosis of multiple sclerosis, myocardial infarction diseases (see Table 2). Some Phase I clinical trials have been completed and a few studies have even advanced to Phase IV.[199,200]

Similarly, AuNPs have been translated into clinical trials since year 2008 and have been used for thermal ablation of tumors.[191,192] However, to the best of our knowledge, AuNPs has advanced to only Phase I clinical trials due to the limitation in penetration depth of laser light during PTT and their application *in vivo*.[17,201,202] The use of a fibre optic NIR laser for deeper laser penetration into tumors or a synergistic PTT and other therapies (or surgery) are some of the possible alternatives to the use of nanomaterials for PTT.[17]

Another addition to clinical trials is the Cornell or C dots which are inorganic protein-coated-fluorescent-silica NPs with potential in theranostics of melanoma.[203] C dots allow real-time pre-operative and intraoperative sentinel lymph node (SLN) tissue localization and retention using a hand-held fluorescent camera.[79] Although complete lymph node dissection for patients who had SLN biopsy was deemed inappropriate as a form of treatment after 2017,[113] the C dots are still believed to possess therapeutic effects by reduction in size of tumor and are currently under further investigation.[203] Phase III trials of both concurrent triplet combination therapy (vemurafenib, cobimetinib, atezolizumab) and sequential combination therapy (vemurafenib and cobimetinib alone) in advanced melanoma patients are ongoing.[204] The results of the trials would allow better understanding of the safety and efficacy of targeted therapy and immunotherapy combinations.

Most of the targeted theranostic probes for ovarian cancer are still in various phases of clinical trials, have yet to be approved by the FDA.[205] For the triple-negative breast cancer,

only paclitaxel and irinotecan loaded liposomes, also known as EndoTAG-1 and MM-398 have proceeded through clinical studies.[206] Phase III trial of EndoTAG-1 in combination with gemcitabine is currently ongoing in patients with pancreatic cancer. Recently, Phase I study to understand the biodistribution of MM-398 and the feasibility of using ferumoxytol as a solid tumor and brain cancer imaging agent has been completed.

Nanomaterials such as carbon nanotubes and graphene are not yet approved for clinical trials as wearable sensors, implantable devices, aid in clinical interventions and treatments of various diseases.[108] Primary challenges including human health risks (biocompatibility, biological toxicity), environmental impact, selectivity for biomarkers detection, long-term stability, should be addressed before clinically approved graphene and its derivatives move forward.

There are various clinical trials that have been terminated due to numerous reasons such as inadequate enrolment, variations in the clinical findings and no improvements compared to controls/placebos. For example, CALAA-01, a targeted nanocomplex that contains anti-ribonucleotide reductase small interfering RNA (siRNA) has been terminated after Phase I. Despite showing the potential in solid tumor, the nature and complexity of CALAA-01 raised several concerns (possible immunostimulation, coagulopathic effects, kidney toxicity, off-target deposition, hepatotoxicity), therefore hindering its clinical translation.[207]

One of the flaws in clinical trials is the disconnection between mice and human models.[202] Nanomaterials showing positive theranostic results in *in vitro* and *in vivo* settings do not grant their applicability in clinical trials, mainly due to a combination of multiple complex bio-nano interactions in the body.[68,208] Research on nanotheranostic nanomaterials is rapidly advancing to incorporate biocompatibility, specific targeting, advanced imaging and diagnosis, as well as localized drug delivery in the human body.[12,17,23,56,138] An increase in knowledge of physiochemical properties of nanomaterials coupled with the design of

multifunctional theranostic platform and microenvironment-priming approaches is likely to radically expedite clinical approval of more nanotheranostic nanomaterials and bring them to clinical applications.

**TABLE OF SUMMARY**

**Table 2 A Summary of Functional Theranostic Nanomaterials Translated into Clinical Studies**

| **Cancer/Disease/ Illness** | **Type of nanomaterial/ Composition** | **Physiochemical properties** | **Therapeutic/ Imaging modality** | **Clinical trial phase/Status** | **Ref.** |
|---|---|---|---|---|---|
| Solid tumors | Ruthenium NPs (NKP-1339) | Targeting of GRP78 (key regulator of misfolded protein processing); mean half-life: 113 hours; mean total clearance (CLtotal): 164 mL/hour | Targeting & therapy | Phase I completed (2012) | [209] |

| | | | | | |
|---|---|---|---|---|---|
| | Gold nanospheres, bounded to PEG-THIOL & recombinant human tumor necrosis factor alpha (rhTNF) | Size: 27 nm; liquid, intravenous injection; net negative surface charge | Targeting & immunostimulant therapy | Phase I completed (2012) | [210,211] |
| | Polymeric NPs, containing cyclodextrin-based polymer, small interfering RNA (siRNA), human transferrin protein (hTf) targeting ligand & hydrophilic PEG (CALAA-01) | Size: 70 nm; liquid, intravenous injection; siRNA is not chemically modified; 1:1 charge ratio of positive charged polymer to negatively charge nucleic acid; endosomal disruption & siRNA release into | Targeting & therapy (RNAi) | Phase I terminated (2012), progressive disease was observed | [207,212] |

| | | | | | |
|---|---|---|---|---|---|
| | | the cytoplasm of target cells due to imidazole residues | | | |
| Advanced solid tumors | Colloidal gold NPs, bounded with recombinant human tumor necrosis factor alpha (rhTNF) & thiolyated PEG (CYT-6091) | Size: 7-20 nm; intra-tumour injection; well-tolerated doses at 50-600 μg/$m^2$; 85 % complete remission rates | Targeting, immunotherapy & imaging | Phase I completed (2009) | [210,213] |
| Breast cancer | Liposome NPs encapsulating DOX & trastuzumab (for targeting of HER2 receptor protein) (MM-302) | Size: 100 nm; enhanced antitumor activity, activation of p53 protein levels phosphorylation/activation; decreased | Targeting & therapy | Phase II/III terminated (2017) (does not show benefit over control & confirmed *via* futility analysis) | [214] |

| | | | | | |
|---|---|---|---|---|---|
| | | intracellular signaling (p-Akt); increased DNA damage signaling | | | |
| | CdS/ZnS core-shell quantum dots, carboxylic acid-functionalized, coated with veldoreotide (VELD) | Size: 1-10 nm; conjugation with VELD at pH 7; somatostatin receptors (SSTR) agonist with anti-cancer activity; in the form of topical cream | Imaging & therapy | Phase I recruiting (estimated completion year 2022) | [215] |
| Squamous cell cancer of the head & neck | Manganese oxide (GC4419) | Intravenous injection; about 2 hours half-life with minimal | Targeting & therapy | Phase I completed (2015) | [216] |

| | | | | | |
|---|---|---|---|---|---|
| | | accumulation upon repeated dosing | | | |
| Head and neck melanoma, breast cancer, colorectal cancer | Silica NPs (cRGDY-PEG-Cy5.5-C dots) | Size: 6-7 nm; superior brightness; enhanced tumor tissue retention with low background signal; portable & real-time optical detection of nodal metastases | Tracking & imaging | Phase II ongoing (estimated completion year 2020) | [79] |
| Head and neck cancer | Ultrasuperparamagnetic nanoparticle iron oxide (Ferumoxytol) | Size: 17-31 nm; 3D quantitative tumor characterization | Targeting & imaging (MRI) | Phase I completed (2019) | [217] |

| | | | | | |
|---|---|---|---|---|---|
| Atherosclerosis | Gold NPs coated on silica/iron oxide shells | Size: 90–150 nm; stenting & micro-infusion of stem cells bearing NPs into the lesion | Targeting & therapy (plasmonic photothermal & stem cell therapy) | Phase I completed (2016) | [218] |
| Myocardial infarction | Ultrasuperparamagnetic nanoparticle iron oxide (Ferumoxytol) | Size: 17-31 nm; 4-6 times enhanced phagocytosis; higher uptake by cells due to cardiac inflammation; possible visualization of heart muscle damage area | Targeting & imaging | N/A Completed (2012) | [219] |

| | | | | | |
|---|---|---|---|---|---|
| Type 1 diabetes | Gold NPs coupled with proinsulin peptide (C19-A3 GNP) | Size: 5 nm; intradermal delivery by microneedles; negatively charged (-40 to -60 mV) | Targeting & therapy | Phase I ongoing (2016) | [220] |
| | Ultra superparamagnetic nanoparticle iron oxide (Ferumoxtran-10), dextran-coated | Size: 30 nm; monocrystalline; with long-circulating properties; real time visualization of inflammatory lesions *in vivo* | Targeting & imaging | N/A completed (2009) | [221] |
| Brain metastases | Gd NPs (AGuIX) | Size: 4.5 nm; can be used in combination with fractionated stereotactic radiation | Targeting & imaging (MRI) | Phase I recruiting (estimated completion year 2020) | [222] |

| | | | | | |
|---|---|---|---|---|---|
| | | in oligo brain metastases | | | |
| Gliosarcoma | Spherical gold NPs carrying nucleic acids & drugs (NU-0129) | Size: 13 nm; can cross the blood-brain barrier; targeting of Bcl2L12 gene to stop cancer cells from growing | Targeting & therapy | Phase I ongoing (2017) | [223] |
| Transthyretin-mediated (hATTR) amyloidosis | Lipid NPs Patisiran (ALN-TTR02) | Size: 60-100 nm; liquid, intravenous injection; prevented the deterioration of left ventricular global longitudinal strain over 18 months | Targeting & therapy (gene silencing) | Phase III completed (2017) | [224] |

| | | | | | |
|---|---|---|---|---|---|
| Thyroid cancer | Lymphotrophic superparamagnetic NPs loaded with drug (Ferumoxytol) | Size: 30 nm; intravenous injection (lyophilized iron oxide injected dose: 2.6 mg per kg of body weight); imaging with high sensitivity & specificity in detecting small lymph nodes (even 2 nm) | Imaging (MRI) & therapy | N/A completed (2015) | [225,226] |
| Prostate cancer | Hafnium oxide NPs (NBTXR3) | Size: 50 nm; liquid, intra-tumoral injection; non-pyrogen, sterile; | Targeting & therapy (radiotherapy) | Phase I & II ongoing (estimated completion year 2020) | [227] |

| | | | | | |
|---|---|---|---|---|---|
| | | white aqueous dispersion; negative surface charge; stable in aqueous solution at pH 6-8; able to deposit high energy within tumors; chemically inert in cellular & subcellular systems; therapy activated by intensity modulated radiotherapy | | | |
| | Silica NPs | Size: sub-8 nm; intravenous injection; targeting of | Targeting & imaging (PET/MRI) | Phase I ongoing (estimated | [228] |

| | | | | | |
|---|---|---|---|---|---|
| | ($^{64}$Cu-NOTA-PSMAi-PEG-Cy5.5-C' dots) | prostate-specific membrane antigen (PSMA); specific uptake at prostate specific (PC-3) cells | | completion year 2021) | |
| | Magnetic iron oxide NPs, conjugated with dual peptides targeting luteinizing hormone-releasing hormone receptor (LHRH-R) & urokinase-type plasminogen activator receptor (uPAR) | Size: 15.74 nm; surface charge: −58.06 ± 1.72 mV; preferential binding & accumulation in PC-3 cells; 2 times enhanced cytotoxicity; 10 times lesser dose required; possess double- | Targeting & imaging (MRI) | Phase I completed (2015) | [104] |

| | | | | | |
|---|---|---|---|---|---|
| | | receptor targeting and imaging capability | | | |
| Cervical cancer | Ultrasuperparamagnetic nanoparticle iron oxide (Ferumoxtran-10) | Size: 30 nm; intravenous injection; increased MRI sensitivity to detect lymph nodes metastasis | Targeting & imaging | N/A completed (2019) | [229] |
| | Gd NPs (AGuIX), grafted with additional DOTA chelates, | Size: 4.5 nm; improved longitudinal relaxivity (4.87 $s^{-1}$ | Theranostic agent (imaging, targeting & therapy) | Phase I ongoing (2019) | [88] |

| | | | | | |
|---|---|---|---|---|---|
| | complexation of bismuth | $mM^{-1}$ & $r_2$/ $r_1$ of 1.46); a contrast of 4.26 Hounsfield unit $mM^{-1}$ (close to those of clinically used CT contrast agents) | | | |
| Multiple sclerosis | Ultra superparamagnetic nanoparticle iron oxide (Ferumoxytol) | Size: 17-31 nm; intravenous injection; contrast agent for brain MRI; ultrahigh-field MRI & phase contrast; highly sensitive | Targeting & imaging (MRI) | Phase I completed (2019) | [230] |
| Pancreatic cancer | Ultrasuperparamagnetic nanoparticle iron oxide (Ferumoxytol) | Size: 17-31 nm; targeting of bombesin receptors; relaxivity: | Targeting & imaging (MRI) | Phase IV completed (2012) | [231] |

| | | | | | |
|---|---|---|---|---|---|
| | | 70 $mM^{-1}s^{-1}$; identification of small/undetectable lymph nodes metastasis | | | |
| Non-small cell lung cancer | Polymeric NPs, with a hydrophobic polylactic acid polymeric core, encapsulating DOX & hydrophilic PEG corona decorated with small molecule prostate-specific membrane antigen | Size: 100 nm; biocompatible; demonstrated dose linear pharmacokinetic profile; prolonged persistence | Targeting & therapy | Phase II completed (2016) | [232] |

| | | | | | |
|---|---|---|---|---|---|
| | (PSMA) targeting ligands (BIND-014) | | | | |
| Relapsed or refractory B cell malignancies | Polyethylenimine NPs, comprised of small interfering RNA–mediated suppression of hypusinated eukaryotic translation initiation factor 5A (eIF5A) & plasmid-based overexpression of a non-hypusinable eIF5A mutant (SNS01-T) | Size: 72 nm; rod-shaped; polydispersity index: 0.197; positive surface charge; inhibits tumor progression in a number of B-cell malignancies | Targeting & therapy (RNAi) | Phase I/II recruitment status (2014) | [233] |

| | | | | | |
|---|---|---|---|---|---|
| Relapsed or refractory leukemia | Lipid NP, composed of cationic DOTIM/cholesterol liposomes & plasmid DNA (JVRS-100) | Size: >100 nm; liquid, intramuscular injection; cationic; with immunostimulatory properties; enhanced humoral & cell-mediated immune responses | Targeting & immunotherapy | Phase I completed (2017) | [234] |
| Parkinson's disease | Gold nanocrystals, modified with montmorillonite | Single crystallized in the face centred cubic lattice; with a preferential growth direction along the (111) plane; specific surface: 327–579 | Therapy & diagnosis | Phase II ongoing (estimated completion year 2020) | [235] |

| | | | | | |
|---|---|---|---|---|---|
| | | $m^2/g$; large specific pore volumes ~0.7 $cm^3/g$; pore diameters: 0–10 nm; synthesized propargylamines with 82–94 % yield & 100 % selectivity | | | |
| Central venous catheter related infections | Impregnated with silver NPs (AgTive) | Size: 50 nm; $10^{-9}$ mol/l required for bactericidal activity; concentration of 0.8 % in an active surface of 450 $cm^2/g$ polyurethane | Targeting & therapy | Phase IV completed (2008) | [236,237] |

## CONCLUSION AND FUTURE PERSPECTIVE

Nanotheranostics refers to the use of nanomaterials capable of providing concurrent diagnostics and therapeutics at the disease sites. In this review, we have discussed the key properties of different nanomaterials, and how these nanomaterials are designed and tuned to meet the selectivity and specificity of the target disease. The specific properties of the nanomaterials in terms of feasibility, drawbacks and their potential applications in nanotheranostics were presented.

Both solid and liquid cancerous tumors are different in regard to their tumor vascularity and heterogeneity, which require different diagnostic treatment and targeting strategies. Au nanostructures are biocompatible and permit facile surface functionalization for wide biological applications. In addition, Au nanostructures serve as a good photothermal transducer. Conjugation of a photosensitizer on the Au-based nanoplatform could generate high singlet oxygen and activate PDT. Most of the nanomaterials presented here are stimuli-responsive, able to kick-start the sequential theranostic effects and release the chemotherapeutic drugs only when reaching tumor sites. If the potential side effects of each drug are well-understood, future studies can be expected on the co-delivery of drug combinations in a single platform for broader pharmacological applications.

Inorganic nanomaterials are relatively stable over large ranges of pH and temperature, yet, concerns are raised over their low biodegradation and biosafety issues. Modification of different molecules (targeting and imaging contrast agents, drugs) on the surface of the inorganic nanomaterials permits diverse applications of the nanomaterials. However, the characterization and fairly weak fundamental understanding of the structure-function correlations often restrict its predictive functions in nanotheranostics. Polymeric and lipid NPs are usually used as nano-vehicles for delivering therapeutics and diagnostics agents to the tumor sites, thanks to their biocompatibility and biostability features. Generally, the poor

spatial resolution, shallow tissue penetration and relatively low quantum yield are some of the challenges of NIR-emissive polymeric NPs in theranostics. Since each drug varies in their surface area and solubility, their loading mechanism into lipid NPs sometimes remain challenging. Knowledge of the drug loading mechanism allows optimal formulation of the nanocarrier system with theranostic properties and minimal limitations or potential side effects.

Being one of the most interesting and versatile materials, graphene and its derivatives offer a relatively simple but highly integrated and multifunctional nanotheranostic platform for biomedical applications. Nevertheless, more systemic investigations are required to better understand its behavior, biodegradability and toxicological profiles in complex biological environment.

Concerning nanotheranostic applications in liquid tumors, researches are still in its infancy compared to solid tumor. Most of the approaches done thus far are directed to the diagnosis and treatment of blood cancers, such as lymphoma and leukemia. It is surprising to note that although the physico-chemical scenario of blood cancers is different to solid tumors, the same types of nanomaterials are being used. This can be clearly observed in the use of metal NPs for thermal ablation in both solid and liquid tumors. In solid tumors, the nanomaterial is anchored to the surface of the tumor leading to an effective and non-invasive ablation, whereas in liquid tumor, the target element is in constant circulation and this can lead to ablation of adjacent tissue. The same phenomenon is observed with the use of polymeric and lipid NPs as drug delivery systems in both solid and liquid tumor, where it is not clear the different requirements in terms of blood-brain barrier penetration, stability and renal clearance. This question needs to be solved and more work should be carried out in order to push the nanotheranostics for *in vivo* applications in circulating tumors.

For neurodegenerative diseases, all the nanotheranostic strategies have been applied for the diagnosis and treatment of Alzheimer disease and interestingly the selection of the nanomaterial is based on the therapeutic strategy (inhibition of Aβ aggregation and $Cu^{2+}$ ions chelation). In both cases, fluorescence imaging modality is selected as a cost-effective and simple alternative to MRI and PET. Moreover, both therapy strategies have proven to be effective in *in vivo* therapy of Alzheimer disease, although it would be important to develop them also for the other neurodegenerative diseases.

The NPs used for the theranostics of autoimmune diseases can be colloidal-based or organic-based. The nanomaterials are mostly designed for targeting of the scavenger receptor present on the activated macrophages. The NPs permit prolonged circulation in the bloodstream and subsequently controlled release of the therapeutic drugs at the inflammation sites. Safety concern (biodistribution in non-targeted tissues, potential inflammation, biodegradability, biocompatibility and clearance) is the biggest obstacle that hampers the clinical application of most of the nanomedicine of RA.

For cardiovascular diseases, the research is mainly focused on the non-invasive imaging modalities such as MRI and NIR fluorescence for detection of atherosclerotic plaque. The pursuit of therapeutic agents for atherosclerosis and its potential impact remains an open field for research. Currently, there is less information about the dose, pharmacokinetics, long-term side effects and toxicology of the NPs employed in most of the studies. Future research should also be emphasized on more detailed biocompatibility (such as blood-half-life) and immunogenicity evaluation of the NPs, as well as development towards precision drug delivery and early detection of atherosclerotic plaque.

Inorganic NPs as antibacterial agents still face drawbacks such as non-specific biological toxicity or potential long-term *in vivo* retention. Applications of metal-free antibacterial agents are limited by poor stability and biocompatibility, complicated synthetic steps, and

limited material structural tunability. Besides, the long-term biosafety of antibacterial nanomaterials is another big concern as it usually associated with possible risks including excessive or insufficient heating, undesired diffusion and potential impact on the immune system.

Continuous and multiple pharmacological and physical approaches have been developed to overcome biological and physiological barriers of the nanomaterials in complex biological systems. The ideal size of the NPs is highly dependent on the cancer type, tumor site and the stage of the diseases. Overall, NPs with a tunable size between 10-100 nm is the most favorable in the development of cancer theranostics, mainly due to enhanced cellular uptake, biodistribution, blood circulation half-life, cellular uptake, tumor penetration and targeting at this size range.

The pH value, antioxidant levels and enzymatic activity belong to endogenous stimuli; while light, ultrasound and magnetic are some of the examples of external stimuli. Theranostic applicability of external stimuli-responsive nanomaterials is less dependent on tumor type or pathological properties. Such nanomaterials can be applied at the diseases site in a controlled manner, but the efficacy is severally compromised in metastasized lesions. In contrast, theranostic efficacy of endogenous stimuli-sensitive nanomaterials is highly heterogeneous between different types of tumors/diseases. Moreover, staging (a process to determine if cancer has spread within the organ or to other parts of the body) is important to determine the stage of the cancer/disease. The design of nanomaterials (dose requirements, efficacy, side effects, *etc*.) must be tuned according to the pathological properties of tumors/diseases.

Safety, efficiency and controllability are the major criteria in biomedical applications. Eco-toxicological, biosafety and biocompatibility evaluation must be conducted for theranostic nanomaterials, taking into account factors including route of administration/exposure, biodistribution, biodegradability, long-term exposure, *etc*. The morphology, size distribution,

nature of interfaces (charges and surface chemistry) and colloidal stability of the nanomaterials in different media might influence the nanotoxicity of nanomaterials. The interaction of NPs with cell organelles also requires further studies as it plays a critical role in impacting the biogenesis and biological activities.

No theranostic nanomaterials have been approved by the FDA for commercialization to date, mainly due to significant heterogeneity in the design, synthesis, safety and efficacy of the nanomaterials in clinical trials. The behavior of the nanomaterials in the dynamic physiological and pathological alterations *in vivo* is not well-defined too. Most of the current nanomaterials are in various phases of clinical trials, though the future perspective is brilliant. Future research should be focused on improving the clinical relevance and translational feasibility of nanomaterials for theranostic applications. The strength and limitations of each nanomaterial, particularly the potential side effects/toxicities, should be comprehensively understood upon developing them with robust efficacy and clinical benefit. Understanding of pharmacokinetic profile of nanomaterials in humans should be emphasized, along with clinical translation in appropriate animal models. After all the concerted efforts from multidisciplinary teams of chemist, pharmacists, physicists and engineers, it is believed that nanomaterials promise revolutionary potential as theranostic agents for a variety of clinical applications and improving the quality of life of the population.

## AUTHOR INFORMATION


### Corresponding authors

* E-mail: Kasturi.Muthoosamy@nottingham.edu.my

* E-mail: arben.merkoci@icn2.cat

### ORCID

Xin Yi Wong: 0000-0002-8673-9345

Amadeo Sena-Torralba: 0000-0003-1340-1383

Ruslan Alvarez Diduk: 0000-0002-9876-1574

Kasturi Muthoosamy: 0000-0003-3752-5794

Arben Merkoçi: 0000-0003-2486-8085

## ACKNOWLEDGMENTS

This work was supported by the Fundamental Research Grant Scheme (FRGS), Ministry of Higher Education (MOHE), Malaysia [FRGS/1/2016/STG07/UNIM/02/1]. This work is also funded by the CERCA Program/ Generalitat de Catalunya. ICN2 acknowledges the support of the Spanish MINECO for the Project MAT2017-87202-P and through the Severo Ochoa Centers of Excellence Program under Grant SEV2201320295.

## VOCABULARY

**nanotheranostics**, development of nanomedicine approaches for advanced theranostics (combined therapeutic and imaging/diagnostic features); **nanomaterials**, materials with one or more external dimensions in the nanoscale (sizes range from about 1-100 nm); **photothermal therapy**, thermal ablation of cancer cells with the use of photoabsorbing agents that could efficiently transfer the absorbed light energy into heat, subsequently leading to cell death; **photodynamic therapy**, an externally activatable treatment with the use of photosensitizer molecules to generate cytotoxic singlet or reactive oxygen species to kill cancer cells *via* oxidative stress; **passive targeting**, delivery of nanoparticles *via* enhanced permeability and retention effect in tumor or any leaky vasculature and anatomic barrier; **active targeting**, delivery of nanoparticles to the tissue of interest based on molecular, ligand/receptor or antibody-antigen recognition. More focused delivery with reduced potential side effects, toxicity and cost of drug/delivery; **graphene**, single-layered carbon atoms packed into a two-dimensional honeycomb lattice.

**REFERENCES**


(1) Jagtap, P.; Sritharan, V.; Gupta, S. Nanotheranostic Approaches for Management of Bloodstream Bacterial Infections. *Nanomedicine Nanotechnology, Biol. Med.* **2017**, *13*, 329–341.

(2) Krishnan, V. Theranostics-Revolutionizing Conventional Orthodontic Care! *J. World Fed. Orthod.* **2019**, *8*, 1–2.

(3) Caldorera-Moore, M. E.; Liechty, W. B.; Peppas, N. A. Responsive Theranostic Systems: Integration of Diagnostic Imaging Agents and Responsive Controlled Release Drug Delivery Carriers. *Acc. Chem. Res.* **2011**, *44*, 1061–1070.

(4) Ko, C.-N.; Li, G.; Leung, C.-H.; Ma, D.-L. Dual Function Luminescent Transition Metal Complexes for Cancer Theranostics: The Combination of Diagnosis and Therapy. *Coord. Chem. Rev.* **2019**, *381*, 79–103.

(5) Yang, Z.; Song, J.; Tang, W.; Fan, W.; Dai, Y.; Shen, Z.; Lin, L.; Cheng, S.; Liu, Y.; Niu, G.; Rong, P.; Wang, W.; Chen, X. Stimuli-Responsive Nanotheranostics for Real-Time Monitoring Drug Release by Photoacoustic Imaging. *Theranostics.* **2019**, *9*, 526–536.

(6) Kim, H.; Kwak, G.; Kim, K.; Yoon, H. Y.; Kwon, I. C. Theranostic Designs of Biomaterials for Precision Medicine in Cancer Therapy. *Biomaterials.* **2019**, *213*, 119207.

(7) Mura, S.; Couvreur, P. Nanotheranostics for Personalized Medicine. *Adv Drug Deliv Rev*. **2012**, *64*, 1394–1416.

(8) Lim, E.-K.; Kim, T.; Paik, S.; Haam, S.; Huh, Y.-M.; Lee, K. Nanomaterials for Theranostics: Recent Advances and Future Challenges. *Chem. Rev.* **2015**, *115*, 327–394.

(9) Patel, K. D.; Singh, R. K.; Kim, H. W. Carbon-Based Nanomaterials As An Emerging Platform for Theranostics. *Mater. Horizons.* **2019**, *6*, 434–469.

(10) Thakor, A. S.; Gambhir, S. S. Nanooncology: The Future of Cancer Diagnosis and Therapy. *CA. Cancer J. Clin.* **2013**, *63*, 395–418.

(11) Kojima, R.; Aubel, D.; Fussenegger, M. Novel Theranostic Agents for Next-Generation Personalized Medicine: Small Molecules, Nanoparticles, and Engineered Mammalian Cells. *Curr. Opin. Chem. Biol.* **2015**, *28*, 29–38.

(12) Roma-Rodrigues, C.; Pombo, I.; Raposo, L.; Pedrosa, P.; Fernandes, A. R.; Baptista, P. V. Nanotheranostics Targeting the Tumor Microenvironment. *Front. Bioeng. Biotechnol.* **2019**, *7*, 197.

(13) Chen, X.; Song, J.; Chen, X.; Yang, H. X-Ray-Activated Nanosystems for Theranostic Applications. *Chem. Soc. Rev.* **2019**, *48*, 3073–3101.

(14) Yang, K.; Feng, L.; Shi, X.; Liu, Z. Nano-Graphene in Biomedicine: Theranostic Applications. *Chem. Soc. Rev.* **2013**, *42*, 530–547.

(15) Qi, C.; Lin, J.; Fu, L. H.; Huang, P. Calcium-Based Biomaterials for Diagnosis, Treatment, and Theranostics. *Chem. Soc. Rev.* **2018**, *47*, 357–403.

(16) Tao, Y.; Li, M.; Ren, J.; Qu, X. Metal Nanoclusters: Novel Probes for Diagnostic and Therapeutic Applications. *Chem. Soc. Rev.* **2015**, *44*, 8636–8663.

(17) Liu, Y.; Bhattarai, P.; Dai, Z.; Chen, X. Photothermal Therapy and Photoacoustic Imaging: *Via* Nanotheranostics in Fighting Cancer. *Chem. Soc. Rev.* **2019**, *48*, 2053–2108.

(18) Meng, H.; Leong, W.; Leong, K. W.; Chen, C.; Zhao, Y. Walking the Line: The Fate of Nanomaterials at Biological Barriers. *Biomaterials.* **2018**, *174*, 41–53.

(19) Nabil, G.; Bhise, K.; Sau, S.; Atef, M.; El-Banna, H. A.; Iyer, A. K. Nano-Engineered Delivery Systems for Cancer Imaging and Therapy: Recent Advances, Future Direction and Patent Evaluation. *Drug Discov. Today.* **2019**, *24*, 462–491.

(20) Zhang, P.; Wang, J.; Chen, H.; Zhao, L.; Chen, B.; Chu, C.; Liu, H.; Qin, Z.; Liu, J.;

Tan, Y.; Chen, X; Liu, G. Tumor Microenvironment-Responsive Ultrasmall Nanodrug Generators with Enhanced Tumor Delivery and Penetration. *J. Am. Chem. Soc.* **2018**, *140*, 14980–14989.

(21) Frost, R.; Langhammer, C.; Cedervall, T. Real-Time *In Situ* Analysis of Biocorona Formation and Evolution on Silica Nanoparticles in Defined and Complex Biological Environments. *Nanoscale.* **2017**, *9*, 3620–3628.

(22) Nierenberg, D.; Khaled, A. R.; Flores, O. Formation of a Protein Corona Influences the Biological Identity of Nanomaterials. *Rep Pract Oncol Radiother.* **2018**, *23*, 300–308.

(23) Zhou, Y.; Dai, Z. New Strategies in the Design of Nanomedicines to Oppose Uptake by the Mononuclear Phagocyte System and Enhance Cancer Therapeutic Efficacy. *Chem. – An Asian J.* **2018**, *13*, 3333–3340.

(24) Oh, J. Y.; Kim, H. S.; Palanikumar, L.; Go, E. M.; Jana, B.; Park, S. A.; Kim, H. Y.; Kim, K.; Seo, J. K.; Kwak, S. K.; Kim, C.; Kang, S.; Ryu, J.-H. Cloaking Nanoparticles with Protein Corona Shield for Targeted Drug Delivery. *Nat. Commun.* **2018**, *9*, 4548.

(25) Kong, H.; Xia, K.; Ren, N.; Cui, Y.; Liu, R.; Li, Q.; Lv, M.; Shi, J.; Yan, Q.; Cui, Z.; Fan, C.; Zhu, Y.; Wang, L. Serum Protein Corona-Responsive Autophagy Tuning in Cells. *Nanoscale.* **2018**, *10*, 18055–18063.

(26) Wang, X.; Zhu, Y.; Chen, M.; Yan, M.; Zeng, G.; Huang, D. How Do Proteins 'Response' to Common Carbon Nanomaterials? *Adv. Colloid Interface Sci.* **2019**, *270*, 101–107.

(27) Franqui, L. S.; De Farias, M. A.; Portugal, R. V; Costa, C. A. R.; Domingues, R. R.; Souza Filho, A. G.; Coluci, V. R.; Leme, A. F. P.; Martinez, D. S. T. Interaction of Graphene Oxide with Cell Culture Medium: Evaluating the Fetal Bovine Serum Protein Corona Formation towards *In Vitro* Nanotoxicity Assessment and Nanobiointeractions. *Mater. Sci. Eng. C.* **2019**, *100*, 363–377.

(28) Zamboni, W. C.; Szebeni, J.; Kozlov, S. V; Lucas, A. T.; Piscitelli, J. A.; Dobrovolskaia, M. A. Animal Models for Analysis of Immunological Responses to Nanomaterials: Challenges and Considerations. *Adv. Drug Deliv. Rev.* **2018**, *136–137*, 82–96.

(29) Pei, Y.; Chen, L.; Huang, Y.; Wang, J.; Feng, J.; Xu, M.; Chen, Y.; Song, Q.; Jiang, G.; Gu, X.; Zhang, Q.; Gao, X.; Chen, J. Sequential Targeting TGF-β Signaling and KRAS Mutation Increases Therapeutic Efficacy in Pancreatic Cancer. *Small.* **2019**, *15*, 1900631.

(30) Peng, J.; Yang, Q.; Shi, K.; Xiao, Y.; Wei, X.; Qian, Z. Intratumoral Fate of Functional Nanoparticles in Response to Microenvironment Factor: Implications on Cancer Diagnosis and Therapy. *Adv. Drug Deliv. Rev.* **2019**, *143*, 37–67.

(31) Li, Z.; Yu, X. F.; Chu, P. K. Recent Advances in Cell-Mediated Nanomaterial Delivery Systems for Photothermal Therapy. *J. Mater. Chem. B.* **2018**, *6*, 1296.

(32) Chen, Y.; Liu, X.; Yuan, H.; Yang, Z.; von Roemeling, C. A.; Qie, Y.; Zhao, H.; Wang, Y.; Jiang, W.; Kim, B. Y. S. Therapeutic Remodeling of the Tumor Microenvironment Enhances Nanoparticle Delivery. *Adv. Sci.* **2019**, *6*, 1802070.

(33) Maloney, E.; Dufort, C. C.; Provenzano, P. P.; Farr, N.; Carlson, M. A.; Vohra, R.; Park, J.; Hingorani, S. R.; Lee, D. Non-Invasive Monitoring of Stromal Biophysics with Targeted Depletion of Hyaluronan in Pancreatic Ductal Adenocarcinoma. *Cancers (Basel).* **2019**, *11*, 772.

(34) Denton, C. P.; Ong, V. H.; Xu, S.; Chen-Harris, H.; Modrusan, Z.; Lafyatis, R.; Khanna, D.; Jahreis, A.; Siegel, J.; Sornasse, T. Therapeutic Interleukin-6 Blockade Reverses Transforming Growth Factor-Beta Pathway Activation in Dermal Fibroblasts: Insights from the FaSScinate Clinical Trial in Systemic Sclerosis. *Ann. Rheum. Dis.* **2018**, *77*, 1362–1371.

(35) DeBerardinis, R. J.; Chandel, N. S. Fundamentals of Cancer Metabolism. *Sci. Adv.* **2016**,

*2*, e1600200. DOI: 10.1126/sciadv.1600200.

(36) Nakamura, Y.; Mochida, A.; Choyke, P. L.; Kobayashi, H. Nanodrug Delivery: Is the Enhanced Permeability and Retention Effect Sufficient for Curing Cancer? *Bioconjug. Chem.* **2016**, *27*, 2225–2238.

(37) Vinhas, R.; Mendes, R.; Fernandes, A. R.; Baptista, P. V. Nanoparticles—Emerging Potential for Managing Leukemia and Lymphoma. *Front. Bioeng. Biotechnol.* **2017**, *5*, 1–10.

(38) Cheng, L.; Wang, C.; Liu, Z. Functional Nanomaterials for Phototherapies of Cancer. *Chinese J. Clin. Oncol.* **2014**, *41*, 18–26.

(39) Ma, Z.; Wan, H.; Wang, W.; Zhang, X.; Uno, T.; Yang, Q.; Yue, J.; Gao, H.; Zhong, Y.; Tian, Y.; Sun, Q.; Liang, Y.; Dai, H. A Theranostic Agent for Cancer Therapy and Imaging in the Second Near-Infrared Window. *Nano Res.* **2019**, *12*, 273–279.

(40) Sun, Q.; Ojha, T.; Kiessling, F.; Lammers, T.; Shi, Y. Enhancing Tumor Penetration of Nanomedicines. *Biomacromolecules.* **2017**, *18*, 1449–1459.

(41) Zhang, D.; Zheng, A.; Li, J.; Wu, M.; Wu, L.; Wei, Z.; Liao, N.; Zhang, X.; Cai, Z.; Yang, H.; Liu, G.; Liu, X.; Liu, J. Smart Cu(II)-Aptamer Complexes Based Gold Nanoplatform for Tumor Micro-Environment Triggered Programmable Intracellular Prodrug Release, Photodynamic Treatment and Aggregation Induced Photothermal Therapy of Hepatocellular Carcinoma. *Theranostics.* **2017**, *7*, 164–179.

(42) Chen, H.; Li, F.; Yao, Y.; Wang, Z.; Zhang, Z.; Tan, N. Redox Dual-Responsive and O2-Evolving Theranostic Nanosystem for Highly Selective Chemotherapy against Hypoxic Tumors. *Theranostics.* **2019**, *9*, 90–103.

(43) Zhou, R.; Wang, H.; Yang, Y.; Zhang, C.; Dong, X.; Du, J.; Yan, L.; Zhang, G.; Gu, Z.; Zhao, Y. Tumor Microenvironment-Manipulated Radiocatalytic Sensitizer Based on Bismuth Heteropolytungstate for Radiotherapy Enhancement. *Biomaterials.* **2019**, *189*,

11–22.

(44) Wei, J.; Li, J.; Sun, D.; Li, Q.; Ma, J.; Chen, X.; Zhu, X.; Zheng, N. A Novel Theranostic Nanoplatform Based on Pd at Pt-PEG-Ce6 for Enhanced Photodynamic Therapy by Modulating Tumor Hypoxia Microenvironment. *Adv. Funct. Mater.* **2018**, *28*, 1706310.

(45) Liu, Y.; Jia, Q.; Guo, Q.; Wei, W.; Zhou, J. Simultaneously Activating Highly Selective Ratiometric MRI and Synergistic Therapy in Response to Intratumoral Oxidability and Acidity. *Biomaterials.* **2018**, *180*, 104–116.

(46) Piao, J. G.; Gao, F.; Li, Y.; Yu, L.; Liu, D.; Tan, Z. Bin; Xiong, Y.; Yang, L.; You, Y. Z. PH-Sensitive Zwitterionic Coating of Gold Nanocages Improves Tumor Targeting and Photothermal Treatment Efficacy. *Nano Res.* **2018**, *11*, 3193–3204.

(47) Zhou, J.; Xue, C.; Hou, Y.; Li, M.; Hu, Y.; Chen, Q.; Li, Y.; Li, K.; Song, G.; Cai, K.; Luo, Z. Oxygenated Theranostic Nanoplatforms with Intracellular Agglomeration Behavior for Improving the Treatment Efficacy of Hypoxic Tumors. *Biomaterials.* **2019**, *197*, 129–145.

(48) Liu, S.; Wang, L.; Zhang, M.; Tao, K.; Wang, B.; Lin, M.; Zhang, X.; Liu, Y.; Hou, Y.; Zhang, H.; Bai, Y. Tumor Microenvironment-Responsive Nanoshuttles with Sodium Citrate Modification for Hierarchical Targeting and Improved Tumor Theranostics. *ACS Appl. Mater. Interfaces.* **2019**, *11*, 25730–25739.

(49) Zhang, W.; Cai, K.; Li, X.; Zhang, J.; Ma, Z.; Foda, M. F.; Mu, Y.; Dai, X.; Han, H. Au Hollow Nanorods-Chimeric Peptide Nanocarrier for NIR-II Photothermal Therapy and Real-Time Apoptosis Imaging for Tumor Theranostics. *Theranostics.* **2019**, *9*, 4971–4981.

(50) Das, P.; Fatehbasharzad, P.; Colombo, M.; Fiandra, L.; Prosperi, D. Multifunctional Magnetic Gold Nanomaterials for Cancer. *Trends Biotechnol.* **2019**, *37*, 995–1010.

(51) Zhang, X.; Xi, Z.; Machuki, J. O.; Luo, J.; Yang, D.; Li, J.; Cai, W.; Yang, Y.; Zhang,

L.; Tian, J.; Guo, K. Gold Cube-in-Cube Based Oxygen Nanogenerator: A Theranostic Nanoplatform for Modulating Tumor Microenvironment for Precise Chemo-Phototherapy and Multimodal Imaging. *ACS Nano.* **2019**, *13*, 5306–5325.

(52) Chen, J.; Glaus, C.; Laforest, R.; Zhang, Q.; Yang, M.; Gidding, M.; Welch, M. J.; Xia, Y. Gold Nanocages As Photothermal Transducers for Cancer Treatment. *Small.* **2010**, *6*, 811–817.

(53) Xing, R.; Zou, Q.; Yuan, C.; Zhao, L.; Chang, R.; Yan, X. Self-assembling Endogenous Biliverdin As a Versatile Near-Infrared Photothermal Nanoagent for Cancer Theranostics. *Adv. Mater.* **2019**, *31*, 1900822.

(54) Chen, J.; Ning, C.; Zhou, Z.; Yu, P.; Zhu, Y.; Tan, G.; Mao, C. Nanomaterials As Photothermal Therapeutic Agents. *Prog. Mater. Sci.* **2019**, *99*, 1–26.

(55) Li, Z.; Aranda-Ramos, A.; Güell-Grau, P.; Tajada, J. L.; Pou-Macayo, L.; Lope Piedrafita, S.; Pi, F.; G. Roca, A.; Baró, M. D.; Sort, J.; Nogués, C.; Nogués, J.; Sepúlveda, B. Magnetically Amplified Photothermal Therapies and Multimodal Imaging with Magneto-Plasmonic Nanodomes. *Appl. Mater. Today.* **2018**, *12*, 430–440.

(56) Lu, J.; Wang, J.; Ling, D. Surface Engineering of Nanoparticles for Targeted Delivery to Hepatocellular Carcinoma. *Small.* **2018**, *14*, 1702037.

(57) Gao, Y.; Zheng, Q. C.; Xu, S.; Yuan, Y.; Cheng, X.; Jiang, S.; Kenry; Yu, Q.; Song, Z.; Liu, B.; Li, M. Theranostic Nanodots with Aggregation-Induced Emission Characteristic for Targeted and Image-Guided Photodynamic Therapy of Hepatocellular Carcinoma. *Theranostics.* **2019**, *9*, 1264–1279.

(58) Mu, W.; Jiang, D.; Mu, S.; Liang, S.; Liu, Y.; Zhang, N. Promoting Early Diagnosis and Precise Therapy of Hepatocellular Carcinoma by Glypican-3-Targeted Synergistic Chemo-Photothermal Theranostics. *ACS Appl. Mater. Interfaces.* **2019**, *11*, 23591–23604.

(59) Han, X.; Xu, K.; Taratula, O.; Farsad, K. Applications of Nanoparticles in Biomedical Imaging. *Nanoscale.* **2019**, *11*, 799–819.

(60) Li, Q.; Hou, M.; Ren, J.; Lu, S.; Xu, Z.; Li, C. M.; Kang, Y.; Xue, P. Co-Delivery of Chlorin E6 and Doxorubicin Using PEGylated Hollow Nanocapsules for 'All-In-One' Tumor Theranostics. *Nanomedicine* **2019**, *14*, 2273-2292.

(61) Shen, S.; Wu, Y.; Li, K.; Wang, Y.; Wu, J.; Zeng, Y.; Wu, D. Versatile Hyaluronic Acid Modified AQ4N-Cu(II)-Gossypol Infinite Coordination Polymer Nanoparticles: Multiple Tumor Targeting, Highly Efficient Synergistic Chemotherapy, and Real-Time Self-Monitoring. *Biomaterials.* **2018**, *154*, 197–212.

(62) Li, Z.; Lopez-Ortega, A.; Aranda-Ramos, A.; Tajada, J. L.; Sort, J.; Nogues, C.; Vavassori, P.; Nogues, J.; Sepulveda, B. Simultaneous Local Heating/Thermometry Based on Plasmonic Magnetochromic Nanoheaters. *Small.* **2018**, *14*, 1800868.

(63) Xiaju, C.; Rui, S.; Ling, Y.; Zhifang, C.; Haibin, S.; Mingyuan, G. Light-Triggered Assembly of Gold Nanoparticles for Photothermal Therapy and Photoacoustic Imaging of Tumors *In Vivo*. *Adv. Mater.* **2017**, *29*, 1604894.

(64) Smith, B. R.; Gambhir, S. S. Nanomaterials for *In Vivo* Imaging. *Chem. Rev.* **2017**, *117*, 901–986.

(65) Yang, H.; Liu, C.; Yang, D.; Zhang, H.; Xi, Z. Comparative Study of Cytotoxicity, Oxidative Stress and Genotoxicity Induced by Four Typical Nanomaterials: The Role of Particle Size, Shape and Composition. *J. Appl. Toxicol.* **2009**, *29*, 69–78.

(66) Liu, Y.; Wu, L.; Tong, R.; Yang, F.; Yin, L.; Li, M.; You, L.; Xue, J.; Lu, Y. PD-1/PD-L1 Inhibitors in Cervical Cancer. *Front. Pharmacol.* **2019**, *10*, 65.

(67) Wang, D.; Meng, L.; Fei, Z.; Hou, C.; Long, J.; Zeng, L.; Dyson, P. J.; Huang, P. Multi-Layered Tumor-Targeting Photothermal-Doxorubicin Releasing Nanotubes Eradicate Tumors: *In Vivo* with Negligible Systemic Toxicity. *Nanoscale* **2018**, *10*, 8536–8546.

(68) Wolfram, J.; Ferrari, M. Clinical Cancer Nanomedicine. *Nano Today.* **2019**, *25*, 85–98.

(69) Maurizi, L.; Papa, A.-L.; Boudon, J.; Sudhakaran, S.; Pruvot, B.; Vandroux, D.; Chluba, J.; Lizard, G.; Millot, N. Toxicological Risk Assessment of Emerging Nanomaterials: Cytotoxicity, Cellular Uptake, Effects on Biogenesis and Cell Organelle Activity, Acute Toxicity and Biodistribution of Oxide Nanoparticles. In *Unraveling the Safety Profile of Nanoscale Particles and Materials - From Biomedical to Environmental Applications*; IntechOpen: London, 2018; pp 17–36.

(70) Veeranarayanan, S.; Mohamed, M. S.; Poulose, A. C.; Rinya, M.; Sakamoto, Y.; Maekawa, T.; Kumar, D. S. Photodynamic Therapy at Ultra-Low NIR Laser Power and X-Ray Imaging Using Cu3BiS3 Nanocrystals. *Theranostics.* **2018**, *8*, 5231–5245.

(71) Hou, G.; Qian, J.; Xu, W.; Sun, T.; Wang, Y.; Wang, J.; Ji, L.; Suo, A. A Novel PH-Sensitive Targeting Polysaccharide-Gold Nanorod Conjugate for Combined Photothermal-Chemotherapy of Breast Cancer. *Carbohydr. Polym.* **2019**, *212*, 334–344.

(72) Li, B.; Wang, Y.; He, J. Gold Nanorods-Based Smart Nanoplatforms for Synergic Thermotherapy and Chemotherapy of Tumor Metastasis. *ACS Appl. Mater. Interfaces.* **2019**, *11*, 7800–7811.

(73) Li, Y.; Zhang, X.; Zhang, Z.; Wu, H.; Xu, X.; Gu, Z. Tumor-Adapting and Tumor-Remodeling AuNR@dendrimer-Assembly Nanohybrids Overcome Impermeable Multidrug-Resistant Cancer. *Mater. Horizons.* **2018**, *5*, 1047–1057.

(74) Gubbels, J. A.; Claussen, N.; Kapur, A. K.; Connor, J. P.; Patankar, M. S. The Detection, Treatment, and Biology of Epithelial Ovarian Cancer. *J. Ovarian Res.* **2010**, *3*, 1–11.

(75) Ju, Y.; Dong, B.; Yu, J.; Hou, Y. Inherent Multifunctional Inorganic Nanomaterials for Imaging-Guided Cancer Therapy. *Nano Today.* **2019**, *26*, 108–122.

(76) Poudel, K.; Gautam, M.; Jin, S. G.; Choi, H.-G.; Yong, C. S.; Kim, J. O. Copper Sulfide: An Emerging Adaptable Nanoplatform in Cancer Theranostics. *Int. J. Pharm.* **2019**, *562*,

135–150.

(77) Liang, L.; Peng, S.; Yuan, Z.; Wei, C.; He, Y.; Zheng, J.; Gu, Y.; Chen, H. Biocompatible Tumor-Targeting Nanocomposites Based on CuS for Tumor Imaging and Photothermal Therapy. *RSC Adv.* **2018**, *8*, 6013–6026. DOI: 10.1039/C7RA12796K

(78) Liu, Z.; Wang, F.; Chen, X. Integrin Avβ3-Targeted Cancer Therapy. *Drug Dev. Res.* **2008**, *69*, 329–339.

(79) Bradbury, M. S.; Phillips, E.; Montero, P. H.; Cheal, S. M.; Stambuk, H.; Durack, J. C.; Sofocleous, C. T.; Meester, R. J. C.; Wiesner, U.; Patel, S. Clinically-Translated Silica Nanoparticles As Dual-Modality Cancer-Targeted Probes for Image-Guided Surgery and Interventions. *Integr. Biol. (Camb).* **2013**, *5*, 74–86.

(80) Liu, Z.; Zhang, S.; Lin, H.; Zhao, M.; Yao, H.; Zhang, L.; Peng, W.; Chen, Y. Theranostic 2D Ultrathin MnO2nanosheets with Fast Responsibility to Endogenous Tumor Microenvironment and Exogenous NIR Irradiation. *Biomaterials.* **2018**, *155*, 54–63.

(81) Liu, L.; Liu, Y.; Ma, L.; Mao, F.; Jiang, A.; Liu, D.; Wang, L.; Jia, Q.; Zhou, J. Artemisinin-Loaded Mesoporous Nanoplatform for PH-Responsive Radical Generation Synergistic Tumor Theranostics. *ACS Appl. Mater. Interfaces.* **2018**, *10*, 6155–6167.

(82) Han, Y.; An, Y.; Jia, G.; Wang, X.; He, C.; Ding, Y.; Tang, Q. Theranostic Micelles Based on Upconversion Nanoparticles for Dual-Modality Imaging and Photodynamic Therapy in Hepatocellular Carcinoma. *Nanoscale.* **2018**, *10*, 6511–6523.

(83) Wang, C.; Cheng, L.; Liu, Z. Upconversion Nanoparticles for Photodynamic Therapy and Other Cancer Therapeutics. *Theranostics.* **2013**, *3*, 317–330.

(84) Shi, X.; He, D.; Tang, G.; Tang, Q.; Xiong, R.; Ouyang, H.; Yu, C. Y. Fabrication and Characterization of a Folic Acid-Bound 5-Fluorouracil Loaded Quantum Dot System for Hepatocellular Carcinoma Targeted Therapy. *RSC Adv.* **2018**, *8*, 19868–19878. DOI:

10.1039/C8RA01025K

(85) Ma, J. J.; Yu, M. X.; Zhang, Z.; Cai, W. G.; Zhang, Z. L.; Zhu, H. L.; Cheng, Q. Y.; Tian, Z. Q.; Pang, D. W. Gd-DTPA-Coupled Ag2Se Quantum Dots for Dual-Modality Magnetic Resonance Imaging and Fluorescence Imaging in the Second Near-Infrared Window. *Nanoscale.* **2018**, *10*, 10699–10704.

(86) Lee, K. E.; Hesketh, A. V.; Kelly, T. L. Chemical Stability and Degradation Mechanisms of Triangular Ag, Ag@Au, and Au Nanoprisms. *Phys. Chem. Chem. Phys.* **2014**, *16*, 12407–12414.

(87) Du, J.; Zheng, X.; Yong, Y.; Yu, J.; Dong, X.; Zhang, C.; Zhou, R.; Li, B.; Yan, L.; Chen, C.; Gu, Z.; Zhao, Y. Design of TPGS-Functionalized Cu3BiS3 Nanocrystals with Strong Absorption in the Second Near-Infrared Window for Radiation Therapy Enhancement. *Nanoscale* **2017**, *9*, 8229–8239.

(88) Lux, F.; Tran, V. L.; Thomas, E.; Dufort, S.; Rossetti, F.; Martini, M.; Truillet, C.; Doussineau, T.; Bort, G.; Denat, F.; Boschetti, F.; Angelovski. G.; Detappe, A.; Crémillieux, Y.; Mignet, N.; Doan, B.T.; Larrat, B.; Meriaux, S.; Barbier, E.; Roux, S; *et al.* AGuIX® from Bench to Bedside—Transfer of an Ultrasmall Theranostic Gadolinium-Based Nanoparticle to Clinical Medicine. *Br. J. Radiol.* **2018**, *92*, 20180365.

(89) Dumoga, S.; Rai, Y.; Bhatt, A. N.; Tiwari, A. K.; Singh, S.; Mishra, A. K.; Kakkar, D. Block Copolymer Based Nanoparticles for Theranostic Intervention of Cervical Cancer: Synthesis, Pharmacokinetics, and *In Vitro*/*In Vivo* Evaluation in HeLa Xenograft Models. *ACS Appl. Mater. Interfaces.* **2017**, *9*, 22195–22211.

(90) Li, X.; Schumann, C.; Albarqi, H. A.; Lee, C. J.; Alani, A. W. G.; Bracha, S.; Milovancev, M.; Taratula, O.; Taratula, O. A Tumor-Activatable Theranostic Nanomedicine Platform for NIR Fluorescence-Guided Surgery and Combinatorial Phototherapy. *Theranostics.* **2018**, *8*, 767–784.

(91) Perry, J. L.; Herlihy, K. P.; Napier, M. E.; Desimone, J. M. PRINT: A Novel Platform toward Shape and Size Specific Nanoparticle Theranostics. *Acc. Chem. Res.* **2011**, *44*, 990–998.

(92) Wu, M.; Wu, L.; Li, J.; Zhang, D.; Lan, S.; Zhang, X.; Lin, X.; Liu, G.; Liu, X.; Liu, J. Self-Luminescing Theranostic Nanoreactors with Intraparticle Relayed Energy Transfer for Tumor Microenvironment Activated Imaging and Photodynamic Therapy. *Theranostics.* **2019**, *9*, 20–33.

(93) Yan, Z.; Wang, Q.; Liu, X.; Peng, J.; Li, Q.; Wu, M.; Lin, J. Cationic Nanomicelles Derived from Pluronic F127 As Delivery Vehicles of Chinese Herbal Medicine Active Components of Ursolic Acid for Colorectal Cancer Treatment. *RSC Adv.* **2018**, *8*, 15906–15914. DOI: 10.1039/c8ra01071d

(94) Beard, P. Biomedical Photoacoustic Imaging. *Interface Focus.* **2011**, *1*, 602–631.

(95) Yao, M.; Ma, M.; Xu, H.; Pan, X.; Xu, G.; Wu, R. Small PLGA Nanocapsules Co-Encapsulating Copper Sulfide Nanodots and Fluorocarbon Compound for Photoacoustic Imaging-Guided HIFU Synergistic Therapy. *RSC Adv.* **2018**, *8*, 4514–4524. DOI: 10.1039/c7ra12074e

(96) Liu, J.; Xu, F.; Huang, J.; Xu, J.; Liu, Y.; Yao, Y.; Ao, M.; Li, A.; Hao, L.; Cao, Y.; Hu, Z.; Ran, H.; Wang, Z.; Li, P. Low-Intensity Focused Ultrasound (LIFU)-Activated Nanodroplets As a Theranostic Agent for Noninvasive Cancer Molecular Imaging and Drug Delivery. *Biomater. Sci.* **2018**, *6*, 2838–2849.

(97) Qian, Y.; Wang, Y.; Jia, F.; Wang, Z.; Yue, C.; Zhang, W.; Hu, Z.; Wang, W. Tumor-Microenvironment Controlled Nanomicelles with AIE Property for Boosting Cancer Therapy and Apoptosis Monitoring. *Biomaterials.* **2019**, *188*, 96–106.

(98) Shen, M.-Y.; Liu, T.-I.; Yu, T.-W.; Kv, R.; Chiang, W.-H.; Tsai, Y.-C.; Chen, H.-H.; Lin, S.-C.; Chiu, H.-C. Hierarchically Targetable Polysaccharide-Coated Solid Lipid

Nanoparticles As an Oral Chemo/Thermotherapy Delivery System for Local Treatment of Colon Cancer. *Biomaterials.* **2019**, *197*, 86–100.

(99) Zhang, K.; Zhang, Y.; Meng, X.; Lu, H.; Chang, H.; Dong, H.; Zhang, X. Light-Triggered Theranostic Liposomes for Tumor Diagnosis and Combined Photodynamic and Hypoxia-Activated Prodrug Therapy. *Biomaterials.* **2018**, *185*, 301–309.

(100) Zhao, H.; Wu, M.; Zhu, L.; Tian, Y.; Wu, M.; Li, Y.; Deng, L.; Jiang, W.; Shen, W.; Wang, Z.; Mei, Z.; Li, P.; Ran, H.; Zhou, Z.; Ren, J. Cell-Penetrating Peptide-Modified Targeted Drug-Loaded Phase-Transformation Lipid Nanoparticles Combined with Low-Intensity Focused Ultrasound for Precision Theranostics against Hepatocellular Carcinoma. *Theranostics.* **2018**, *8*, 1892–1910.

(101) Chen, Q.; Liang, C.; Sun, X.; Chen, J.; Yang, Z.; Zhao, H.; Feng, L.; Liu, Z. $H_2O_2$-Responsive Liposomal Nanoprobe for Photoacoustic Inflammation Imaging and Tumor Theranostics *via In Vivo* Chromogenic Assay. *Proc. Natl. Acad. Sci.* **2017**, *114*, 5343–5348.

(102) Luo, Y.; Tang, Y.; Liu, T.; Chen, Q.; Zhou, X.; Wang, N.; Ma, M.; Cheng, Y.; Chen, H. Engineering Graphene Oxide with Ultrasmall SPIONs and Smart Drug Release for Cancer Theranostics. *Chem. Commun.* **2019**, *55*, 1963–1966.

(103) Dadfar, S. M.; Roemhild, K.; Drude, N. I.; von Stillfried, S.; Knüchel, R.; Kiessling, F.; Lammers, T. Iron Oxide Nanoparticles: Diagnostic, Therapeutic and Theranostic Applications. *Adv. Drug Deliv. Rev.* **2019**, *138*, 302–325.

(104) Ahmed, M. S. U.; Salam, A. Bin; Yates, C.; Willian, K.; Jaynes, J.; Turner, T.; Abdalla, M. O. Double-Receptor-Targeting Multifunctional Iron Oxide Nanoparticles Drug Delivery System for the Treatment and Imaging of Prostate Cancer. *Int. J. Nanomedicine.* **2017**, *12*, 6973–6984.

(105) Cisterna, B. A.; Kamaly, N.; Choi, W. Il; Tavakkoli, A.; Farokhzad, O. C.; Vilos, C.

Targeted Nanoparticles for Colorectal Cancer. *Nanomedicine.* **2016**, *11*, 2443–2456.

(106) Bai, R. G.; Ninan, N.; Muthoosamy, K.; Manickam, S. Graphene: A Versatile Platform for Nanotheranostics and Tissue Engineering. *Prog. Mater. Sci.* **2017**, *91*, 24–69.

(107) Lamb, J.; Fischer, E.; Rosillo-Lopez, M.; Salzmann, C. G.; Holland, J. P. Multi-Functionalised Graphene Nanoflakes As Tumour-Targeting Theranostic Drug-Delivery Vehicles. *Chem. Sci.* **2019**, *10*, 8880-8888.

(108) Huang, H.; Su, S.; Wu, N.; Wan, H.; Wan, S.; Bi, H.; Sun, L. Graphene-Based Sensors for Human Health Monitoring. *Front. Chem.* **2019**, *7*, 399.

(109) Karimi Shervedani, R.; Samiei Foroushani, M.; Kefayat, A.; Torabi, M.; Rahnemaye Rahsepar, F. Construction and Characterization of a Theranostic System Based on Graphene/Manganese Chelate. *Biosens. Bioelectron.* **2018**, *117*, 794–801.

(110) Hwang, D. W.; Kim, H. Y.; Li, F.; Park, J. Y.; Kim, D.; Park, J. H.; Han, H. S.; Byun, J. W.; Lee, Y.-S.; Jeong, J. M.; Char, K.; Lee, D. S. *In Vivo* Visualization of Endogenous MiR-21 Using Hyaluronic Acid-Coated Graphene Oxide for Targeted Cancer Therapy. *Biomaterials.* **2017**, *121*, 144–154.

(111) Zhao, X.; Wei, Z.; Zhao, Z.; Miao, Y.; Qiu, Y.; Yang, W.; Jia, X.; Liu, Z.; Hou, H. Design and Development of Graphene Oxide Nanoparticle/Chitosan Hybrids Showing PH-Sensitive Surface Charge-Reversible Ability for Efficient Intracellular Doxorubicin Delivery. *ACS Appl. Mater. Interfaces.* **2018**, *10*, 6608–6617.

(112) Owens, B. Melanoma. *Nature.* **2014**, *515*, S109.

(113) Schadendorf, D.; van Akkooi, A. C. J.; Berking, C.; Griewank, K. G.; Gutzmer, R.; Hauschild, A.; Stang, A.; Roesch, A.; Ugurel, S. Melanoma. *Lancet.* **2018**, *392*, 971–984.

(114) Kalluru, P.; Vankayala, R.; Chiang, C.-S.; Hwang, K. C. Nano-Graphene Oxide-Mediated *In Vivo* Fluorescence Imaging and Bimodal Photodynamic and Photothermal

Destruction of Tumors. *Biomaterials.* **2016**, *95*, 1–10.

(115) Sun, B.; Wu, J.; Cui, S.; Zhu, H.; An, W.; Fu, Q.; Shao, C.; Yao, A.; Chen, B.; Shi, D. *In Situ* Synthesis of Graphene Oxide/Gold Nanorods Theranostic Hybrids for Efficient Tumor Computed Tomography Imaging and Photothermal Therapy. *Nano Res.* **2017**, *10*, 37–48.

(116) Li, Y.; Liu, H.; Liu, X. Q.; Li, S.; Wang, L.; Ma, N.; Qiu, D. Free-Radical-Assisted Rapid Synthesis of Graphene Quantum Dots and Their Oxidizability Studies. *Langmuir.* **2016**, *32*, 8641–8649.

(117) Ye, R.; Peng, Z.; Metzger, A.; Lin, J.; Mann, J. A.; Huang, K.; Xiang, C.; Fan, X.; Samuel, E. L. G.; Alemany, L. B.; Marti, A. A.; Tour, J. M. Bandgap Engineering of Coal-Derived Graphene Quantum Dots. *ACS Appl. Mater. Interfaces.* **2015**, *7*, 7041–7048.

(118) Ge, J.; Lan, M.; Zhou, B.; Liu, W.; Guo, L.; Wang, H.; Jia, Q.; Niu, G.; Huang, X.; Zhou, H.; Meng, X.; Wang, P.; Lee, C.-S.; Zhang, W.; Han, X. A Graphene Quantum Dot Photodynamic Therapy Agent with High Singlet Oxygen Generation. *Nat. Commun.* **2014**, *5*, 1–8.

(119) Li, S.; Zhou, S.; Li, Y.; Li, X.; Zhu, J.; Fan, L.; Yang, S. Exceptionally High Payload of the IR780 Iodide on Folic Acid-Functionalized Graphene Quantum Dots for Targeted Photothermal Therapy. *ACS Appl. Mater. Interfaces.* **2017**, *9*, 22332–22341.

(120) Zhang, D.; Wen, L.; Huang, R.; Wang, H.; Hu, X.; Xing, D. Mitochondrial Specific Photodynamic Therapy by Rare-Earth Nanoparticles Mediated Near-Infrared Graphene Quantum Dots. *Biomaterials.* **2018**, *153*, 14–26.

(121) Hao, S.; Chen, G.; Yang, C. Sensing Using Rare-Earth-Doped Upconversion Nano-Particles. *Theranostics.* **2013**, *3*, 331–345.

(122) Tabish, T. A.; Scotton, C. J.; J Ferguson, D. C.; Lin, L.; der Veen, A. van; Lowry, S.;

Ali, M.; Jabeen, F.; Ali, M.; Winyard, P. G.; Zhang, S. Biocompatibility and Toxicity of Graphene Quantum Dots for Potential Application in Photodynamic Therapy. *Nanomedicine.* **2018**, *13*, 1923–1937.

(123) Zhang, C.; Liu, Z.; Zheng, Y.; Geng, Y.; Han, C.; Shi, Y.; Sun, H.; Zhang, C.; Chen, Y.; Zhang, L.; Zhou, X.; Kong, L. Glycyrrhetinic Acid Functionalized Graphene Oxide for Mitochondria Targeting and Cancer Treatment *In Vivo*. *Small.* **2018**, *14*, 1703306.

(124) Li, J.; Cai, C.; Li, J.; Li, J.; Li, J.; Sun, T.; Wang, L.; Wu, H.; Yu, G. Chitosan-Based Nanomaterials for Drug Delivery. *Molecules.* **2018**, *23*, 2661.

(125) Bourgeois, M.; Bailly, C.; Frindel, M.; Guerard, F.; Chérel, M.; Faivre-Chauvet, A.; Kraeber-Bodéré, F.; Bodet-Milin, C. Radioimmunoconjugates for Treating Cancer: Recent Advances and Current Opportunities. *Expert Opin. Biol. Ther.* **2017**, *17*, 813–819.

(126) Wang, S.; Zhang, Q.; Yang, P.; Yu, X.; Huang, L.-Y.; Shen, S.; Cai, S. Manganese Oxide-Coated Carbon Nanotubes As Dual-Modality Lymph Mapping Agents for Photothermal Therapy of Tumor Metastasis. *ACS Appl. Mater. Interfaces.* **2016**, *8*, 3736–3743.

(127) Bonvin, D.; Bastiaansen, J. A. M.; Stuber, M.; Hofmann, H.; Mionic Ebersold, M. Folic Acid on Iron Oxide Nanoparticles: Platform with High Potential for Simultaneous Targeting, MRI Detection and Hyperthermia Treatment of Lymph Node Metastases of Prostate Cancer. *Dalt. Trans.* **2017**, *46*, 12692–12704.

(128) Hurley, K. R.; Ring, H. L.; Etheridge, M.; Zhang, J.; Gao, Z.; Shao, Q.; Klein, N. D.; Szlag, V. M.; Chung, C.; Reineke, T. M.; Garwood, M.; Bischof, J. C.; Haynes, C. L. Predictable Heating and Positive MRI Contrast from a Mesoporous Silica-Coated Iron Oxide Nanoparticle. *Mol. Pharm.* **2016**, *13*, 2172–2183.

(129) Ye, X.; Shi, H.; He, X.; Yu, Y.; He, D.; Tang, J.; Lei, Y.; Wang, K. Cu-Au Alloy

Nanostructures Coated with Aptamers: A Simple, Stable and Highly Effective Platform for *In Vivo* Cancer Theranostics. *Nanoscale.* **2016**, *8*, 2260–2267.

(130) Tang, L.; Yang, X.; Yin, Q.; Cai, K.; Wang, H.; Chaudhury, I.; Yao, C.; Zhou, Q.; Kwon, M.; Hartman, J. A.; Dobrucki, I. T.; Dobrucki, L. W.; Borst, L. B.; Lezmi, S.; Helferich, W. G.; Ferguson, A. L.; Fan, T. M.; Cheng, J. Investigating the Optimal Size of Anticancer Nanomedicine. *Proc. Natl. Acad. Sci.* **2014**, *111*, 15344–15349.

(131) Niu, F.; Yan, J.; Ma, B.; Li, S.; Shao, Y.; He, P.; Zhang, W.; He, W.; Ma, P. X.; Lu, W. Lanthanide-Doped Nanoparticles Conjugated with an Anti-CD33 Antibody and a P53-Activating Peptide for Acute Myeloid Leukemia Therapy. *Biomaterials.* **2018**, *167*, 132–142.

(132) Nagahama, K.; Kumano, T.; Oyama, N.; Kawakami, J. Curcumisome Nanovesicles Generated by Self-Assembly of Curcumin Amphiphiles toward Cancer Theranostics. *Biomater. Sci.* **2015**, *3*, 1566–1578.

(133) Belletti, D.; Riva, G.; Luppi, M.; Tosi, G.; Forni, F.; Vandelli, M. A.; Ruozi, B.; Pederzoli, F. Anticancer Drug-Loaded Quantum Dots Engineered Polymeric Nanoparticles: Diagnosis/Therapy Combined Approach. *Eur. J. Pharm. Sci.* **2017**, *107*, 230–239.

(134) Torino, E.; Auletta, L.; Vecchione, D.; Orlandella, F. M.; Salvatore, G.; Iaccino, E.; Fiorenza, D.; Grimaldi, A. M.; Sandomenico, A.; Albanese, S.; Sarnataro, D.; Gramanzini, M.; Palmieri, C.; Scala, G.; Quinto, I.; Netti, P. A.; Salvatore, M.; Greco, A. Multimodal Imaging for a Theranostic Approach in a Murine Model of B-Cell Lymphoma with Engineered Nanoparticles. *Nanomedicine Nanotechnology, Biol. Med.* **2018**, *14*, 483–491.

(135) Yang, Z.; Tian, R.; Wu, J.; Fan, Q.; Yung, B. C.; Niu, G.; Jacobson, O.; Wang, Z.; Liu, G.; Yu, G.; Huang, W.; Song, J.; Chen, X. Impact of Semiconducting Perylene Diimide

Nanoparticle Size on Lymph Node Mapping and Cancer Imaging. *ACS Nano.* **2017**, *11*, 4247–4255.

(136) Saesoo, S.; Sathornsumetee, S.; Anekwiang, P.; Treetidnipa, C.; Thuwajit, P.; Bunthot, S.; Maneeprakorn, W.; Maurizi, L.; Hofmann, H.; Rungsardthong, R. U.; Saengkrit, N.. Characterization of Liposome-Containing SPIONs Conjugated with Anti-CD20 Developed As a Novel Theranostic Agent for Central Nervous System Lymphoma. *Colloids Surf B Biointerfaces.* **2018**, *161*, 497–507.

(137) Daneman, R.; Prat, A. The Blood-Brain Barrier. *Cold Spring Harb. Perspect. Biol.* **2015**, *7*, a020412. DOI: 10.1101/cshperspect.a020412

(138) Sharma, M.; Dube, T.; Chibh, S.; Kour, A.; Mishra, J.; Panda, J. J. Nanotheranostics, a Future Remedy of Neurological Disorders. *Expert Opin. Drug Deliv.* **2019**, *16*, 113–128.

(139) Lin, M. T.; Beal, M. F. Mitochondrial Dysfunction and Oxidative Stress in Neurodegenerative Diseases. *Nature.* **2006**, *443*, 787.

(140) Wang, X.; Wang, X.; Guo, Z. Metal-Involved Theranostics: An Emerging Strategy for Fighting Alzheimer's Disease. *Coord. Chem. Rev.* **2018**, *362*, 72–84.

(141) Li, Y.; Xu, D.; Ho, S.-L.; Li, H.-W.; Yang, R.; Wong, M. S. A Theranostic Agent for *In Vivo* Near-Infrared Imaging of β-Amyloid Species and Inhibition of β-Amyloid Aggregation. *Biomaterials.* **2016**, *94*, 84–92.

(142) Chen, Q.; Du, Y.; Zhang, K.; Liang, Z.; Li, J.; Yu, H.; Ren, R.; Feng, J.; Jin, Z.; Li, F.; Sun, J.; Zhou, M.; He, Q.; Sun, X.; Zhang, H.; Tian, M.; Ling, D. Tau-Targeted Multifunctional Nanocomposite for Combinational Therapy of Alzheimer's Disease. *ACS Nano.* **2018**, *12*, 1321–1338.

(143) Li, G.; Shao, K.; Umeshappa, C. S. Recent Progress in Blood-Brain Barrier Transportation Research. In *Brain Targeted Drug Delivery System*; Gao, H., Gao, X., Eds.; Academic Press: London, 2019; pp 33–51.

(144) Yang, T.; Yang, L.; Zhang, C.; Wang, Y.; Ma, X.; Wang, K.; Luo, J.; Yao, C.; Wang, X.; Wang, X. A Copper-Amyloid-β Targeted Fluorescent Chelator As a Potential Theranostic Agent for Alzheimer's Disease. *Inorg. Chem. Front.* **2016**, *3*, 1572–1581.

(145) Cui, Z.; Bu, W.; Fan, W.; Zhang, J.; Ni, D.; Liu, Y.; Wang, J.; Liu, J.; Yao, Z.; Shi, J. Sensitive Imaging and Effective Capture of Cu2+: Towards Highly Efficient Theranostics of Alzheimer's Disease. *Biomaterials.* **2016**, *104*, 158–167.

(146) Serra, P.; Santamaria, P. Nanoparticle-Based Approaches to Immune Tolerance for the Treatment of Autoimmune Diseases. *Eur. J. Immunol.* **2018**, *48*, 751–756.

(147) Prosperi, D.; Colombo, M.; Zanoni, I.; Granucci, F. Drug Nanocarriers to Treat Autoimmunity and Chronic Inflammatory Diseases. *Semin in Immunol*. **2017**, *34*, 61–67.

(148) Wang, Q.; Sun, X. Recent Advances in Nanomedicines for the Treatment of Rheumatoid Arthritis. *Biomater. Sci.* **2017**, *5*, 1407–1420.

(149) Yang, M.; Ding, J.; Feng, X.; Chang, F.; Wang, Y.; Gao, Z.; Zhuang, X.; Chen, X. Scavenger Receptor-Mediated Targeted Treatment of Collagen-Induced Arthritis by Dextran Sulfate-Methotrexate Prodrug. *Theranostics.* **2017**, *7*, 97–105.

(150) Heo, R.; You, D. G.; Um, W.; Choi, K. Y.; Jeon, S.; Park, J. S.; Choi, Y.; Kwon, S.; Kim, K.; Kwon, I. C.; Jo, D. G.; Kang, Y. M.; Park, J. H. Dextran Sulfate Nanoparticles As a Theranostic Nanomedicine for Rheumatoid Arthritis. *Biomaterials.* **2017**, *131*, 15–26.

(151) Chuang, S.-Y.; Lin, C.-H.; Huang, T.-H.; Fang, J.-Y. Lipid-Based Nanoparticles As a Potential Delivery Approach in the Treatment of Rheumatoid Arthritis. *Nanomaterials.* **2018**, *8*, 42.

(152) Zhou, M.; Hou, J.; Zhong, Z.; Hao, N.; Lin, Y.; Li, C. Targeted Delivery of Hyaluronic Acid-Coated Solid Lipid Nanoparticles for Rheumatoid Arthritis Therapy. *Drug Deliv.*

**2018**, *25*, 716–722.

(153) Kim, H. J.; Lee, S. M.; Park, K. H.; Mun, C. H.; Park, Y. B.; Yoo, K. H. Drug-Loaded Gold/Iron/Gold Plasmonic Nanoparticles for Magnetic Targeted Chemo-Photothermal Treatment of Rheumatoid Arthritis. *Biomaterials.* **2015**, *61*, 95–102.

(154) Tang, Q.; Cui, J.; Tian, Z.; Sun, J.; Wang, Z.; Chang, S.; Zhu, S. Oxygen and Indocyanine Green Loaded Phase-Transition Nanoparticle-Mediated Photo-Sonodynamic Cytotoxic Effects on Rheumatoid Arthritis Fibroblast-Like Synoviocytes. *Int. J. Nanomedicine.* **2017**, *12*, 381–393.

(155) Rehman, F. U.; Zhao, C.; Wu, C.; Li, X.; Jiang, H.; Selke, M.; Wang, X. Synergy and Translation of Allogenic Bone Marrow Stem Cells after Photodynamic Treatment of Rheumatoid Arthritis with Tetra Sulfonatophenyl Porphyrin and TiO2 Nanowhiskers. *Nano Res.* **2016**, *9*, 3305–3321.

(156) Yao, L.; Lihua, L.; Zefeng, L.; Liping, W.; Lijun, L.; Mei, L.; Yu, Z.; Qingshui, Y.; Qi, L.; Hong, X. A New Treatment Modality for Rheumatoid Arthritis: Combined Photothermal and Photodynamic Therapy Using Cu7.2S4 Nanoparticles. *Adv. Healthc. Mater.* **2018**, *7*, 1800013.

(157) Li, C.; Li, H.; Wang, Q.; Zhou, M.; Li, M.; Gong, T.; Zhang, Z.; Sun, X. PH-Sensitive Polymeric Micelles for Targeted Delivery to Inflamed Joints. *J. Control. Release.* **2017**, *246*, 133–141.

(158) Yuan, F.; Quan, L. dong; Cui, L.; Goldring, S. R.; Wang, D. Development of Macromolecular Prodrug for Rheumatoid Arthritis. *Adv. Drug Deliv. Rev.* **2012**, *64*, 1205–1219.

(159) Joshi, N.; Yan, J.; Levy, S.; Bhagchandani, S.; Slaughter, K. V.; Sherman, N. E.; Amirault, J.; Wang, Y.; Riegel, L.; He, X.; Tan, S. R.; Valic, M.; Vemula, P. K.; Miranda, O. R.; Levy, O.; Gravallese, E. M.; Aliprantis, A. O.; Ermann, J.; Karp, J. M.. Towards

an Arthritis Flare-Responsive Drug Delivery System. *Nat. Commun.* **2018**, *9*, 1–11.

(160) Gustafson, H. H.; Holt-Casper, D.; Grainger, D. W.; Ghandehari, H. Nanoparticle Uptake: The Phagocyte Problem. *Nano Today.* **2015**, *10*, 487–510.

(161) Kim, K. S.; Song, C. G.; Kang, P. M. Targeting Oxidative Stress Using Nanoparticles As a Theranostic Strategy for Cardiovascular Diseases. *Antioxid. Redox Signal.* **2017**, *30*, 7428.

(162) Suntiparpluacha, M.; Tammachote, N.; Tammachote, R. Triamcinolone Acetonide Reduces Viability, Induces Oxidative Stress, and Alters Gene Expressions of Human Chondrocytes. *Eur. Rev. Med. Pharmacol. Sci.* **2016**, *20*, 4985–4992.

(163) Dormont, F.; Varna, M.; Couvreur, P. Nanoplumbers: Biomaterials to Fight Cardiovascular Diseases. *Mater. Today.* **2018**, *21*, 122–143.

(164) Gao, W.; Sun, Y.; Cai, M.; Zhao, Y.; Cao, W.; Liu, Z.; Cui, G.; Tang, B. Copper Sulfide Nanoparticles As a Photothermal Switch for TRPV1 Signaling to Attenuate Atherosclerosis. *Nat. Commun.* **2018**, *9*, 1–10.

(165) Kang, C.; Gwon, S.; Song, C.; Kang, P. M.; Park, S.-C.; Jeon, J.; Hwang, D. W.; Lee, D. Fibrin-Targeted and H2O2-Responsive Nanoparticles As a Theranostics for Thrombosed Vessels. *ACS Nano.* **2017**, *11*, 6194–6203.

(166) Sun, X.; Li, W.; Zhang, X.; Qi, M.; Zhang, Z.; Zhang, X. E.; Cui, Z. *In Vivo* Targeting and Imaging of Atherosclerosis Using Multifunctional Virus-Like Particles of Simian Virus 40. *Nano Lett.* **2016**, *16*, 6164–6171.

(167) Zhang, W.; Zhang, X. E.; Li, F. Virus-Based Nanoparticles of Simian Virus 40 in the Field of Nanobiotechnology. *Biotechnol. J.* **2018**, *13*, 1700619.

(168) Lusis, A. J. Atherosclerosis: Insight Review Article. *Nature.* **2000**, *407*, 233–241.

(169) Chan, C. K. W.; Zhang, L.; Cheng, C. K.; Yang, H.; Huang, Y.; Tian, X. Y.; Choi, C. H. J. Recent Advances in Managing Atherosclerosis *via* Nanomedicine. *Small.* **2018**, *14*,

1702793.

(170) Jung, E.; Lee, J.; Jeong, L.; Park, S.; Lee, M.; Song, C.; Lee, D. Stimulus-Activatable Echogenic Maltodextrin Nanoparticles As Nanotheranostic Agents for Peripheral Arterial Disease. *Biomaterials.* **2019**, *192*, 282–291.

(171) Jung, E.; Kang, C.; Lee, J.; Yoo, D.; Hwang, D. W.; Kim, D.; Park, S. C.; Lim, S. K.; Song, C.; Lee, D. Molecularly Engineered Theranostic Nanoparticles for Thrombosed Vessels: H2O2-Activatable Contrast-Enhanced Photoacoustic Imaging and Antithrombotic Therapy. *ACS Nano.* **2018**, *12*, 392–401.

(172) Nandwana, V.; Ryoo, S. R.; Kanthala, S.; McMahon, K. M.; Rink, J. S.; Li, Y.; Venkatraman, S. S.; Thaxton, C. S.; Dravid, V. P. High-Density Lipoprotein-Like Magnetic Nanostructures (HDL-MNS): Theranostic Agents for Cardiovascular Disease. *Chem. Mater.* **2017**, *29*, 2276–2282.

(173) Marin, R.; Skripka, A.; Besteiro, L. V.; Benayas, A.; Wang, Z.; Govorov, A. O.; Canton, P.; Vetrone, F. Highly Efficient Copper Sulfide-Based Near-Infrared Photothermal Agents: Exploring the Limits of Macroscopic Heat Conversion. *Small*. **2018**, *14*, 1803282.

(174) Li, B.; Aid-Launais, R.; Labour, M. N.; Zenych, A.; Juenet, M.; Choqueux, C.; Ollivier, V.; Couture, O.; Letourneur, D.; Chauvierre, C. Functionalized Polymer Microbubbles As New Molecular Ultrasound Contrast Agent to Target P-Selectin in Thrombus. *Biomaterials.* **2019**, *194*, 139–150.

(175) Liu, Z.; Liu, J.; Wang, R.; Du, Y.; Ren, J.; Qu, X. An Efficient Nano-Based Theranostic System for Multi-Modal Imaging-Guided Photothermal Sterilization in Gastrointestinal Tract. *Biomaterials.* **2015**, *56*, 206–218.

(176) Xia, J.; Li, T.; Lu, C.; Xu, H. Selenium-Containing Polymers: Perspectives toward Diverse Applications in Both Adaptive and Biomedical Materials. *Macromolecules.*

**2018**, *51*, 7435–7455.

(177) Sahu, A. K.; Dash, D. K.; Mishra, K.; Mishra, S. P.; Yadav, R.; Kashyap, P. Properties and Applications of Ruthenium. In *Noble and Precious Metals - Properties, Nanoscale Effects and Applications*; IntechOpen: London, 2018; pp 377–390.

(178) Huang, N.; Chen, X.; Zhu, X.; Xu, M.; Liu, J. Ruthenium Complexes/Polypeptide Self-Assembled Nanoparticles for Identification of Bacterial Infection and Targeted Antibacterial Research. *Biomaterials.* **2017**, *141*, 296–313.

(179) Dizaj, S. M.; Mennati, A.; Jafari, S.; Khezri, K.; Adibkia, K. Antimicrobial Activity of Carbon-Based Nanoparticles. *Adv. Pharm. Bull.* **2015**, *5*, 19–23.

(180) Miller, K. P.; Wang, L.; Benicewicz, B. C.; Decho, A. W. Inorganic Nanoparticles Engineered to Attack Bacteria. *Chem. Soc. Rev.* **2015**, *44*, 7787–7807.

(181) Mao, D.; Hu, F.; Kenry; Ji, S.; Wu, W.; Ding, D.; Kong, D.; Liu, B. Metal–Organic-Framework-Assisted *In Vivo* Bacterial Metabolic Labeling and Precise Antibacterial Therapy. *Adv. Mater.* **2018**, *30*, 1706831.

(182) Chen, X.; Wo, F.; Jin, Y.; Tan, J.; Lai, Y.; Wu, J. Drug-Porous Silicon Dual Luminescent System for Monitoring and Inhibition of Wound Infection. *ACS Nano.* **2017**, *11*, 7938–7949.

(183) Zhao, Z.; Yan, R.; Yi, X.; Li, J.; Rao, J.; Guo, Z.; Yang, Y.; Li, W.; Li, Y. Q.; Chen, C. Bacteria-Activated Theranostic Nanoprobes against Methicillin-Resistant *Staphylococcus Aureus* Infection. *ACS Nano.* **2017**, *11*, 4428–4438.

(184) Zhou, J.; Yao, D.; Qian, Z.; Hou, S.; Li, L.; Jenkins, A. T. A.; Fan, Y. Bacteria-Responsive Intelligent Wound Dressing: Simultaneous *In Situ* Detection and Inhibition of Bacterial Infection for Accelerated Wound Healing. *Biomaterials.* **2018**, *161*, 11–23.

(185) Xie, Y.; Liu, Y.; Yang, J.; Liu, Y.; Hu, F.; Zhu, K.; Jiang, X. Gold Nanoclusters for Targeting Methicillin-Resistant *Staphylococcus Aureus In Vivo*. *Angew. Chemie - Int.*

*Ed.* **2018**, *57*, 3958–3962.

(186) Zheng, K.; Setyawati, M. I.; Leong, D. T.; Xie, J. Surface Ligand Chemistry of Gold Nanoclusters Determines Their Antimicrobial Ability. *Chem. Mater.* **2018**, *30*, 2800–2808.

(187) Kim, T.; Zhang, Q.; Li, J.; Zhang, L.; Jokerst, J. V. A Gold/Silver Hybrid Nanoparticle for Treatment and Photoacoustic Imaging of Bacterial Infection. *ACS Nano.* **2018**, *12*, 5615–5625.

(188) Gao, G.; Jiang, Y. W.; Jia, H. R.; Wu, F. G. Near-Infrared Light-Controllable On-Demand Antibiotics Release Using Thermo-Sensitive Hydrogel-Based Drug Reservoir for Combating Bacterial Infection. *Biomaterials.* **2019**, *188*, 83–95.

(189) Di Venosa, G.; Hermida, L.; Batlle, A.; Fukuda, H.; Defain, M. V.; Mamone, L.; Rodriguez, L.; MacRobert, A.; Casas, A. Characterisation of Liposomes Containing Aminolevulinic Acid and Derived Esters. *J. Photochem. Photobiol. B Biol.* **2008**, *92*, 1–9.

(190) Bobo, D.; Robinson, K. J.; Islam, J.; Thurecht, K. J.; Corrie, S. R. Nanoparticle-Based Medicines: A Review of FDA-Approved Materials and Clinical Trials to Date. *Pharm. Res.* **2016**, *33*, 2373–2387.

(191) Anselmo, A. C.; Mitragotri, S. A Review of Clinical Translation of Inorganic Nanoparticles. *AAPS J.* **2015**, *17*, 1041–1054. DOI: 10.1208/s12248-015-9780-2.

(192) Anselmo, A. C.; Mitragotri, S. Nanoparticles in the Clinic. *Bioeng. Transl. Med.* **2016**, *1*, 10–29.

(193) El-Boubbou, K. Magnetic Iron Oxide Nanoparticles As Drug Carriers: Clinical Relevance. *Nanomedicine.* **2018**, *13*, 953–971.

(194) Ehlerding, E. B.; Grodzinski, P.; Cai, W.; Liu, C. H. Big Potential from Small Agents: Nanoparticles for Imaging-Based Companion Diagnostics. *ACS Nano.* **2018**, *12*, 2106–

2121.

(195) Hu, P.; Fu, Z.; Liu, G.; Tan, H.; Xiao, J.; Shi, H.; Cheng, D. Gadolinium-Based Nanoparticles for Theranostic MRI-Guided Radiosensitization in Hepatocellular Carcinoma. *Front. Bioeng. Biotechnol.* **2019**, *7*, 368.

(196) Thakare, V.; Tran, V.-L.; Natuzzi, M.; Thomas, E.; Moreau, M.; Romieu, A.; Collin, B.; Courteau, A.; Vrigneaud, J.-M.; Louis, C.; Roux, S.; Boschetti, F.; Tillement, O.; Lux, F.; Denat, F. Functionalization of Theranostic AGuIX® Nanoparticles for PET/MRI/Optical Imaging. *RSC Adv.* **2019**, *9*, 24811–24815. DOI: 10.1039/c9ra00365g

(197) Dufort, S.; Appelboom, G.; Verry, C.; Barbier, E. L.; Lux, F.; Bräuer-Krisch, E.; Sancey, L.; Chang, S. D.; Zhang, M.; Roux, S.; Tillement, O.; Le, D. G. Ultrasmall Theranostic Gadolinium-Based Nanoparticles Improve High-Grade Rat Glioma Survival. *J. Clin. Neurosci.* **2019**, *67*, 215–219.

(198) Miller, M. A.; Arlauckas, S.; Weissleder, R. Prediction of Anti-Cancer Nanotherapy Efficacy by Imaging. *Nanotheranostics.* **2017**, *1*, 296–312.

(199) Nardecchia, S.; Sánchez-Moreno, P.; Vicente, J. de; Marchal, J. A.; Boulaiz, H. Clinical Trials of Thermosensitive Nanomaterials: An Overview. *Nanomater. (Basel, Switzerland).* **2019**, *9*, 191.

(200) Chang, D.; Lim, M.; Goos, J. A. C. M.; Qiao, R.; Ng, Y. Y.; Mansfeld, F. M.; Jackson, M.; Davis, T. P.; Kavallaris, M. Biologically Targeted Magnetic Hyperthermia: Potential and Limitations. *Front. Pharmacol.* **2018**, *9*, 831.

(201) Singh, P.; Pandit, S.; Mokkapati, V. R. S. S.; Garg, A.; Ravikumar, V.; Mijakovic, I. Gold Nanoparticles in Diagnostics and Therapeutics for Human Cancer. *Int. J. Mol. Sci.* **2018**, *19*, 1979.

(202) Pedrosa, P.; Vinhas, R.; Fernandes, A.; Baptista, P. V. Gold Nanotheranostics: Proof-Of-Concept or Clinical Tool? *Nanomater. (Basel, Switzerland).* **2015**, *5*, 1853–1879.

(203) Ventola, C. L. Progress in Nanomedicine: Approved and Investigational Nanodrugs. *P T.* **2017**, *42*, 742–755.

(204) Pelster, M. S.; Amaria, R. N. Combined Targeted Therapy and Immunotherapy in Melanoma: A Review of the Impact on the Tumor Microenvironment and Outcomes of Early Clinical Trials. *Ther. Adv. Med. Oncol.* **2019**, *11*, 1758835919830826.

(205) Navyatha, B.; Nara, S. Theranostic Nanostructures for Ovarian Cancer. *Crit. Rev. Ther. Drug Carrier Syst.* **2019**, *36*, 305–371.

(206) Thakur, V.; Kutty, R. V. Recent Advances in Nanotheranostics for Triple Negative Breast Cancer Treatment. *J. Exp. Clin. Cancer Res.* **2019**, *38*, 430.

(207) Zuckerman, J. E.; Gritli, I.; Tolcher, A.; Heidel, J. D.; Lim, D.; Morgan, R.; Chmielowski, B.; Ribas, A.; Davis, M. E.; Yen, Y. Correlating Animal and Human Phase Ia/Ib Clinical Data with CALAA-01, a Targeted, Polymer-Based Nanoparticle Containing SiRNA. *Proc. Natl. Acad. Sci. U. S. A.* **2014**, *111*, 11449–11454.

(208) Li, Y.; Yang, S.; Zheng, J.; Zou, Z.; Yang, R.; Tan, W. "Trojan Horse" DNA Nanostructure for Personalized Theranostics: Can It Knock on the Door of Preclinical Practice? *Langmuir.* **2018**, *34*, 15028–15044.

(209) Burris, H. A.; Bakewell, S.; Bendell, J. C.; Infante, J.; Jones, S. F.; Spigel, D. R.; Weiss, G. J.; Ramanathan, R. K.; Ogden, A.; Von Hoff, D. Safety and Activity of IT-139, a Ruthenium-Based Compound, in Patients with Advanced Solid Tumours: A First-In-Human, Open-Label, Dose-Escalation Phase I Study with Expansion Cohort. *ESMO Open.* **2016**, *1*, e000154. DOI: 10.1136/esmoopen-2016-000154.

(210) Libutti, S. K.; Paciotti, G. F.; Byrnes, A. A.; Alexander Jr, H. R.; Gannon, W. E.; Walker, M.; Seidel, G. D.; Yuldasheva, N.; Tamarkin, L. Phase I and Pharmacokinetic Studies of CYT-6091, A Novel PEGylated Colloidal Gold-RhTNF Nanomedicine. *Clin. Cancer Res.* **2010**, *16*, 6139–6149.

(211) Paciotti, G. F.; Myer, L.; Weinreich, D.; Goia, D.; Pavel, N.; McLaughlin, R. E.; Tamarkin, L. Colloidal Gold: A Novel Nanoparticle Vector for Tumor Directed Drug Delivery. *Drug Deliv.* **2004**, *11*, 169–183.

(212) Davis, M. E.; Zuckerman, J. E.; Choi, C. H. J.; Seligson, D.; Tolcher, A.; Alabi, C. A.; Yen, Y.; Heidel, J. D.; Ribas, A. Evidence of RNAi in Humans from Systemically Administered SiRNA *via* Targeted Nanoparticles. *Nature* **2010**, *464*, 1067–1070.

(213) Paciotti, G. F.; Kingston, D. G. I.; Tamarkin, L. Colloidal Gold Nanoparticles: A Novel Nanoparticle Platform for Developing Multifunctional Tumor-Targeted Drug Delivery Vectors. *Drug Dev. Res.* **2006**, *67*, 47–54.

(214) Espelin, C. W.; Leonard, S. C.; Geretti, E.; Wickham, T. J.; Hendriks, B. S. Dual HER2 Targeting with Trastuzumab and Liposomal-Encapsulated Doxorubicin (MM-302) Demonstrates Synergistic Antitumor Activity in Breast and Gastric Cancer. *Cancer Res.* **2016**, *76*, 1517–1527.

(215) Abdellatif, A. A. H.; Tawfeek, H. M. Development and Evaluation of Fluorescent Gold Nanoparticles. *Drug Dev. Ind. Pharm.* **2018**, *44*, 1679–1684.

(216) Anderson, C. M.; Sonis, S. T.; Lee, C. M.; Adkins, D.; Allen, B. G.; Sun, W.; Agarwala, S. S.; Venigalla, M. L.; Chen, Y.; Zhen, W.; Mould, D. R.; Holmlund, J. T.; Brill, J. M.; Buatti, J. M. Phase 1b/2a Trial of the Superoxide Dismutase Mimetic GC4419 to Reduce Chemoradiotherapy-Induced Oral Mucositis in Patients with Oral Cavity or Oropharyngeal Carcinoma. *Int. J. Radiat. Oncol. Biol. Phys.* **2018**, *100*, 427–435.

(217) Ng, S. P.; Bahig, H.; Wang, J.; Cardenas, C. E.; Lucci, A.; Hall, C. S.; Meas, S.; Sarli, V. N.; Yuan, Y.; Urbauer, D. L.; Ding, Y.; Ikner, S.; Dinh, V.; Elgohari, B. A.; Johnson, J. M.; Skinner, H. D.; Gunn, G. B.; Garden, A. S.; Phan, J.; Rosenthal, D. I.; *et al.* Predicting Treatment Response Based on Dual Assessment of Magnetic Resonance Imaging Kinetics and Circulating Tumor Cells in Patients with Head and Neck Cancer

(PREDICT-HN): Matching “Liquid Biopsy” and Quantitative Tumor Modeling. *BMC Cancer.* **2018**, *18*, 903.

(218) Kharlamov, A. N.; Feinstein, J. A.; Cramer, J. A.; Boothroyd, J. A.; Shishkina, E. V; Shur, V. Plasmonic Photothermal Therapy of Atherosclerosis with Nanoparticles: Long-Term Outcomes and Safety in NANOM-FIM Trial. *Future Cardiol.* **2017**, *13*, 345–363.

(219) Alam, S. R.; Shah, A. S.; Richards, J.; Lang, N. N.; Barnes, G.; Joshi, N.; MacGillivray, T.; McKillop, G.; Mirsadraee, S.; Payne, J.; Fox, K.A.; Henriksen, P.; Newby, D. E.; Semple, S. I. Ultrasmall Superparamagnetic Particles of Iron Oxide in Patients with Acute Myocardial Infarction Early Clinical Experience. *Circ. Cardiovasc. Imaging.* **2012**, *5*, 559–565.

(220) Dul, M.; Nikolic, T.; Stefanidou, M.; McAteer, M. A.; Williams, P.; Mous, J.; Roep, B. O.; Kochba, E.; Levin, Y.; Peakman, M.; Wong, F. S.; Dayan, C. M.; Tatovic, D.; Coulman, S. A.; Birchall, J. C. Conjugation of a Peptide Autoantigen to Gold Nanoparticles for Intradermally Administered Antigen Specific Immunotherapy. *Int. J. Pharm.* **2019**, *562*, 303–312.

(221) Turvey, S. E.; Swart, E.; Denis, M. C.; Mahmood, U.; Benoist, C.; Weissleder, R.; Mathis, D. Noninvasive Imaging of Pancreatic Inflammation and Its Reversal in Type 1 Diabetes. *J. Clin. Invest.* **2005**, *115*, 2454–2461.

(222) Tanguy, R.; Métellus, P.; Mornex, F.; Mazeron, J.-J. Stereotactic Radiosurgery and Radiotherapy for Brain Metastases. *Bull. Cancer.* **2013**, *100*, 75–81.

(223) Kumthekar, P.; Rademaker, A.; Ko, C.; Dixit, K.; Schwartz, M. A.; Sonabend, A. M.; Sharp, L.; Lukas, R. V.; Stupp, R.; Horbinski, C.; McCortney, K.; Stegh, A. H. A Phase 0 First-In-Human Study Using NU-0129: A Gold Base Spherical Nucleic Acid (SNA) Nanoconjugate Targeting BCL2L12 in Recurrent Glioblastoma Patients. *J. Clin. Oncol.* **2019**, *37*, 3012.

(224) Minamisawa, M.; Claggett, B.; Adams, D.; Kristen, A. V; Merlini, G.; Slama, M. S.; Dispenzieri, A.; Shah, A. M.; Falk, R. H.; Karsten, V.; Sweetser, M. T.; Chen, J.; Riese, R.; Vest, J.; Solomon, S. D. Association of Patisiran, an RNA Interference Therapeutic, with Regional Left Ventricular Myocardial Strain in Hereditary Transthyretin Amyloidosis: The APOLLO Study. *JAMA Cardiol.* **2019**, *4*, 466–472.

(225) Harisinghani, M. G.; Barentsz, J.; Hahn, P. F.; Deserno, W. M.; Tabatabaei, S.; van de Kaa, C. H.; de la Rosette, J.; Weissleder, R. Noninvasive Detection of Clinically Occult Lymph-Node Metastases in Prostate Cancer. *N. Engl. J. Med.* **2003**, *348*, 2491–2499.

(226) Mao, Y.; Hedgire, S.; Harisinghani, M. Radiologic Assessment of Lymph Nodes in Oncologic Patients. *Curr. Radiol. Rep.* **2013**, *2*, 36.

(227) Bonvalot, S.; Le Pechoux, C.; De Baere, T.; Kantor, G.; Buy, X.; Stoeckle, E.; Terrier, P.; Sargos, P.; Coindre, J. M.; Lassau, N.; Ait, S. R.; Dimitriu, M.; Borghi, E.; Levy, L.; Deutsch, E.; Soria, J. C. First-In-Human Study Testing a New Radioenhancer Using Nanoparticles (NBTXR3) Activated by Radiation Therapy in Patients with Locally Advanced Soft Tissue Sarcomas. *Clin. Cancer Res.* **2017**, *23*, 908–917.

(228) Chen, F.; Ma, K.; Zhang, L.; Madajewski, B.; Turker, M. Z.; Gallazzi, F.; Cruickshank, K.; Zhang, X.; Jenjitranant, P.; Touijer, K. A.; Quinn, T. P.; Zanzonico, P.; Wiesner, U.; Bradbury, M. S. Ultrasmall Renally Clearable Silica Nanoparticles Target Prostate Cancer. *ACS Appl. Mater. Interfaces.* **2019**, *11*, 43879–43887.

(229) Atri, M.; Zhang, Z.; Marques, H.; Gorelick, J.; Harisinghani, M.; Sohaib, A.; Koh, D.-M.; Raman, S.; Gee, M.; Choi, H.; Landrum, L.; Mannel, R.; Chuang, L.; Yu, J. Q.; McCourt, C. K.; Gold, M. Utility of Preoperative Ferumoxtran-10 MRI to Evaluate Retroperitoneal Lymph Node Metastasis in Advanced Cervical Cancer: Results of ACRIN 6671/GOG 0233. *Eur. J. Radiol. Open.* **2015**, *2*, 11–18.

(230) Absinta, M.; Sati, P.; Gaitán, M. I.; Maggi, P.; Cortese, I. C. M.; Filippi, M.; Reich, D.

S. Seven-Tesla Phase Imaging of Acute Multiple Sclerosis Lesions: A New Window into the Inflammatory Process. *Ann. Neurol.* **2013**, *74*, 669–678.

(231) Montet, X.; Weissleder, R.; Josephson, L. Imaging Pancreatic Cancer with a Peptide−Nanoparticle Conjugate Targeted to Normal Pancreas. *Bioconjug. Chem.* **2006**, *17*, 905–911.

(232) Von Hoff, D. D.; Mita, M. M.; Ramanathan, R. K.; Weiss, G. J.; Mita, A. C.; LoRusso, P. M.; Burris, H. A.; Hart, L. L.; Low, S. C.; Parsons, D. M.; Zale, S. E.; Summa, J. M.; Youssoufian, H.; Sachdev, J. C. Phase I Study of PSMA-Targeted Docetaxel-Containing Nanoparticle BIND-014 in Patients with Advanced Solid Tumors. *Clin. Cancer Res.* **2016**, *22*, 3157–3163.

(233) Francis, S. M.; Taylor, C. A.; Tang, T.; Liu, Z.; Zheng, Q.; Dondero, R.; Thompson, J. E. SNS01-T Modulation of EIF5A Inhibits B-Cell Cancer Progression and Synergizes with Bortezomib and Lenalidomide. *Mol. Ther.* **2014**, *22*, 1643–1652.

(234) Lay, M.; Callejo, B.; Chang, S.; Hong, D. K.; Lewis, D. B.; Carroll, T. D.; Matzinger, S.; Fritts, L.; Miller, C. J.; Warner, J. F.; Liang, L.; Fairman, J. Cationic Lipid/DNA Complexes (JVRS-100) Combined with Influenza Vaccine (Fluzone) Increases Antibody Response, Cellular Immunity, and Antigenically Drifted Protection. *Vaccine.* **2009**, *27*, 3811–3820.

(235) Borah, B. J.; Borah, S. J.; Saikia, K.; Dutta, D. K. Efficient One-Pot Synthesis of Propargylamines Catalysed by Gold Nanocrystals Stabilized on Montmorillonite. *Catal. Sci. Technol.* **2014**, *4*, 4001–4009.

(236) Guggenbichler, J. P.; Böswald, M.; Lugauer, S.; Krall, T. A New Technology of Microdispersed Silver in Polyurethane Induces Antimicrobial Activity in Central Venous Catheters. *Infection.* **1999**, *27*, S16-23.

(237) Antonelli, M.; De Pascale, G.; Ranieri, V. M.; Pelaia, P.; Tufano, R.; Piazza, O.;

Zangrillo, A.; Ferrario, A.; De Gaetano, A.; Guaglianone, E.; Donelli, G. Comparison of Triple-Lumen Central Venous Catheters Impregnated with Silver Nanoparticles (AgTive®) *vs* Conventional Catheters in Intensive Care Unit Patients. *J. Hosp. Infect.* **2012**, *82*, 101–107.